AD-A190 507 THE GROWTH POTENTIAL OF CORONA DISCHARGES FROM AIRCRAFT FLYING IN PRECIPI..(U) UNIVERSITY OF MANCHESTER INST OF SCIENCE AND TECHNOLOGY (ENGL.. J A BICKNELL 12 NOV 87 1/2

UNCLASSIFIED AFOSR-TR-87-1781 AFOSR-83-0003 F/G 4/1 NL

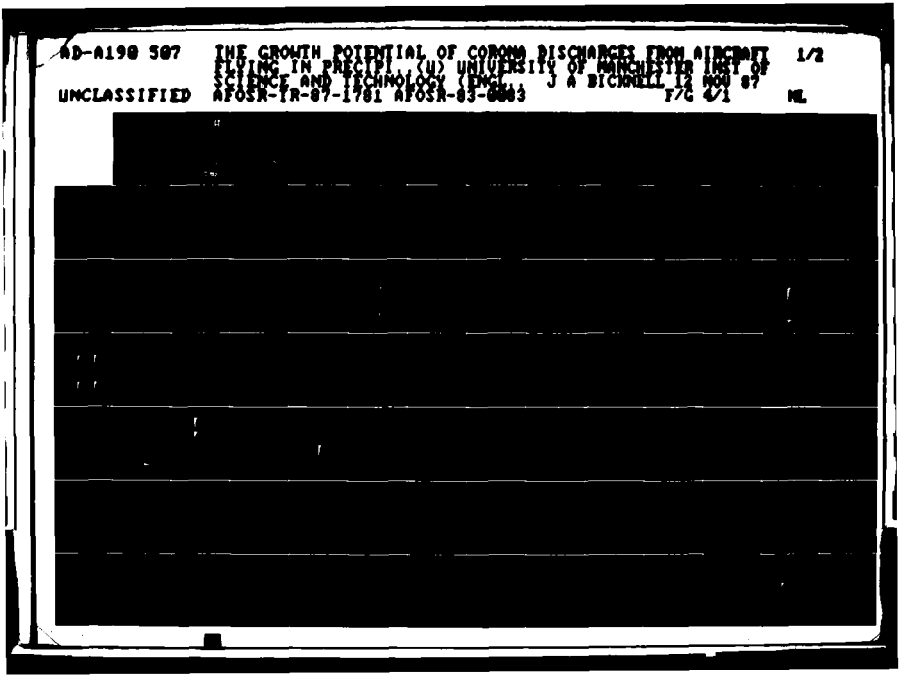

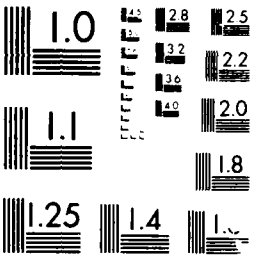

Illinois Institute of Science and Technology

2

FINAL SCIENTIFIC REPORT

GRANT AFOSR 83-0083

The Growth Potential of Corona Discharges from Aircraft Flying in Precipitation

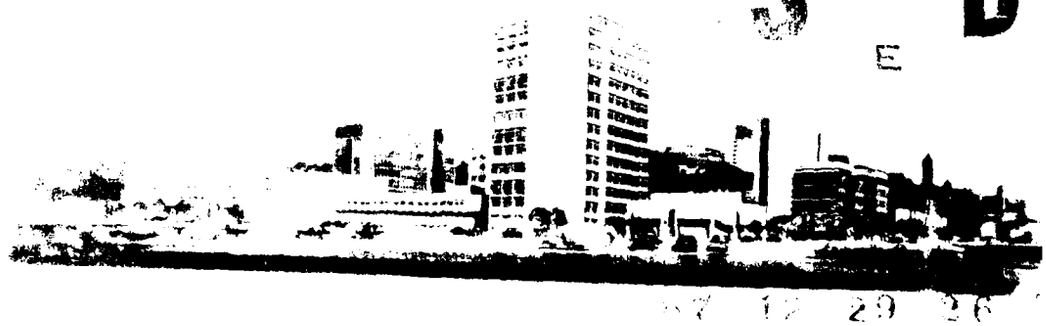

2 4

2

AFOSR-TR. 87-1781

FINAL SCIENTIFIC REPORT

GRANT AFOSR 83-0083

The Growth Potential of Corona Discharges from Aircraft Flying in Precipitation

by

Dr J A Bicknell

Principal Investigator

UMIST

Manchester M60 1QD

England

UNCLASSIFIED
SECURITY CLASSIFICATION OF THIS PAGE

REPORT DOCUMENTATION PAGE

Form Approved OMB No 0704-0188

1a. REPORT SECURITY CLASSIFICATION: UNCLASSIFIED	1b RESTRICTIVE MARKINGS
2a. SECURITY CLASSIFICATION AUTHORITY	3 DISTRIBUTION/AVAILABILITY OF REPORT: Approved for public release; Distribution unlimited
2b. DECLASSIFICATION/DOWNGRADING SCHEDULE	
4. PERFORMING ORGANIZATION REPORT NUMBER(S)	5 MONITORING ORGANIZATION REPORT NUMBER(S): AFOSR-TR- 87-1781
6a. NAME OF PERFORMING ORGANIZATION: University of Manchester Inst. of Science & Technology; 6b OFFICE SYMBOL (If applicable)	7a. NAME OF MONITORING ORGANIZATION: AFOSR/NC
6c. ADDRESS (City, State, and ZIP Code): P.O. Box 88 Manchester M60 1QD, England	7b ADDRESS (City, State, and ZIP Code): Bolling AFB, DC 20332-6448
8a. NAME OF FUNDING/SPONSORING ORGANIZATION: AFOSR; 8b OFFICE SYMBOL (If applicable): NC	9 PROCUREMENT INSTRUMENT IDENTIFICATION NUMBER: AFOSR-83-0083
8c. ADDRESS (City, State, and ZIP Code): Bolling AFB, DC 20332-6448	10 SOURCE OF FUNDING NUMBERS: PROGRAM ELEMENT NO 61102F; PROJECT NO 2310; TASK NO A1; WORK UNIT ACCESSION NO

11. TITLE (Include Security Classification)

THE GROWTH POTENTIAL OF CORONA DISCHARGES FROM AIRCRAFT FLYING IN PRECIPITATION

12 PERSONAL AUTHOR(S)

Dr. J.A. Bicknell

13a. TYPE OF REPORT	13b TIME COVERED	14 DATE OF REPORT (Year, Month, Day)	15 PAGE COUNT
FINAL	FROM 830101 TO 851231	871112	145

16. SUPPLEMENTARY NOTATION

17. COSATI CODES			18 SUBJECT TERMS (Continue on reverse if necessary and identify by block number)
FIELD	GROUP	SUB-GROUP	corona, model, lightning

19. ABSTRACT (Continue on reverse if necessary and identify by block number)

The behavior of positive streamers in fields near and above the stability field has been studied in quasi-uniform fields of up to 18 cm in extent with the aim of producing a model of the behavior so that predictions can be made for much greater distances. In particular the evolution in air of free charge produced by the propagation has been monitored and the effect of pressure and propagation distance on this evolution studied. A frequency and a coefficient have been defined and measured which characterize the growth of free charge. The Schockley-Ramo theorem has been used to analyze the data which not only provides values for other relevant parameters such as attachment coefficient and streamer velocity but also provides a novel way of observing prebreakdown streamer modes. A model has been constructed which adequately accounts for the observed behavior in small gaps but which predicts unrealistically large amounts of free charge in large gaps (greater than 1m). This suggests that some other mechanism might predominate in this case; an increase in electron density leading to channel thermalization is suggested as a possibility.

20 DISTRIBUTION/AVAILABILITY OF ABSTRACT	21 ABSTRACT SECURITY CLASSIFICATION
☒ UNCLASSIFIED/UNLIMITED ☒ SAME AS RPT ☐ DTIC USERS	UNCLASSIFIED
22a NAME OF RESPONSIBLE INDIVIDUAL: James P. Koermer, Lt Col, USAF	22b TELEPHONE (Include Area Code): (202) 767-4960; 22c OFFICE SYMBOL: NC

DD Form 1473, JUN 86 Previous editions are obsolete

SECURITY CLASSIFICATION OF THIS PAGE
UNCLASSIFIED

ABSTRACT

The Growth Potential of Corona Discharges from Aircraft Flying in Precipitation

The behaviour of positive streamers in fields near and above the stability field has been studied in quasi-uniform fields of up to 18cm in extent with the aim of producing a model of the behaviour so that predictions can be made for much greater distances. In particular the evolution in air of free charge produced by the propagation has been monitored and the effect of pressure and propagation distance on this evolution studied. A frequency (Γ) or coefficient (γ) has been defined and measured which characterises the growth of free charge. The Schockley-Ramo theorem has been used to analyse the data which not only provides values for other relevant parameters such as attachment coefficient and streamer velocity but also provides a novel way of observing prebreakdown streamer modes. A model has been constructed which adequately accounts for the observed behaviour in small gaps but which predicts unrealistically large amounts of free charge in large gaps (>1m). This suggests that some other mechanism might predominate in this case; an increase in electron density leading to channel thermalisation is suggested as a possibility.

Section 1: Introduction

The most remarkable single event in atmospheric physics is surely the lightning discharge so that it comes as no surprise that the study of the event has an impressive history together with an equally impressive list of, in many cases, legendary investigators (Franklin, C T R Wilson, Schonland and others). Over the years an enormous quantity of data has been garnered from numerous programmes conducted around the world, most notably in those regions where the lightning stroke is an devastating as it is spectacular. In view of this, what is surprising is that the entire mechanism from the initial charge separation through onset and leader development to the final arc is not satisfactorily understood. For example, there is still a certain controversy surrounding even the physics of the charge separation whilst the measured electric fields in the vicinity of thunderclouds (1-2kV/cm) are substantially lower than those encountered in laboratory long gap breakdowns. The investigation reported here was, and still is, concerned with the onset of the discharge. That is to say, given the thundercloud environment - with fields of measured magnitudes and precipitation of various sorts - together with a knowledge of laboratory breakdown processes - could the onset of the discharge be reasonably well predicted? There is an additional question involving aircraft as will shortly become clear.

Most breakdowns originate with corona and its subsequent development or growth; the exception being breakdown between parallel electrodes involving a strictly uniform field. In order to obtain corona, which is a property of high fields, in the low field of a thundercloud, demands the assumption that precipitation be present - a not too severe limitation for a thundercloud! The geometrically enhanced electric fields at the surface of the precipitation would then reach the level required for corona onset. However, it turns out that the fields required to generate corona from ice and water particles of the anticipated size are still significantly larger than those commonly encountered in a thundercloud. The exception here is the long water filament drawn out when water droplets collide - an event which combines a low onset field with relative rarity; desirable

features when seeking the cause of what is after all a triggered discharge. Of course, aircraft offer exactly the same characteristics - indeed the onset field is likely to be even lower - so if the argument that corona is a discharge prerequisite is acceptable it follows that aircraft can trigger a lightning flash. It is probably worth adding at this point that the overwhelming experimental evidence does currently point to a positive confirmation of aircraft triggered discharges. Mazur, for example, has identified, using radar, the source of several f hes as an aircraft flying through a thunderstorm; rocket triggered discharges provide additional support. When the investigation reported here was undertaken in 1984 this was not the common view (e.g. Clifford).

Of course, corona is not the sole requirement. Generally speaking, corona production will tend to dissipate the field which produces it. To understand corona driven breakdown from essentially isolated conductors (no discrete power source) a distinction must be made between the two forms of corona - negative and positive - both of which will usually occur simultaneously at opposite extremes of such a conductor located in a suitable field. Note this is not the same as monopolar corona from a charged conductor with or without an ambient field. The key difference lies in the concept of a stability field; this is the minimum ambient field in which the corona will propagate. Negative corona requires a much higher field for propagation than positive corona. The propagating corona is usually termed a streamer and the positive streamer stability field is some 4kV/cm only at atmospheric pressure. Since this field is pressure dependent then the lower pressures in a thundercloud lower the stability field to values not untypical of measured thundercloud fields. It is for this reason that the growth of the positive streamers for $E > E_{stability}$ is believed to be of key importance.

This investigation then is concerned almost entirely with the behaviour of such streamers. Establishing suitable conditions is not as easy as would appear because of the large voltages involved. Even 1MV would only allow propagation distances of 2.5m to be studied and then because of the size of the electrodes required to guarantee quasi-uniform fields (~7.5m in diameter) only measurements at atmospheric pressure could be made. The investigation has been confined for these reasons to gaps of only 20cm but

with the electrode structure contained in a vacuum chamber which allows the pressure to be varied from 200 torr to 760 torr - below 200 torr streamers are difficult to generate. An outline of the arrangement is contained in Section 2. The theoretical treatment required to interpret the results is in Section 3 with some typical results in Section 4. Most of the data obtained is contained in Section 5 with some discussion of these results in Section 6 and a broad conclusion presented in Section 7.

Section 2. Experimental Arrangement

2.1 Electrode System

The arrangements consists of two plane parallel electrodes. A third needle electrode is inserted in a hole in the plane anode, the needle being earthed. The redesigned upper electrode (Fig.2.1) is a 25cm diameter aluminium toroid, with a flat face. The 7cm diameter edge profile is intended to prevent natural corona inception from the cathode by keeping the field divergence at the edge low and the 12cm clearance from the GRP vessel walls prevents surface discharges along these to the lower electrode.

This is a 42cm diameter copper plate, 5mm thick, and stands on three spacers, resting on adjustable feet. Changing spacers allows electrode separations from 5 to 20cm to be used. A 6mm diameter stainless steel needle protrudes through a 2cm hole in the centre of the lower electrode, set by line-of-sight against a block, to be 12mm above the lower electrode surface (for easily repeatable consistency) whatever the electrode spacing. Both are earthed via (nominally) 50Ω resistors (see schematic Fig.2.2). The earth point is a copper strip, connected to a mains earth. Subsequent measurement of the resistance of the signal resistors used showed them to be 55 and 56Ω for the conduction and displacement circuit respectively. The cables used to connect with the oscilloscope were found by a resonant method to have a dynamic impedance of 76Ω. All these values are built into the computer program which finds the currents from the voltage waveforms.

Up to-100kV is applied to the upper electrode either directly or via a 200 Ω high voltage resistor from a Brandenburg Γ-series supply. The high voltage charging resistor was incorporated to prevent the formation of an arc.

Assuming the physical circuit between the HT supply and the electrodes to be circular and of radius 40cm, its inductance, $L = \mu_0 \pi r/2 \sim 0.8\mu H$. The capacitance of the electrodes, $C = \epsilon_0 A/d \sim 10pF$ and hence the time-constant for recharging the cathode directly, $\tau = LC \sim 3ns$.

If the cathode charge $Q = CV \sim 15\mu C$, is signficantly depleted inside $\sim 3ns$, the voltage falls, choking off the discharge. The risetime of a corona pulse may be $\sim 100ns$

and a time-to-spark is typically $\sim 1\mu s$; hence corona and arc processes can develop uninhibited if the charging resistor is left out of the circuit. If the cathode must recharge via the 200MΩ resistor, then $\tau = CR \sim 48ms$ and a high current arc cannot be sustained.

2.2 Digitizing System

The voltages across the signal resistors are taken down coaxial cable and digitized by a Philips PM315 125MHz digital storage oscilloscope (256 sample memory). Typical voltage pulses obtained with a Tektronix 300MHz bandwidth analogue oscilloscope show some oscillation but no short timescale events. Though the PM315 has an internal 60MHz filter, no data, therefore, is lost on account of this. It became apparent that the two channels were imperfectly synchronized. The rise in the conduction current circuit occurred one sample later than the rise in the diplacement circuit. This has quite severe consequences for the analysis routines used, as discussed later.

The high speed digital oscilloscope can be pre-triggered. The data is continually read in and once a trigger is experienced, the read-in of data stops. Hence data can be gathered from before the triggering point. This is an improvement over traditional oscilloscope measurements where the very first portion of the event is always absent from the records. (The streamer inception is irregular and so repetitive sampling techniques cannot be used.)

The data recorded by the digital scope were recorded using a Z80-based microcomputer via a GPIB-418 IEEE standard interface. The Pascal source code of the algorithm for handling this is reprinted in the Appendix but the implementation is heavily machine-specific and the code is particularly inefficient. This aspect of the measuring system leaves considerable scope for improvement.

The (integer) data from the scope are stored in a disk file and converted to an array of real data representing the currents calculated using the measured values of the signal resistances and dynamic cable impedances in parallel.

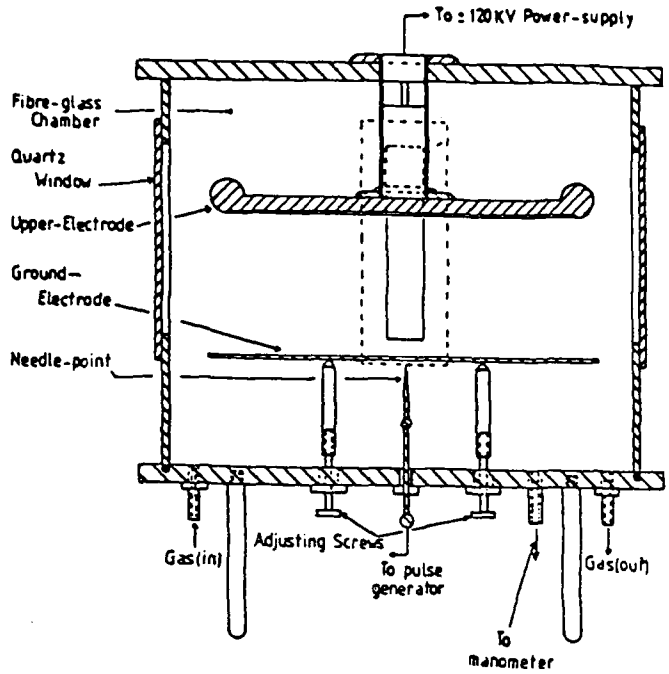

Figure 2.1 Section through the chamber

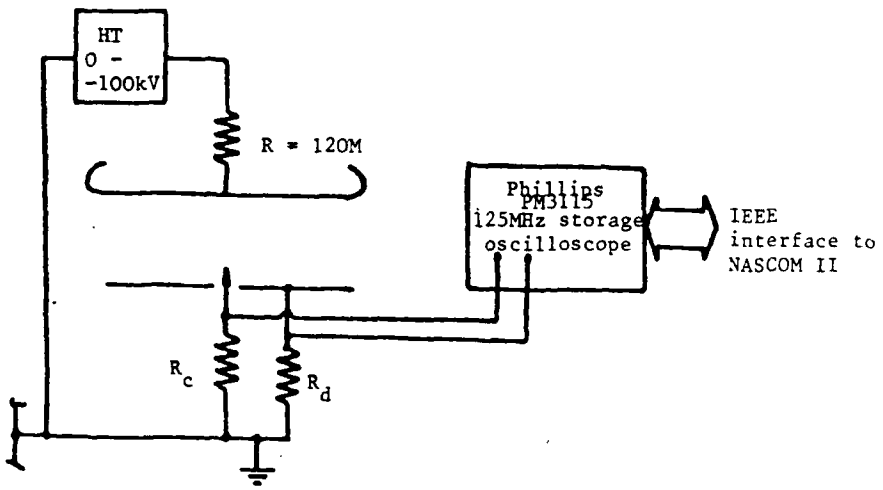

Figure 2.2

2.3 Experiments Carried Out

The needle projected by 12mm above the plane to generate natural corona. In this polarity, positive streamers were produced in the high field induced at the needle end and propagate into the gap. The needle is at earth potential and this falls quite rapidly to the potential which would have been experienced at this level in the plane-parallel gap were there no needle present. This potential drop is En, though it must be stressed that the needle itself is at earth. The potential drop in the enhanced field at the needle end depends on the field and needle height, n, and so keeping the needle height constant will ensure that the potential drop in the gas at its end is the same whatever the gap length or cathode potential. This is rather different from the situation in an inverted point-plane gap (the high voltage is usually applied to the point), where the potential drop at the needle-end does depend on the applied potential.

To produce streamers is no easy task, for the field produced in the gas at the needle-end must be high enough and of a large enough extent. The geometry of the needle is crucial and some considerable time was spent producing a sharp needle with a small, uniformly rounded tip. The idea being to increase the size of the critical volume by having a smoothly rounded tip, but to increase the field enhancement by having a narrow cone angle. The eventual needle profile, arrived at by trial and error had 30^{o} cone-angle, with a tip of radius $\sim 20\mu m$ (measured with a travelling microscope). It was necessary to electrolyse the tip in order to get a smooth profile of this small radius.

This gave satisfactory inception at high pressures but, as described in section 4, not so good an inception at lower pressures, where the critical avalanche must be larger for inception. On occasion, the inception was very infrequent, as the critical volume for those particular conditions was very small. To overcome this difficulty, an ionizing -source (50μCurie Americium) was mounted on the shaft of the needle just below the hole in the plane anode to provide excess starter electrons. The ionizing source did not affect the clearing time of the ions and so under conditions where the source was not needed, it could be left in the electrode chamber and have no effect at all on the discharge.

The primary aim of this work was to investigate the influence of propagation length on the corona characteristics. Accordingly streamers were generated and digital records of the induced currents made, with various different pressures and electrode separations. The data, stored on disk, was then analyzed to provide several fundamental parameters of the streamer's propagation, described in section 3.

It should be noted at this stage that as the data was digital, with a full scale deflection of 8 bits, the display (on a monitor with similar resolution) was scaled so that as much information as possible was visible. An autoranging algorithm was used to find a scale factor such that as much of the screen was used up and then rounded up so that inconvenient numbers were not involved. The zero level was determined by averaging the first 5 points in the record, and the data from the oscilloscope converted into a real number array for further analysis. When the scaling for the screen display was obtained a zero level was chosen such that the real zero level corresponded to a line on the graticule drawn on the screen.

The effect of this variable scaling though is that when making direct comparison of different pulses on the screen (or on the screen dumped copies used herein for illustrations) the scaling must always be borne in mind.

The electrodes are contained in a 50cm diameter GRP vessel, which was pumped out using a throttled-back rotary vacuum pump. Gas was let in through a mixing unit, where the flow could be controlled. The pressure established in the chamber by this flow ($\sim$10l/min), was monitored by a simple rotary dial gauge. Room air was drawn though a silica-gel dryer, which was regularly re-filled with fresh silica gell. Though the influence of humidity was not studied because of the time spent analysing the large quantity of dry gas data, the facilities exist for doing so.

Section 3: Theoretical Considerations

Introduction

An unavoidable paradox arises when studying streamer growth behaviour in a quasi-uniform field in that the generation of the streamer requires highly divergent field conditions, albeit localised. In general terms, the analysis of charge evolution in a uniform field from the behaviour of externally induced currents is relatively straightforward; in two electrode divergent field geometry progress can only be made given at least a detailed knowledge of the field distribution, but even then a derived charged distribution may be ambiguous. The present geometry, detailed in Section 2, contains elements of both. The treatment presented below indicates how the two contributions (uniform and non-uniform) may be separated leading to an estimate of the free charge and its rate of generation. The approach also highlights the importance of obtaining the data in digitised form even though some loss of resolution is inevitable.

3.1 Basic Processes

3.1.1 Induced Charge

Shockley (1938) and Ramo (1939) have shown, as an extension of the Reciprocity theorem (Jeans, 1927), that the charge q_k induced on the k-th conductor in a system S_n of conductors, due to the presence of a point charge q, at r, is given by:

$$q_k^* = -qV_k^*(r) \tag{3.1}$$

where $V_k^*(r)$ is a dimensionless quantity, the per-unit-potential, the potential at r if S_k is at unit potential, and all other conductors, $S_{n\neq k}$, in the system are grounded (Fig.3.1). It is a geometrical property of the electrode system.

3.1.2 Induced Current

Differentiating Eq. 3.1 yields the induced current i_k^* drawn by S_k:

$$i_k^* = -q\nabla V_k^*(\underline{r}).\dot{\underline{r}} = q\underline{E}_k^*(\underline{r}).\underline{v}$$

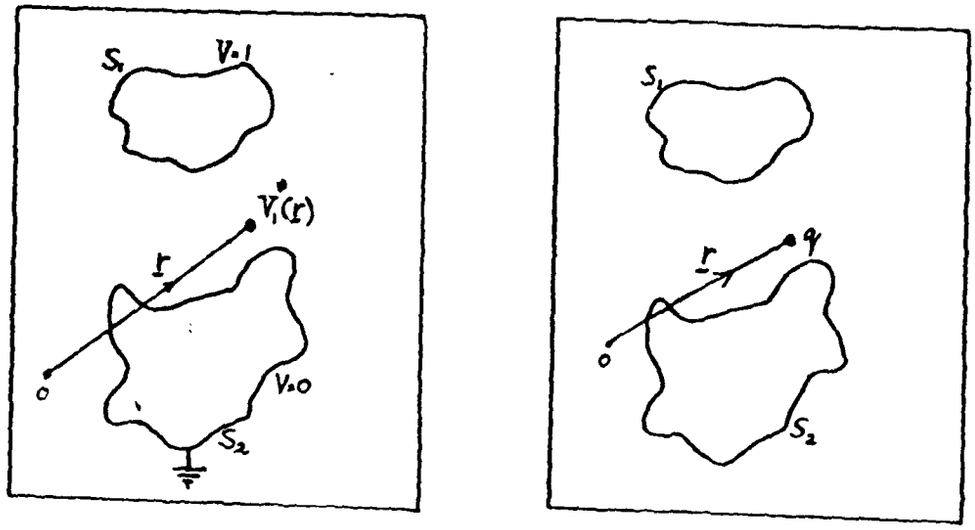

Fig 3.1

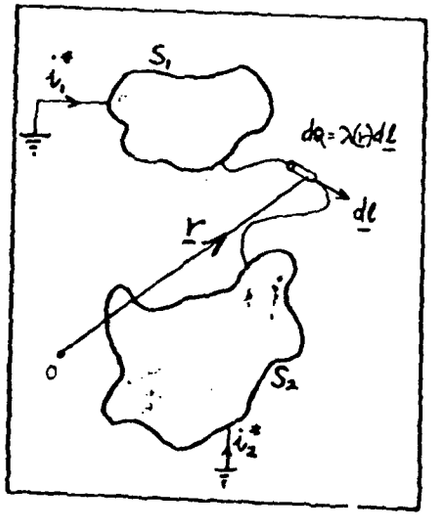

Fig 3.2

where $\underline{E}_k^*(\underline{r})$ is the corresponding per unit field at $\underline{r}$ (dimension L^{-1}), the charge q having instantaneous velocity $\underline{v}$. Since potential fields are superposable, generality is not lost by summing over all free charge in the system and for an axial conducting filament of linear charge density $\lambda(\underline{r})$ (Fig.3.2), the induced current is the line integral:

$$i_k^* = \int \lambda(\underline{r}) E_k^*(\underline{r}) v(\underline{r}) \, d\underline{\ell} = \int E_k^*(\underline{r}) j(\underline{r}) \, d\underline{\ell} \qquad (3.3)$$

$\underline{\ell}$ is a vector along the filament. The current, j, in the filament is given by $j(r) = \lambda(\underline{r})\underline{v}_e$ (the current is overwhelmingly electronic, since $v_e \gg v_{\pm}$).

3.1.3 Parallel Electrodes

For plane parallel electrodes, Fig. 3.3 shows V_k^*, $\underline{E}_k^*$, q_k^* and i_k^* for both electrodes (k=1,2). As a charge q moves from S_1 to S_2, V_1^* falls off linearly and hence q^* is progessively transferred from S_1 to S_2. That is to say, induced charge is conserved.

$$\sum_{k=1}^{n} q_k = -q \qquad (3.4)$$

Since the per-unit field, $E^* = 1/d$ everywhere and in the uniform externally applied field E the charge q has a constant velocity, the induced current is,

$$i^* = qE^*v = qv/d \qquad (3.5)$$

The current is almost entirely electronic, since $v_e \gg v_{\pm}$ and only free electrons contribute significantly to the induced current. By the same token, q is almost entirely composed of free electrons; ions - including negative ions - make little contribution to the induced current.

This induced current is now defined as i_e, and will be referred to as the electron current. This will be used as a theoretical concept in geometries where it cannot be defined as an induced current in a particular electrode. In such geometries, i_e represents the current due to all free electrons weighted uniformly (i.e. as if the per-unit field were uniform throughout the electrode volume). So in the three electrode system used in this study, the electron current is a concept, namely the current which would have been

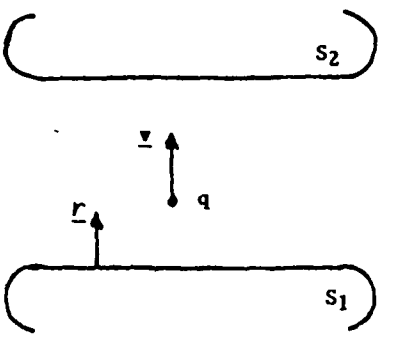

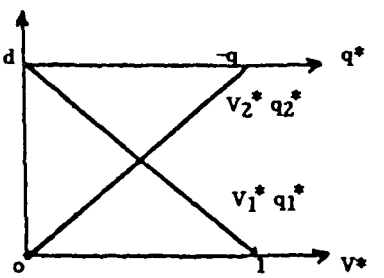

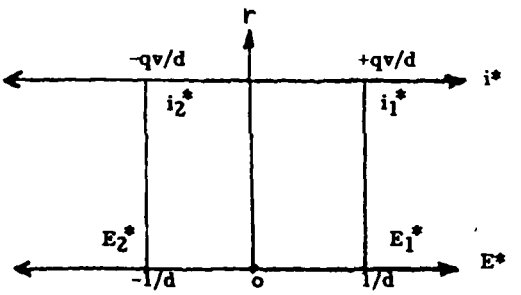

Fig 3.3

V* E* q* and i* for plane parallel electrodes. q from S_1 —> S_2

induced in the lower plane electrode if the point were not there.

3.1.4 Significance of i_e

To further understand i_e let a point charge q move between plane parallel electrodes and consider that:

$$\int_{t_1}^{t_2} i_e\,dt = \frac{q}{d}\int_{t_1}^{t_2} v\,dt = q\,\delta x/d$$

the dipole moment caused by this translation per unit electrode separation between the electron and the positive ion left behind. In this special geometry, $\delta x/d$ is just the change in per-unit potential along the path δx. In a general electrode system then, if one electron created by ionization in the gap drifts by δx, and is neutralized at an electrode and if the difference in V^* along this path is δV^* then the charge transported to that particular electrode is just $\delta V^* q$, which will be less than q. (This is not affected by the physical arrival of the charge, for the electron will be neutralized by the charge built up on the electrode, and no further current will flow to the electrode through the external circuit.)

Furthermore, the net charge in the gap is now q. The remainder of the induced charge resides on the other electrodes. Care must therefore be exercised when considering the induced currents, particularly where distributed charge is concerned, as free charge is not conserved (some may attach, for example); the integral of the free electron current may not then be easy to interpret.

3.1.5 External Current

In general, the conservation of induced charge (Eq.3.4) is the same as conservation of per-unit potential, since $q_k^* = -qV_k^*$:

$$\sum_1^N q_k = -q = \sum_1^N -q V_k^* \Rightarrow \sum_1^N V_k^* = 1$$

which means, for two electrode systems, that $V_1^* + V_2^* = 1 \Rightarrow E_1^* = -E_2^*$ or $i_1^* = -i_2^*$, which is hardly surprising as there is continuity of current in the external circuit. Note that as i^* is found by differentiating q^*, the sign of i^* is not related to the coordinate system used, but to the external circuit. In this case the current into S_1 equals the

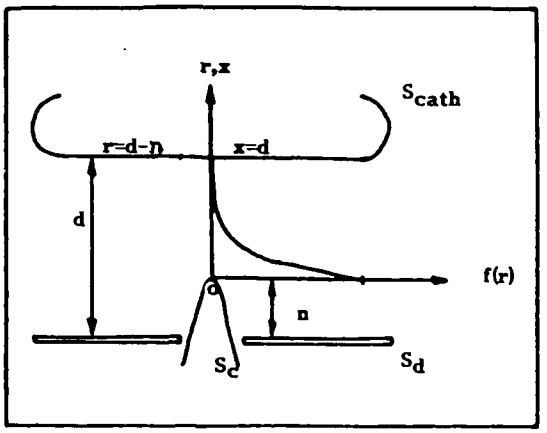

Fig 3.4

Showing f(r) and the coordinate system

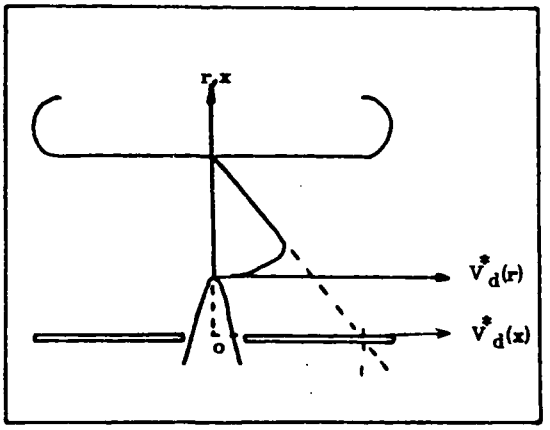

Fig 3.5

Effect of needle on the displacement current

(___) axial trajectory

(- - -) off axis trajectory

current out of S_2. This highlights a fundamental limitation of current measurement in two-electrode systems, i.e. since $i_1^* = -i_2^*$, there is only one degree of freedom. The electron current is defined as the induced current in plane parallel geometry. In point-plane geometry, the electrons moving near the point are weighted considerably more heavily than those further away, and the conceptually defined electron current, the induced current if the electrons are all given equal weight is not recoverable from the actual induced current. It will be shown that this is at least approximately possible in three electrode geometry where there is an extra degree of freedom and a particularly discrete boundary condition.

It can be added that the same analysis is applicable to any two groups of all the electrodes in a system. In the case of those used throughout this study, the external circuit is formed from the needle and the lower plane (i_c and i_d) and the cathode i_{cath}. Then the external current is $(i_c + i_d)$, and is equal to $-i_{cath}$. This is a very interesting observation, for (i_c+i_d) is the current which would be measured by physically combining the plane and point. In this case, however, the electrical interconnection of these electrodes is effected via the signal resistors and an earth point. They are electrically decoupled; the coupling occurs via the physical processes in the gap.

3.2 Three Electrode System

3.2.1 Three Electrode System

Fig 3.4 is an exaggerated sketch of the electrodes used in this study. To maintain consistency with what follows, the point will be referred to as S_c, the plane anode as S_d and the cathode as S_{cath}. It will be shown that the needle, S_c, introduces an effective boundary condition and to emphasize the generality of this, a purely geometric function, f(r), will be used.

A one dimensional filament is considered. Two coordinate frames are used, one, x, having its origin at the anode, S_d, the other, r, having its origin at the end of the needle, S_c, where x=n, the height of the needle above the anode (Fig3.4).

3.2.2 Conduction Current

To find V_c^*, S_c is at unit, and S_a, S_{cath} at zero potential (Section 3.1.1). Accepting for now that the per-unit potential V_c^*, only has an appreciable value near the needle end, $r \lesssim ar_t$ where ar_t is a multiple of the tip radius) [this would seem reasonable if the needle tip were an isolated sphere of radius r_t, then if the surface is at unit potential, beyond the surface the potential will be r_t/r. The earthed anode will exaggerate this fall-off.[9]), the general form expected of V_c^* is given by the dimensionless function f(r) (Fig.3.4) which has the following properties:

$$f(r=0) = 1;\ f(r=d-n) = 0;\ f'(r=d-n) = 0 = f^{(n)}(r=d-n);$$

$$f(r) \sim 0 \text{ unless } r \lesssim ar_t \quad (3.6)$$

From Eq. 3.3, with $V_c^* = f(r)$,

$$i_c = \int_{r=0}^{r=d-n} E_c^* j \, dr = -\int f'(r) \, dr \quad (3.7)$$

and is hence the average current flowing in the portion of the channel where f(r) is appreciable, so given that the spatial extent of f(r) is small, i_c will be the same as the conduction current in the channel base.

The per-unit field is confined to a small region near the tip and a charge travelling across this region will pass through a difference ΔV^* in V^* of ~ 1. So during this transit, the whole charge q is transported to the point. If the size of this region is so small that the electrons cross it quickly compared with their arrival rate, or compared with the temporal resolution of the oscilloscope, then the current in this electrode approximates to the arrival rate of the charge.

3.2.3 Displacement Current

V_d^* for off-axis charge trajectories, is exactly the same as for plane parallel electrodes, and $i_d = i_e$ (section 3.1.3), but because the needle, S_c, is earthed when finding

V^*_d (rather than linearly rising as a charge across the gap, as in section 3.1.3, Fig.3.3) along the gap axis q_d must fall abruptly to zero as $r \rightarrow 0$ (Fig.3.5). The charge induced on the plane will rise linearly as q moves across the gap, only to fall abruptly back to zero as the needle-end is approached. The charge built up on the plane as q traversed the gap is transferred rapidly to the point. (This is a slight simplification: the charge built-up on the plane is (d-n)q/d, and that remaining on the cathode is nq/d both of these are transferred to the point as the test charge traverses the high field region at the needle-end. Of course the charge induced on the plane is a function of the position of q, not its path. The discussion is couched in terms of the trajectory of q to make visualization of the spatial variations clearer.) From the point of view of the conservation of induced charge, (Eq.3.4), it is self-evident that the only possible solution for V^*_d is:

$$V_d^* = \left\{1 - \frac{x}{d}\right\} - \left\{1 - \frac{n}{d}\right\} f(r) = \left\{\frac{d-r-n}{d}\right\} - \left\{\frac{d-n}{d}\right\} f(r) \tag{3.8}$$

and

$$E_d^* = -\frac{\partial}{\partial r} V_d^* = \frac{1}{d} + \frac{d-n}{d} f'(r) \tag{3.9}$$

then $$i_d = \int_{r=0}^{r=d-n} j(r)\left\{\frac{1}{d} + \frac{d-n}{d} f'(r)\right\} dr = \frac{1}{d}\int_{r=0}^{d-n} j(r)\,dr + \frac{d-n}{d}\int_0^{d-n} j(r) f'(r)\,dr$$

that is, $$i_e = i_d + \frac{d-n}{d} i_c \tag{3.10}$$

Since it is contributed to by the displacement of charge across the gap, this is called the displacement current. Rearranging Eq.3.10 we have i_e, the current which would have been recorded in plane parallel geometry:

$$i_e = i_d + \frac{d-n}{d} i_c \tag{3.11}$$

This addition of a negative contribution to i_d from i_c formalizes the rapid drop in V^*_d near the needle end, and will turn out to be a useful analytical tool. This rapid drop-off in V^*_d is due to an effective boundary condition, since the defining equations for V^*_d require the needle to be at earth potential. This is where the i_c term in Eq.3.10 comes from and is a fundamental result.

Fig 3.6

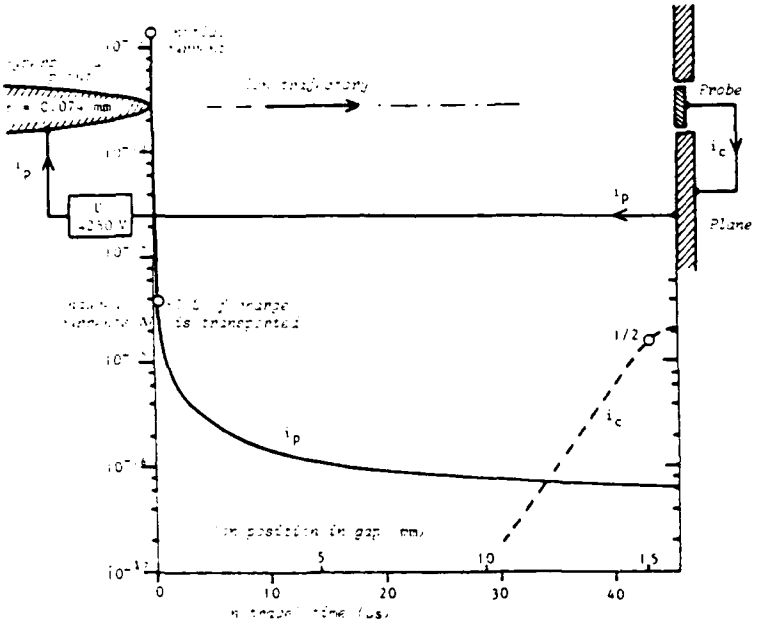

Illustrating the Shockley-Ramo theorem: Point current i_p and center probe current i_c induced by one O_2^- ion drifting from the hyperboloid point to the plane through the Laplacian field in 87.6 kPa dry air (Sigmond, 1978).

Idealised i_c - i_d current profiles

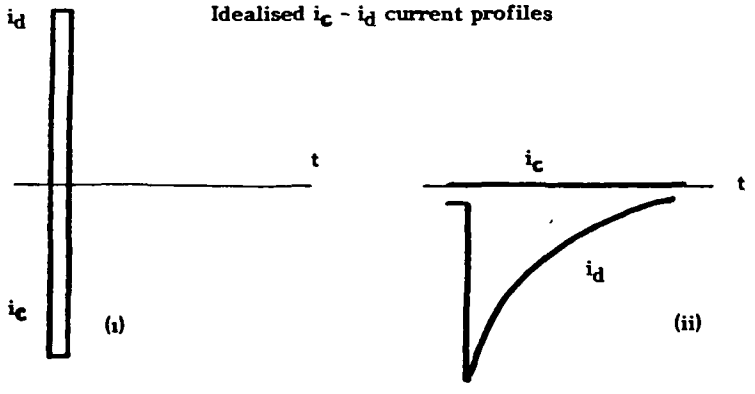

Fig 3.8

This technique for recovering i_e is not dependent on the extent of f(r). Nor is Eq.3.7 for i_c. The only place in this discussion where the spatial extent of f(r) is important is in ascribing i_c to be the physical current in the channel base. This will be discussed later in connection with the space-charge field at the channel base.

3.2.4 Free Charge Reconstruction

As already mentioned, the electron drift speed is $\gg$ ion drift speeds and only the electronic component of the current is observed. Note that this implies that free (electron) charge is NOT conserved; an electron attaching to an oxygen molecule, for example, contributes little to the induced current.

If the free electron charge in the gap totals G_g, and IF these electrons have the same drift speed v_e (the field is uniform, and v_e is found from well-established expressions) then $i_e = G_g v_e/d$ or:

$$G_g = i_e d/v_e \tag{3.12}$$

and the free electron charge in the gap, G_g can be found by simply scaling i_e. This reconstruction of G_g from instantaneous value of the induced currents relies on some fairly gross assumptions, and the validity of these is considered below (section 3.3).

3.2.5 Three Electrode Point-Plane System

Sigmond (1978) has calculated the per-unit potentials and fields for an ingenious three electrode point-plane system used by Marode (1975a,b) (Fig.3.6). The cathode is here divided into two, with a small, isolated central portion. Note how the drop-off of V_c^* is so steep that the charge is transported almost instantaneously to the point as q traverses the high field region. To a lesser extent this occurs as q reaches the central portion of the cathode too, and hence the currents measured will be nearly equal to the charge arrival rates, as outlined above. Thus for this arrangement, as expected for the system used here, the current to the point is effectively equal to the arrival rate of charge.

3.2.6 Polarity of Induced Currents

The applied field is supplied by S_{cath}, and charges of either polarity drift in opposite directions (according to the coordinate system of Fig.3.4) to produce a +ve conventional current j (directed upward in the figure). From Eq.3.7 and Eq.3.5 (f'(r) is -ve), it can be seen that i_c and i_e will always be +ve, and hence will always cause a -ve voltage across the signal resistor R in the external circuit.

All references to currents induced from now on will refer to the voltages across the resistors as though they were currents. So a -ve conduction current waveform (for example) is produced by an upward directed conventional current in the base of the channel.

The only +ve voltage (-ve current) induced in the external circuit to the lower electrodes is the $(-(d-n)/d)i_c$ contribution to i_d. If there were a positive voltage in i_d therefore, it can be inferred that there is current flowing in the region where the per-unit-potential of the needle is appreciable. This is a result of there being an effective boundary condition at the needle-end and is unambiguous. The only ambiguity in the analysis lies in the spatial extent of the needle-end region. In the sense indicated above, positive electron currents i_e, and conduction currents, i_c are physically not possible.

3.3 Limitations/Problems

The above treatment of the induced currents relies on some fairly gross assumptions; however it will now be shown that these can largely be avoided when the particular magnitudes of the parameters involved are considered more carefully.

3.3.1 Space-Charge Field

Section 3.2.4 ignored the space-charge field. Firstly, electron velocities in the active region are $\sim 10^7$ cm/s. The contribution from the space-charge field of the tip, where the electron speed is the highest is considered below (section 3.3.2). Even excepting the tip, for G_g to be recoverable from i_e, the electron speed, and therefore the local field everywhere must be the same. But is this a reasonable assumption? Can the

space-charge field of the channel at least be ignored?

Phelps (1976) asserts that the field along the channel is just the geometric, or applied field; whereas Marode (1981) emphasizes that conductivity is the more important, E being determined such that there is current continuity along the channel.

Phelps would have the space-charge distributed by the applied field: Marode, the conductivity (charge density) determining the field.

A simple calculation shows that for a channel of net charge $\lambda L \sim 10nC$ (typical value of $\int i_c dt$), the space-charge field, $E'_{max} \sim 0.4$ KV/cm, compared with an ambient field of some 4KV/cm. Hence the space charge field can safely be ignored in the channel.

There is an exception. It will be recalled that the development of further streamers is supposed to be suppressed by a positive space-charge local to the needle-tip. The suppression of further streamers is indeed good evidence that the field at the tip is reduced by a positive space-charge. Certainly the geometric field here is high, causing electrons to be swept out of the gap more efficiently than they are swept into this region from the rest of the channel. It will tend to accumulate a positive charge until the local field is uniform along the channel. But this will occur only whilst the electrons in the needle-region remain unattached. This is essentially either the development of compensation zone process of Phelps or the secondary streamer process of Marode.

In this case the space-charge field works in favour of the theory developed here. With the reduced local field due to this space-charge, the electron drift speed will be the same in the base of the channel as it is in the remainder, and the recovery of the free charge (section 3.2.4) thus makes a valid assumption. The electron drift speed can be obtained accurately enough by using the applied field and pressure for a given gas - it does not change significantly because of the space-charge.

Furthermore, the superposition principle permits the effect of individual charges to be considered in isolation and simply summed up (section 3.1.2), so the space-charge does not influence the per-unit-potential; V' is a property of the electrodes.

It has been indicated (section 3.2.2) that the time taken to cross the needle-region is important. If this occurs within the sample time of the oscilloscope, the charge transfer can be considered to have occurred instantaneously. The shortest sample interval used was 16ns and for an electron drift speed of ~40km/s (in the whole length of the channel), this corresponds to a needle-end region 640μm in extent. Since the tip radius of the needle used was ~20μm, the conduction current can safely be identified with the arrival rate of charge at the tip. The transit time of the enhanced per-unit-field region is clearly less than it would have been without the positive space-charge, but it has been shown that the overall effect of this does not affect the identification of the conduction current with the arrival rate of charge at the tip.

3.3.2 Streamer Active Region

A major problem in the analysis of the discharge currents is the different drift speeds in the active region and in the channel. The field in the active region (Hartmann, 1974) may be 120V/cm.torr or more. The corresponding electron speed is ~350km/s, or 20 times greater than the ~35km/s in the drift region (the channel). However, typical free charge values before cathode impact may be up to 100nC, 10^4 x the charge in a streamer tip (10^{-11}C) and thus for a single tip the channel current would be ~10^3x greater than the tip current.

3.4 Application

Turning now from generalities to some specific predictions about the induced currents, etc. expected from particular discharges, there are three cases to consider.

The current may be confined entirely to the tip region (i) or distant from the tip region (ii), or a combination of both (iii).

3.4.1 Case (i)

If the current were confined to the tip region, the electrons would drift to the

anode surface very quickly and be neutralized there. Thus only a brief pulse of current would be observed. As discussed above, there would be a large contribution to the conduction current, because of the relatively large per-unit field, accompanied by a large positive contribution to the displacement current. This positive-going displacement current is the clearest evidence for this phenomenon, as it can arise from no other situation (negative currents are always expected). This kind of event would look much as sketched in Fig. 3.8(i).

3.4.2 Case (ii)

If the charge is distant from the point, then no contribution would be expected to the conduction current; the per-unit field with respect to the tip is negligible at any significant distance from the needle end. The most practical visualization of this kind of behaviour is charge injection from the cathode arising from the impact of the streamer. In this case there would be a continuum of current from whatever processes are occurring in the remainder of the discharge immediately before the impact, and the burst of charge released from the cathode will be superimposed upon this. The electrons liberated from the cathode will then attach over a period, producing the waveforms in Fig. 3.8(ii).

As the electrons from the cathode are distant from the point, there will be no induced conduction current. The electron current i_e will be very much like the displacement current and both will be negative. The situation is similar to plane-plane geometry, for which the displacement current would be identically equal to the electron current. An electron generating event in mid-gap would have produced the same effect.

3.4.4 Case (iii)

Where there is a channel growing into the gap from the point, the situation is more complex. The relative growth and attachment rates need to be considered. There are three main cases, (a) below, (b) at, and (c) well above the stability field. Based on a simple model of the discharge (section 3.5.6 ff) the electron currents are indicated in

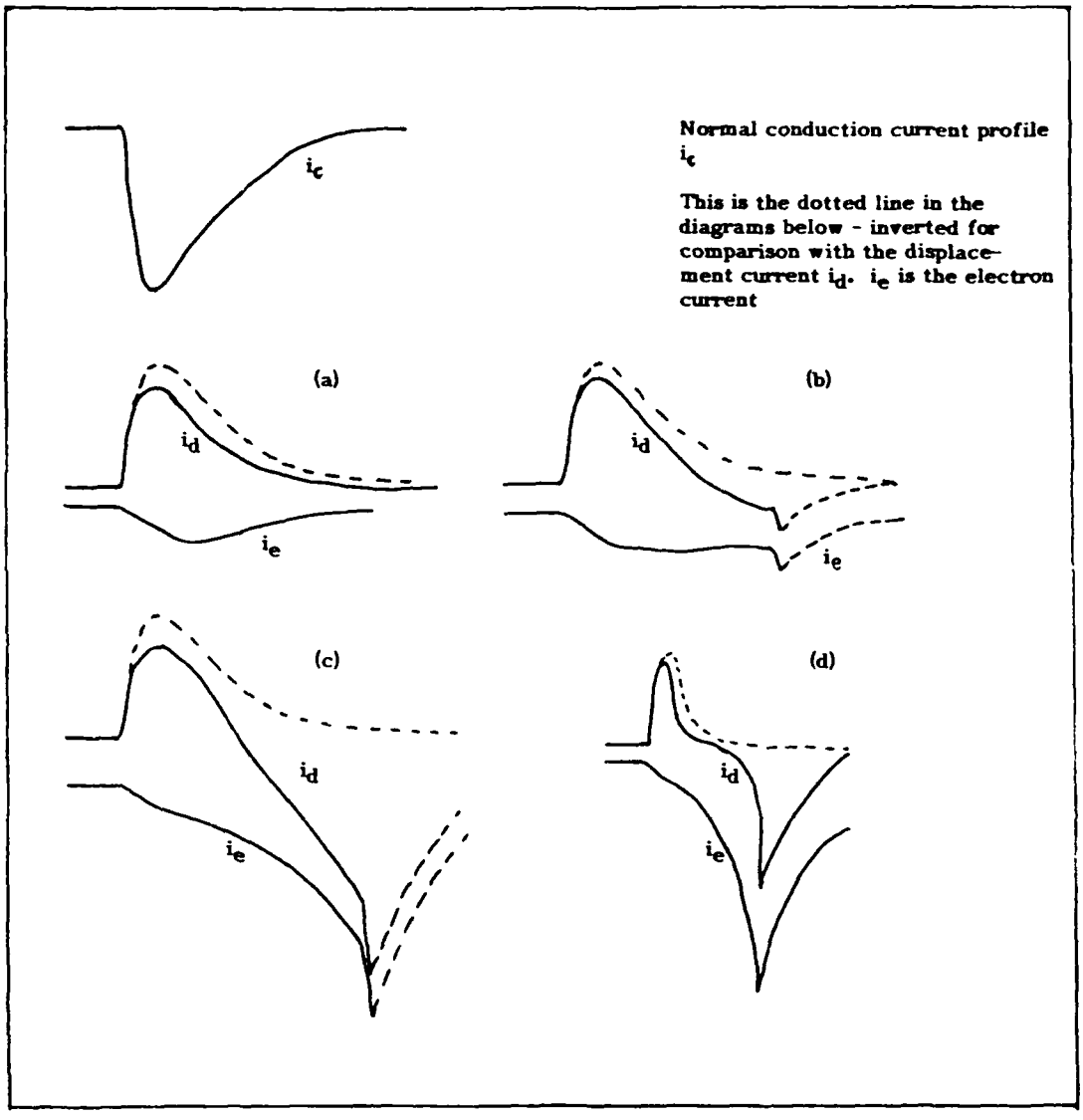
Normal conduction current profile i_c
This is the dotted line in the diagrams below - inverted for comparison with the displacement current i_d. i_e is the electron current
(a)
i_d
i_e
(b)
i_d
i_e
(c)
i_d
i_e
(d)
i_d
i_e

Fig 3.9

Fig.3.9 for each case. As the channel is built up the electron current increases initially, falling again for (a), flattening out for (b) and subsequently rising in case (c). The influence of this on the displacement current can be calculated with the aid of Eq. 3.10 and i_d is sketched for (a), (b) and (c), assuming the case of a standard conduction current pulse in Fig. 3.9.

It can be seen that the dying streamer has a displacement current wholly positive, only marginally different from the conduction current. The stability streamer displacement current does dip below the axis, and a little charge injection from the cathode has been marked in (according to section 3.4.2). Above the stability field the displacement current dips very strongly below the axis, and the charge injection has been drawn in more heavily also. In this example the second derivative of i_d has changed from a concave slope below E_{stab} to a convex slope above E_{stab}. If the attachment is very strong (Fig.3.9(d)), then a point of inflexion is expected to appear.

3.5 Further Analysis

3.5.1 Generated Charge

Consider a channel, length L_1 and charge Q_1 at time t_1, developing to (L_2, Q_2, t_2). Then since $\int_{t_1}^{t_2} i_c dt$ is removed, and the remainder gets attached, one may write:

$$Q_2 = \left(Q_1 - \int_{t_1}^{t_2} i_c\, dt\right) e^{\nu_a (t_2 - t_1)} + \delta Q \qquad (3.14)$$

where the generated charge δQ is introduced to satisfy charge conservation. In a growing streamer system, this is in effect the total streamer tip current integrated over a sample interval. In all calculations, it will be divided by the sample interval, to give a charge injection, or charge generation rate. It will be ~0 after the streamer transit, unless some other electron-detaching or ionizing process is occurring.

3.5.2 Attachment Frequency

To find δQ from Eq.3.14 requires a knowledge of ν_a and this is not well defined experimentally. However, if the channel is decaying without any new electron

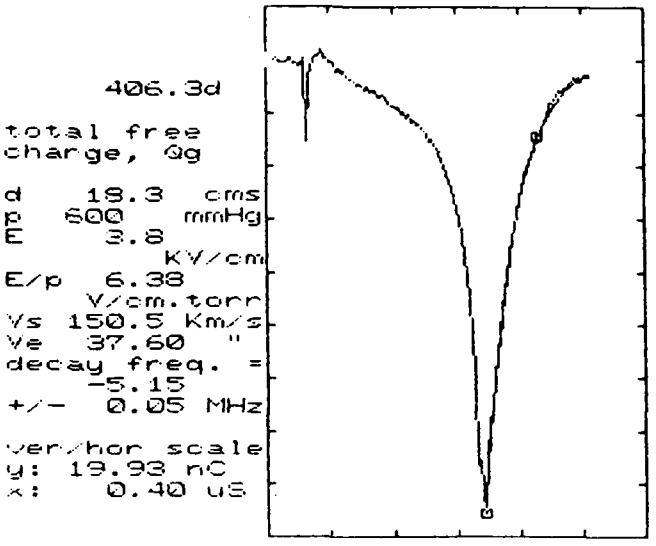

Fig 3.10

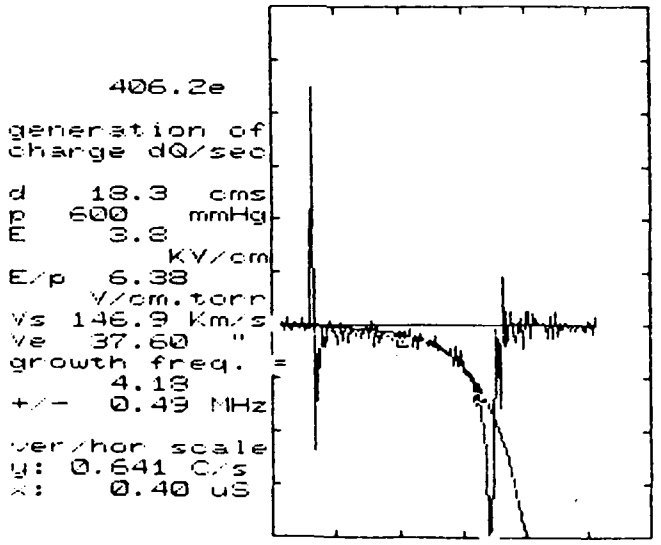

Fig 3.11

detachment or ionization, $\delta Q = 0$. In most cases, the channel has decayed substantially by the time the streamers cross the gap and $\int i_c dt$ in Eq.3.14 can be neglected by comparison with the magnitude of Q_g. Typical values are for Q_g to change by 2-3nC at an attachment frequency of ~3MHz compared with ~320pC extracted from the channel base in the same time. So unless the attachment frequency is very low and there is appreciable conduction current at this point, ν_a can be found by performing a least-squares exponential fit on the Q_g data. An example of this is shown in Fig3.10 where this has been performed between the two cursor markers. In this way, using the fitted value of ν_a from a portion of the discharge when $\delta Q = 0$, allows δQ to be found for portions of the curve when it is non-zero (Fig.3.11).

3.5.3 Streamer Velocity

The large pulse of electrons released when the streamer arrives at the cathode, is seen as a sharp increase in δQ (Fig.3.11). From the transit time of the streamer, t_N, the mean streamer speed, $v_s = (d-n)/t_N$ can be found. This time-of-flight method is rather crude compared with considerably more sophisticated photomultiplier studies, but the results are useful as confirmation or for comparison.

3.5.4. Streamer Function, A(x)

In attempting to identify a formal growth parameter for a streamer consider that a streamer system "creates" an elementary line charge $dQ = A(x)dx$, at x, at time $t=x/v_s$ (Fig.3.12): this charge then drifts at v_e back toward the point, arriving x/v_e seconds later at time $T=x/v_s + x/v_e = x/V$ where it is convenient to define an effective velocity V. After attachment, the charge dQ laid down becomes upon arriving at the point, $dQ' = dQe^{-\eta x} = A(x)e^{-\eta x}dx$. But with $x=VT$, $dx=VdT$, and $dQ'=A(TV)e^{-\eta TV}VdT$, then:

$$i_c = \frac{dQ'}{dT} = A(TV)e^{-\eta TV}V \qquad (3.15)$$

or

$$A(x) = i_c\left(\frac{x}{V}\right)e^{\eta x}/V \qquad (3.16)$$

$$dQ' = A(x)e^{-\eta x}dx$$

$$= A(TV)e^{-\eta TV}\,V\,dT$$

$$i_c(T) = dQ'/dt = A(TV)e^{-\eta TV}V$$

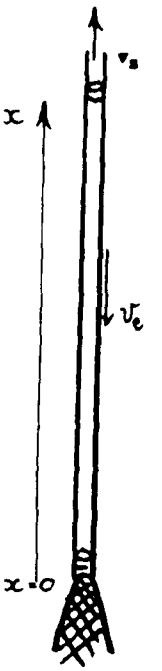

$dQ = A(x)dx$
(created at time $t = x/v_s$)

Fig 3.12

charge
dQ' $'\cdot e^{-\eta x}$
s' $= o$ at time T
T $x/v_e = x/V$

$t = t_1 + t_2$

$d/v_s = X/v_s + X/v_e - x/v_e$

$\Rightarrow X = (d/v_s + x/v_e)V$

$\lambda(x,t) = A(X)e^{-\eta(X-x)}$

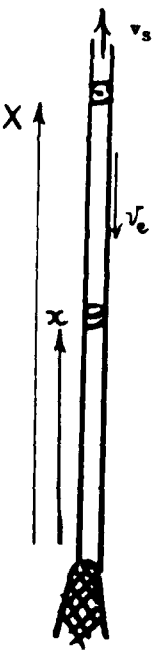

streamer reaches $d = v_s t$

charge deposited at X is $A(X)dX$
at time $t_1 = X/v_s$

drifts to x in
time $t_2 = (X-x)/v_e$
and is $A(X)e^{-\eta(X-x)}dX$

Fig 3.13

Calculation of $A(x)$ from i_c is only possible while significant current survives to reach the point. Noise otherwise dominates the calculation of $A(x)$, and the limited information yielded by this technique limits its use. This demonstrates the dominance of attachment in the channel. Compared with the attachment effect, $A(x)$ has negligible influence upon the form of it.

3.5.5 Channel Function, $\lambda(x)$

The instantaneous electron distribution along the channel, $\lambda(x)$, may be more useful than $A(x)$. Clearly $Q_g = \int_0^d \lambda(x)dx$, and $\lambda(x)$ is related to $A(x)$ by the following relation, (see Fig.3.13)

$$\lambda(x,t) = A(X)e^{-\eta(X-x)} \qquad X = (t+\frac{x}{v_e})V \tag{3.17}$$

In this case, $t=d/v_s$. Substituting this into Eq.3.17 and integrating the electron charge for a streamer which has extended a distance d, and putting $A(X)=\Lambda e^{\gamma X}$ for the streamer function, one has:

$$\begin{aligned} Q_g(d) &= \int_0^d \lambda(x)\,dx \\ &= \Lambda \int_0^d \exp \gamma V\left(\frac{d}{v_s}+\frac{x}{v_e}\right) \exp -\eta\left(\frac{Vd}{v_s}+\frac{x[V-v_e]}{v_e}\right) dx \\ &= \Lambda \frac{v_e}{\gamma V-\eta(V-v_e)} \exp \frac{dV(\gamma-\eta)}{v_s}\left[\exp\left(\frac{\gamma V-\eta(V-v_e)}{v_e}\right)d - 1\right] \end{aligned} \tag{3.18}$$

This has been evaluated with the following values of the coefficients involved: $\eta = 100(m^{-1})$, $v_e=40km/s$, $v_s=150km/s$ (.. $V=31.5km/s$). The result is plotted as $Q_g(d)/\Lambda$ for various values of d and γ in Fig.3.14 and shows that this general picture of the discharge is reasonable insofar as it produces results which agree with the phenomena and with the general idea of a growing streamer.

If the streamer is dying, $\gamma<0$, then Q_g decreases with d. Q_g is stable, reaching a constant level when $\gamma=0$, and rises rapidly when there is strong growth, $\gamma>0$. Initially, as the channel is being established, all values of γ imply growth in Q_g. The stability field

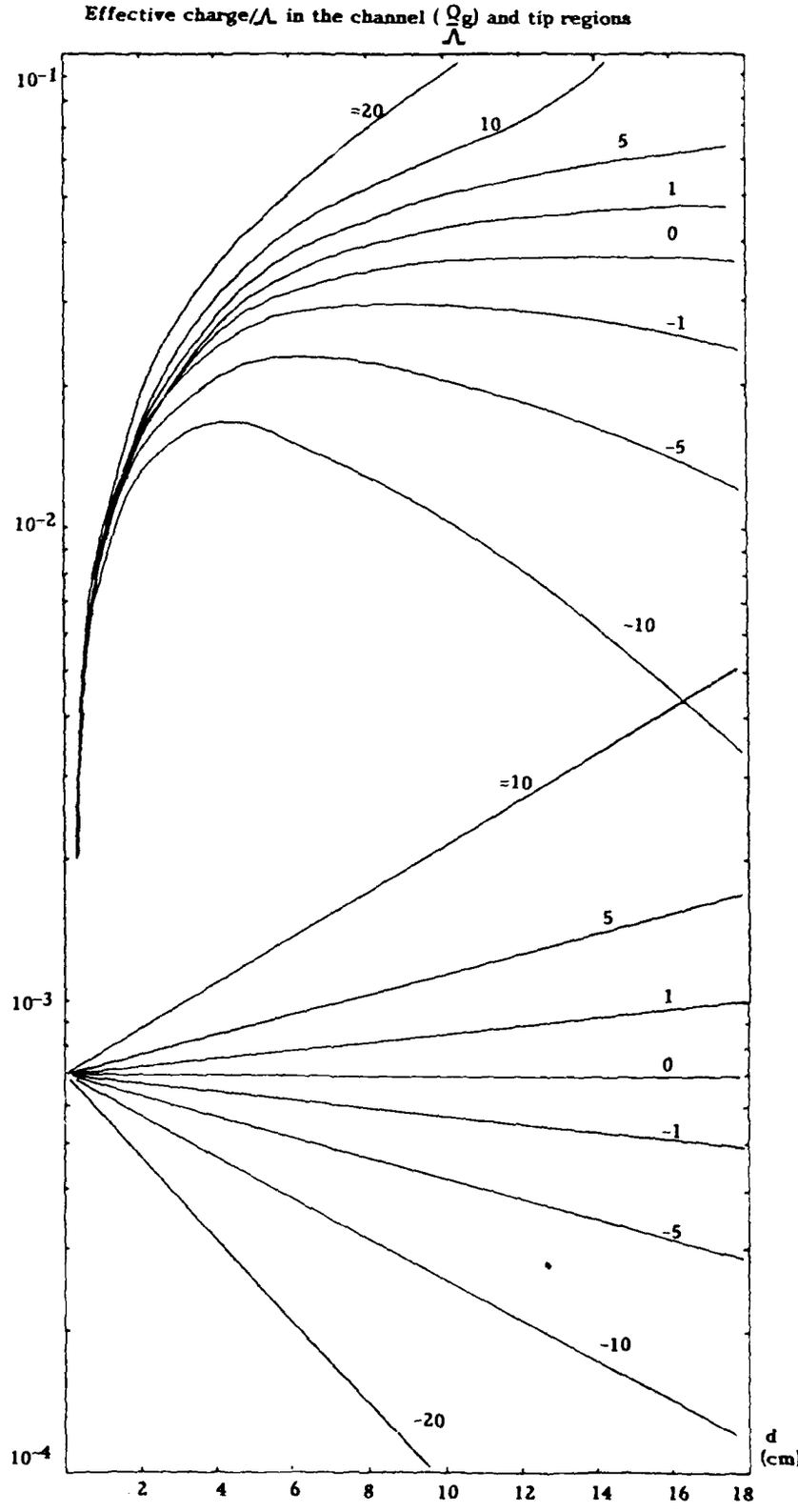
Effective charge/Λ in the channel (Qg/Λ) and tip regions
10⁻¹
10⁻²
10⁻³
10⁻⁴
=20
10
5
1
0
-1
-5
-10
=10
5
1
0
-1
-5
-10
-20
2
4
6
8
10
12
14
16
18
d
(cm)

Fig 3.14

corresponds to $\gamma=0$, but this graph (Fig3.14) makes clear a difficulty in determining the stability field from deciding whether or not the streamers cross the gap. Pre-stability streamers take some time to die, and might reach the cathode in the small $\gtrsim 10$cm or so gaps used experimentally. This analysis shows unequivocally that if C_g holds level throughout the life of the discharge then the streamer is at the stability field.

3.5.6 Formal Growth Parameter

$A(x)$ is the better growth parameter, despite the measurement problems noted in section 3.5.4. An alternative is to use δC for it seems reasonable to write:

$$\delta Q(t) = A(v_s t)v_s, \tag{3.19}$$

as the charge C added to the channel is clearly just the charge $A(x)$ laid down by the streamer. This relation is needed to convert between the spatial and temporal growth rates of the streamer.

Section 4: Typical Results

Introduction

The input data consists of just two time dependent currents (viz. conduction and displacement) but, as indicated in Section3, a number of derived quantities are obtained for each corona event (e.g. free electron magnitude Q_f, generated charge δQ). Naturally, the temporal development of these quantities is field and pressure dependent. In this section some typical results are presented for various field/pressure regimes together with an explanation of these profiles in terms of the microphysics of the event.

4.1 Regular Corona

The bulk of the work concerns conventional streamers at sub-breakdown fields and at different pressures and/or propagation lengths. Subsequently, as the field is increased, a number of corona modes are observed, which are associated with pre-breakdown phenomena. These corona modes are interesting as their elucidation bears upon the topic of the glow-to-arc transition in uniform fields which is commonly encountered in overvolted gaps, at a reduced field nearly always greater than 34V/cm.torr (for air); by comparison, the breakdown in the present study occurs at 8 to 10V/cm.torr. We deal here with the sub-breakdown streamer event.

4.1.1 Inception Field

At reduced pressure, the lateral diffusion of electron avalanches increases. To generate a critical avalanche then, a greater charge is required in this larger volume to raise the tip field to the level where the replication mechanism can operate. So a higher reduced field is needed before onset occurs. Replotting Phelps' stability field data as reduced stability field, E_{stab}/p, shows on the contrary that the stability field is lower at lower pressure (Fig.4.1). The combined effect of these two variations is that at a certain pressure (about ~500 torr in the present study), the onset and stability fields coincide.

Below this value, onset streamers always grow throughout their life, and regrettably no sub-stability field measurements can be made.

4.1.2 Pre-stability Field Streamers

As mentioned above, observations of this regime are restricted to high pressures. The displacement current at low reduced field is entirely positive (Fig. 4.2,#408.2) indicating that there is a lot of current at the base, and very little in the body of the channel. (It will be recalled that a positive displacement current is fundamentally related to the current at the needle-tip, section 3.2.6). The conduction current shows no fine structure (more of this later) and the small electron current (Fig. 4.3) ensures that i_c and i_d are almost anti-symmetric (Fig. 4.4,#408.3).

The electron charge, Q_g, falls off throughout the discharge (Q_g and i_e have the same form, as they are related by a simple scaling factor (section 3.2.4) and all the figures are drawn with a dual scale representing this). The form of Q_g in fact follows that presented in Fig.3.14 for the case of a strongly decaying streamer system. Common to all records is the initial rise in Q_g. Following this the particular features of interest are the peak $\sim$0.23μs after the event began and following that the subsequent strong decay of Q_g. The simple calculation of the charge in the gap (section 3.5.6) shows a similarly broad peak, which indeed (for example with the growth parameter used in the model γ=-10), occurs at around $\sim$0.27μs. All this shows clearly that the low reduced field in the example studied cannot support streamer propagation, even though a critical avalanche can be created at the needle tip. Once the high field region at the needle end has been left behind, the streamer travels a cm or so using its internal energy to compensate for the inadequate supply from the external field and finally dies. Visual observation of the corona confirmed that it did not propagate to the cathode.

It has been observed though that streamers below the stability field may still survive to the cathode. Figure 4.5 shows a sequence of records, as E/p is increased. The event just considered, #408.2, was obtained at the very low ambient reduced field of

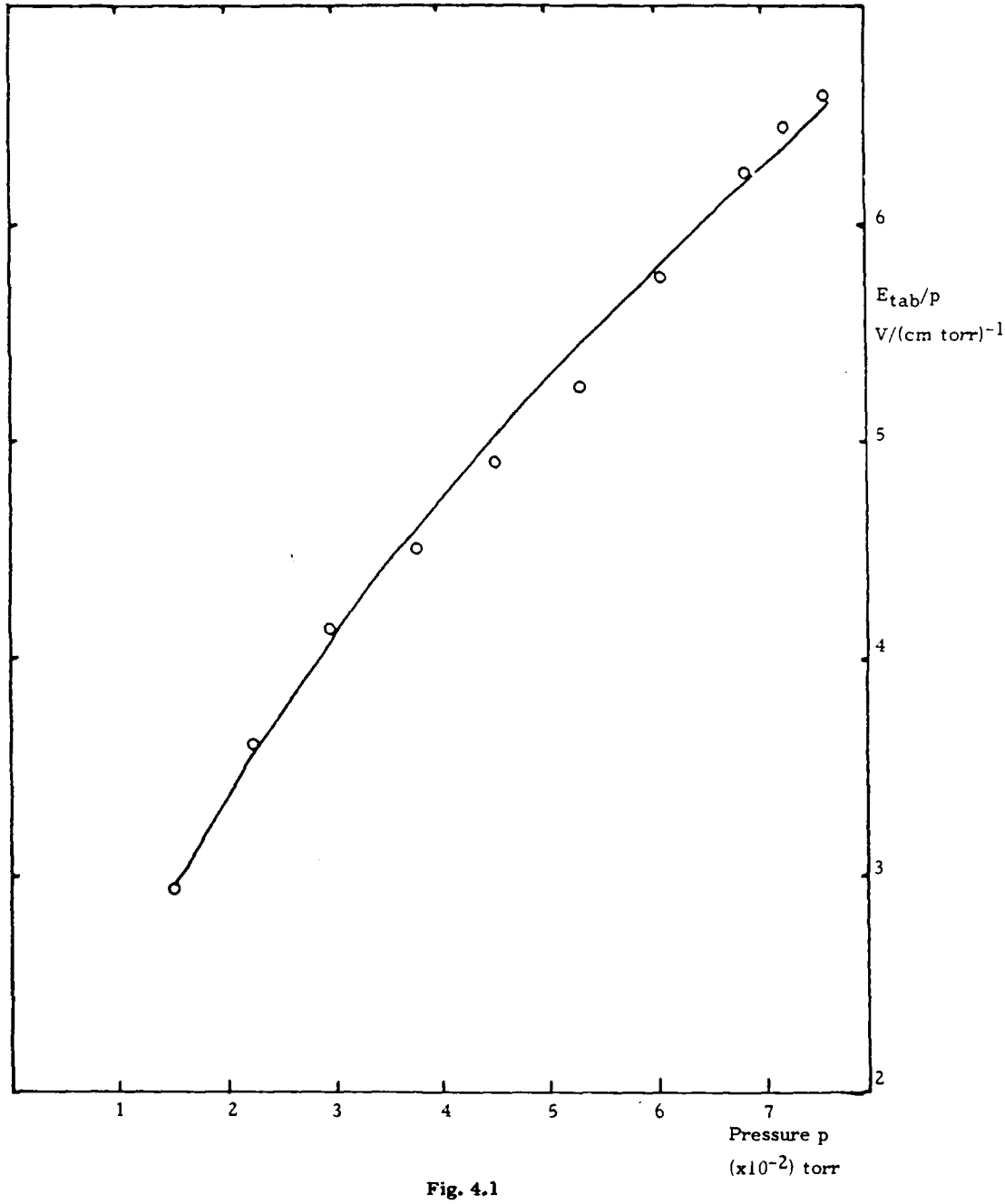

Fig. 4.1

E_{stab}/p v p

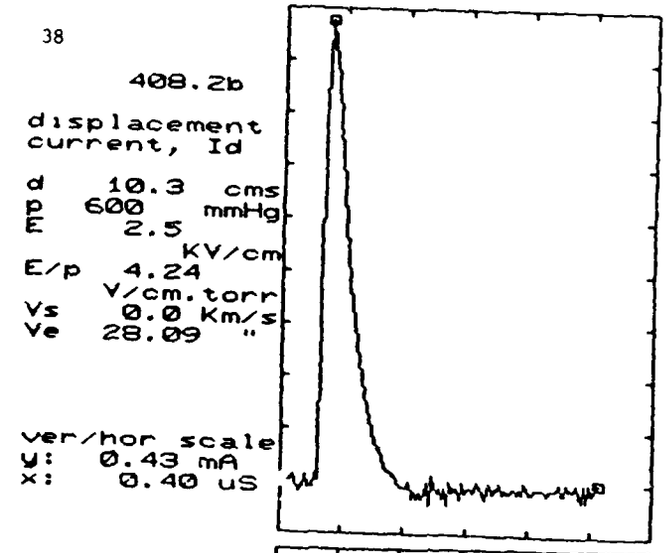

Fig. 4.2

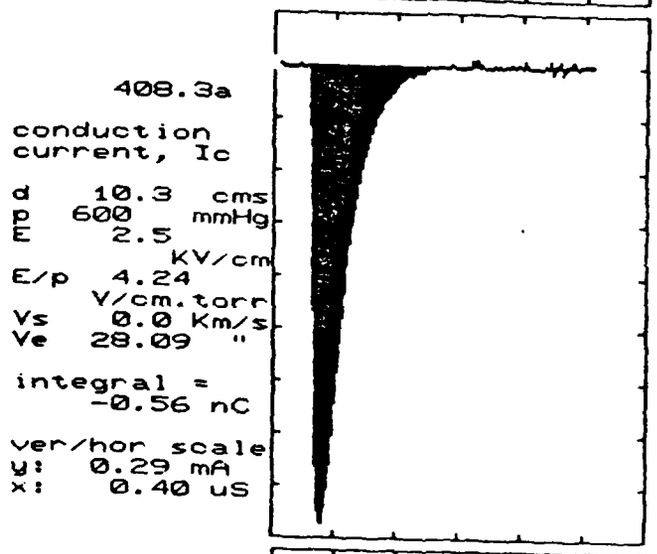

Fig. 4.3

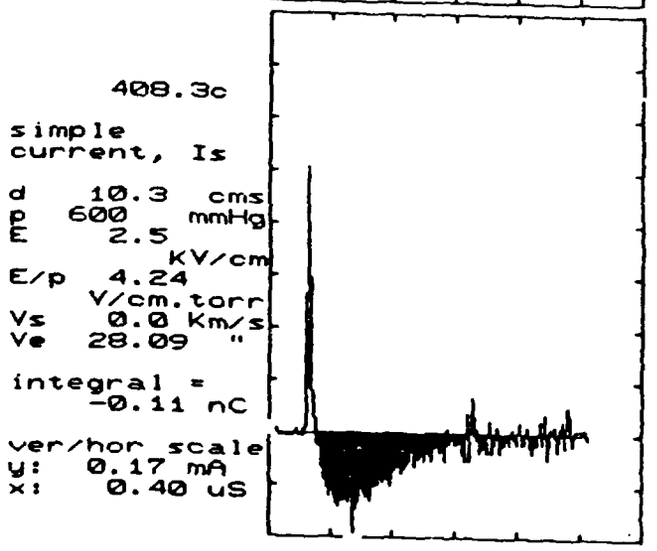

Fig. 4.4

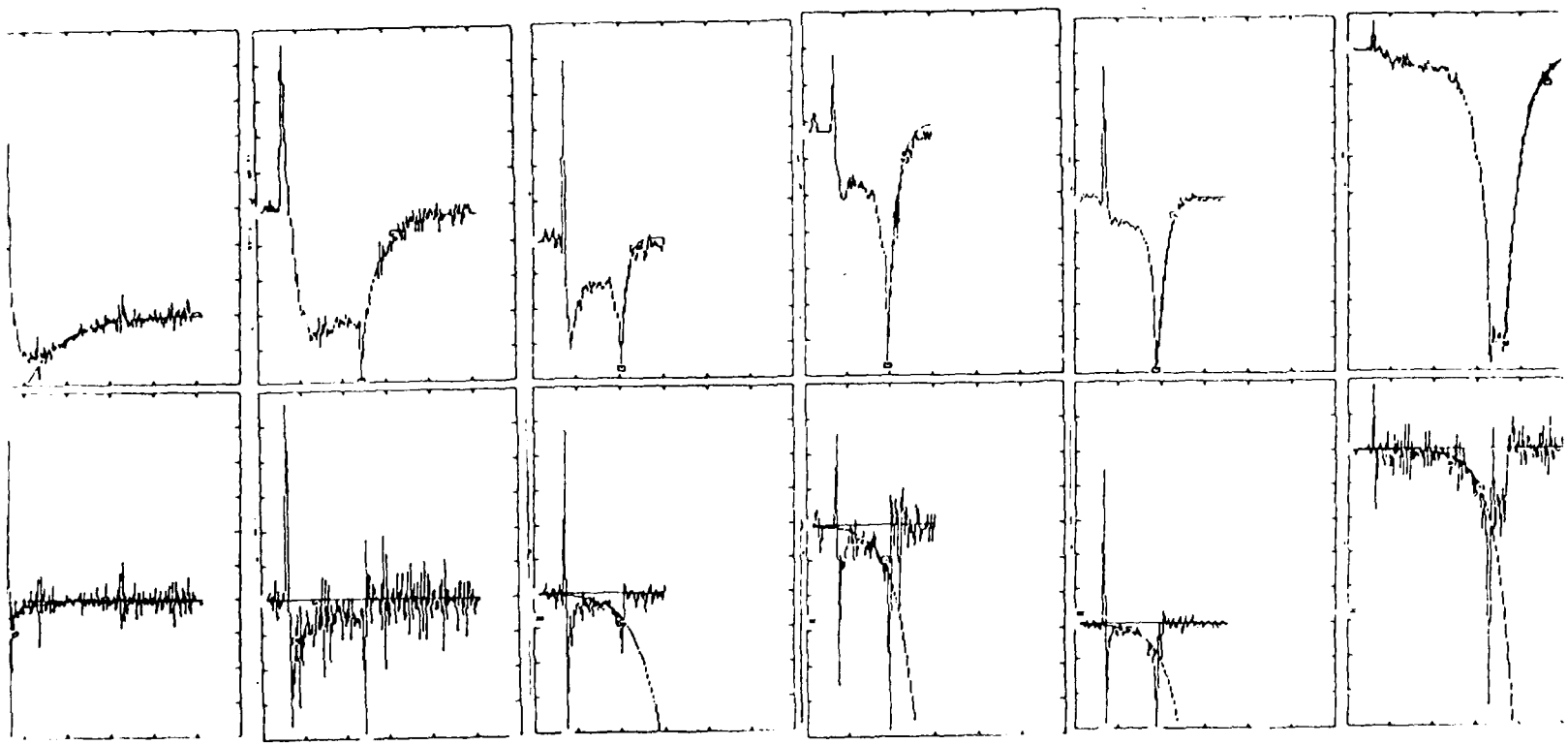

(i) #408.3,
.3cm, 600torr, 4.24V/cm.torr
top, Q_g: 1.16nC/box
below, δQ: 0.072A/box
t: 0.4μs/box

(ii) #409.3,
10.3cm, 600torr, 4.50V/cm.torr
top, Q_g: 0.99nC/box
[i_e: 0.28mA/box]
below, δQ: 0.033A/box
t: 0.4μs/box

(iii) #97.0,
16.4cm, 600torr, 4.67V/cm.torr
top, Q_g: 1.27nC/box
[i_e: 0.23mA/box]
below, δQ: 0.035A/box
t: 1.0μs/box

(iv) #99.1,
16.4cm, 600torr, 4.88V/cm.torr
top, Q_g: 2.29nc/box
[i_e: 0.43mA/box]
below, δQ: 0.035mA/box
t: 1.0μs/box

(v) #101.2
16.4cm, 600torr, 5.28V/cm.torr
top, Q_g: 4.92nC/box
[i_e: 0.96mA/box]
below, δQ: 0.10A/box
t: 1.0μs/box

(vi) #110.2
16.4cm, 600torr, 6.10V/cm.t
top, Q_g: 5.14nC/box
[i_e: 1.14mA/box]
below, δQ: 0.14A/box
t: 0.4μs/box.

Fig. 4.5 (i) - (vi)

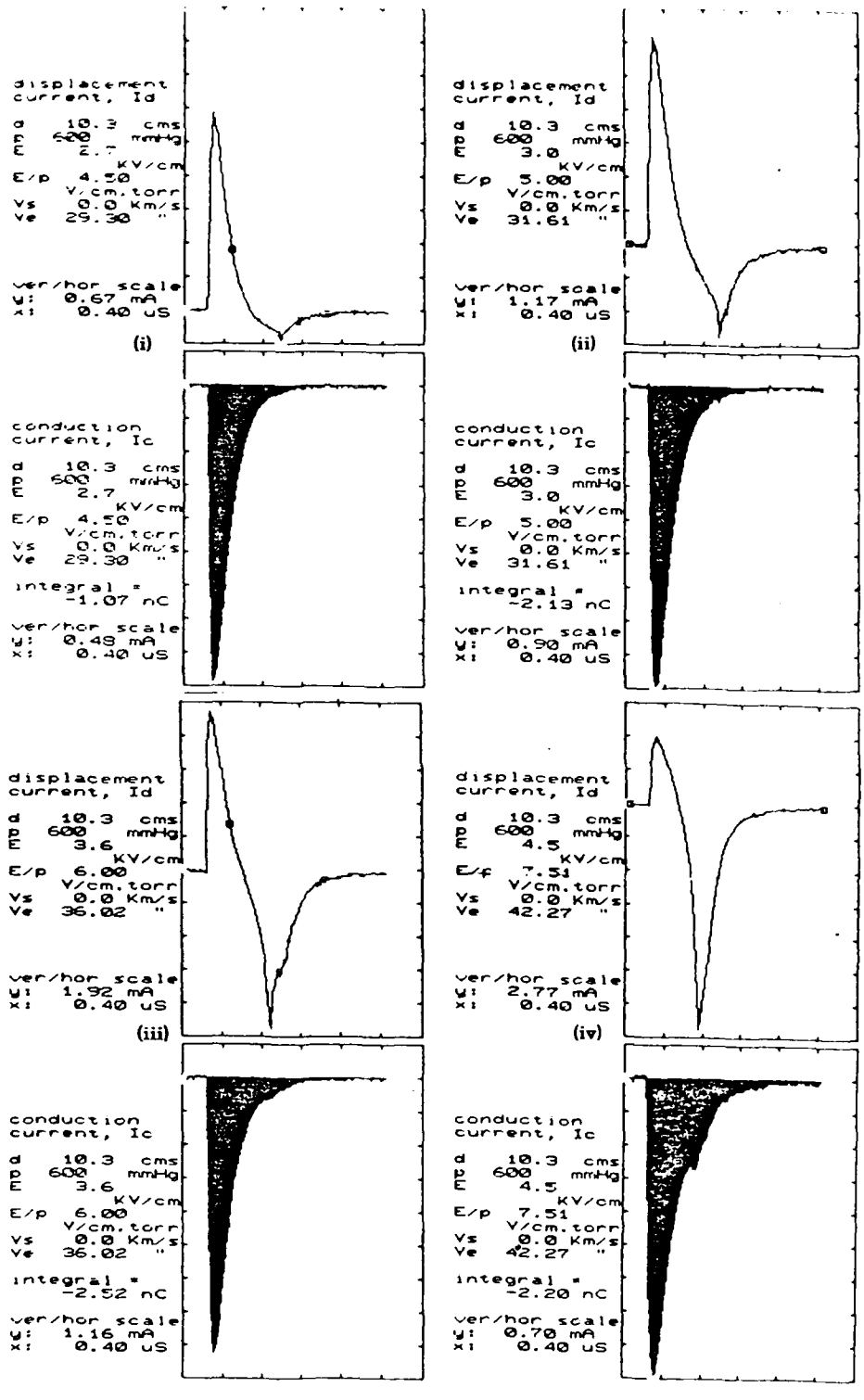
displacement current, Id
d 10.3 cms
p 600 mmHg
E 2.7 KV/cm
E/p 4.50 V/cm.torr
Vs 0.0 Km/s
Ve 29.30 "
ver/hor scale
y: 0.67 mA
x: 0.40 uS
(i)
conduction current, Ic
d 10.3 cms
p 600 mmHg
E 2.7 KV/cm
E/p 4.50 V/cm.torr
Vs 0.0 Km/s
Ve 29.30 "
integral = -1.07 nC
ver/hor scale
y: 0.48 mA
x: 0.40 uS
displacement current, Id
d 10.3 cms
p 600 mmHg
E 3.6 KV/cm
E/p 6.00 V/cm.torr
Vs 0.0 Km/s
Ve 36.02 "
ver/hor scale
y: 1.92 mA
x: 0.40 uS
(iii)
conduction current, Ic
d 10.3 cms
p 600 mmHg
E 3.6 KV/cm
E/p 6.00 V/cm.torr
Vs 0.0 Km/s
Ve 36.02 "
integral = -2.52 nC
ver/hor scale
y: 1.16 mA
x: 0.40 uS
displacement current, Id
d 10.3 cms
p 600 mmHg
E 3.0 KV/cm
E/p 5.00 V/cm.torr
Vs 0.0 Km/s
Ve 31.61 "
ver/hor scale
y: 1.17 mA
x: 0.40 uS
(ii)
conduction current, Ic
d 10.3 cms
p 600 mmHg
E 3.0 KV/cm
E/p 5.00 V/cm.torr
Vs 0.0 Km/s
Ve 31.61 "
integral = -2.13 nC
ver/hor scale
y: 0.90 mA
x: 0.40 uS
displacement current, Id
d 10.3 cms
p 600 mmHg
E 4.5 KV/cm
E/p 7.51 V/cm.torr
Vs 0.0 Km/s
Ve 42.27 "
ver/hor scale
y: 2.77 mA
x: 0.40 uS
(iv)
conduction current, Ic
d 10.3 cms
p 600 mmHg
E 4.5 KV/cm
E/p 7.51 V/cm.torr
Vs 0.0 Km/s
Ve 42.27 "
integral = -2.20 nC
ver/hor scale
y: 0.70 mA
x: 0.40 uS

Fig. 4.6 (i) - (iv)

4.24V/cm.torr. At a slightly higher reduced field, 4.5V/cm.torr, the streamers reach the cathode, and a small current pulse is seen demonstrating this (Fig.4.5ii). This record though (#409.3) shows that Q_g was decreasing throughout the streamer propagation. Thus although it reached the cathode, this streamer was not growing, and according to section 3.4 was below the stability field. The decay is more clearly exhibited in Fig.4.5iii, showing Q_g for event #97.0. This was for a longer propagation distance (16.4cm) than for the previous example (10.3cm), and so the reduction in Q_g has a longer time to manifest itself. The reduced field of 4.67V/cm.torr for event#97.0 is actually higher than the 4.5V/cm.torr used in the previous example (#409.3) though the decay seems stronger: this is of course partly caused by the relative timescales of the plots and partly by the longer total discharge time in the latter event. Fig.4.5iv shows an event (# 99.1) where the streamers grew slightly throughout the discharge; Q_g increases continually up to cathode arrival. This trend is confirmed by Figs.4.5v and 4.5vi where the growth in Q_g increases with the reduced field.

4.1.3 Streamers at the Stability Field or Greater

Streamers can cross a gap at fields below the stability field. There is a range of fields at which a proportion of the streamers cross the gap and a proportion do not. This can be clearly seen from the displacement current records, which either do or do not contain a sharp negative feature as the streamers reach the cathode (or not). This feature is considered here.

4.1.3a Injection from Cathode

Fig.4.6 shows a sequence of streamer displacement and conduction current records for an increasing reduced field. They all show a sharp negative feature in the displacement current, which is accompanied, if at all, by only a relatively insigificant feature in the conduction current. The peak in the displacement current is evidence that there has been a sharp increase in the free charge in the gap, for i_e must have in-

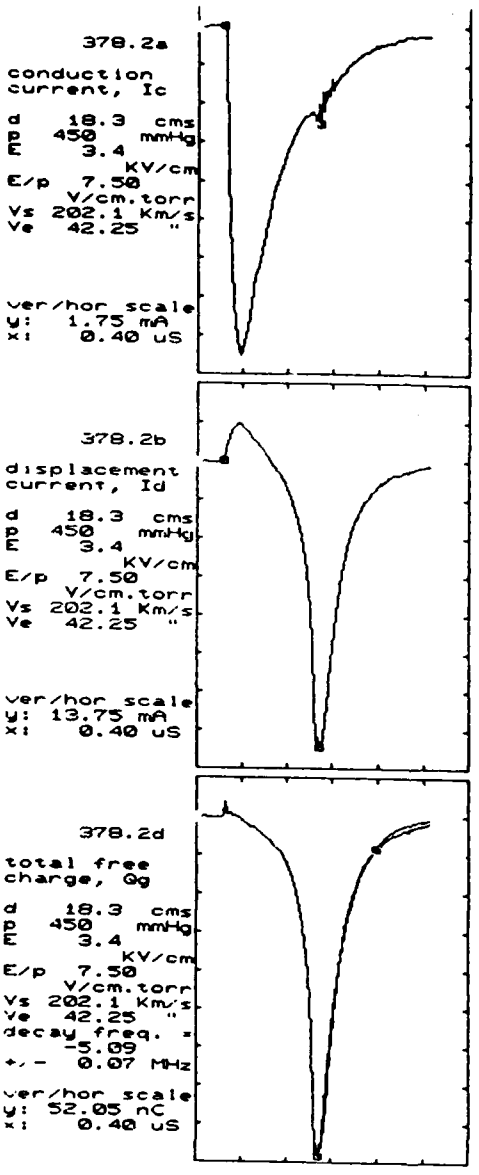
378.2a
conduction
current, Ic
d 18.3 cms
p 450 mmHg
E 3.4
KV/cm
E/p 7.50
V/cm.torr
Vs 202.1 Km/s
Ve 42.25 "
ver/hor scale
y: 1.75 mA
x: 0.40 uS
378.2b
displacement
current, Id
d 18.3 cms
p 450 mmHg
E 3.4
KV/cm
E/p 7.50
V/cm.torr
Vs 202.1 Km/s
Ve 42.25 "
ver/hor scale
y: 13.75 mA
x: 0.40 uS
378.2d
total free
charge, Qg
d 18.3 cms
p 450 mmHg
E 3.4
KV/cm
E/p 7.50
V/cm.torr
Vs 202.1 Km/s
Ve 42.25 "
decay freq. =
-5.09
+/- 0.07 MHz
ver/hor scale
y: 52.05 nC
x: 0.40 uS

Fig. 4.7

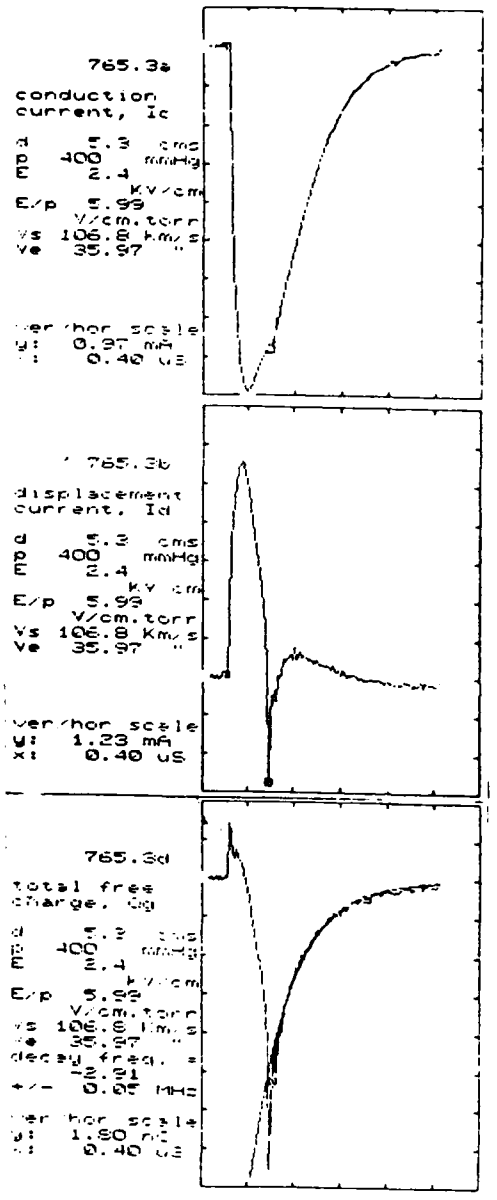
765.3a
conduction
current, Ic
765.3b
displacement
current, Id
765.3d
total free
charge, Qg

Fig. 4.8

creased. The lack of a correspondingly large signal simultaneously in i_c indicates that the charge generation responsible for this feature occurs well away from the point (section 3.4). It has been assumed, since visual observation confirms that the streamers cross the gap when this negative feature in i_d is present, that this generation of charge occurs at the cathode when the streamers arrive and the cathode region is established.

This rapid injection of charge is superimposed upon the now growing Q_g for the system as a whole. The two are partially separable by calculating δQ as described in section 3.5.1. Fig.4.5 shows the δQ records corresponding to the Q_g records already presented for various reduced fields. The impulsive nature of the charge injection can be seen more clearly when plotted as δQ demonstrating that this feature increases in size with E/p; this can be linked with the ultimate size of the streamer system. It would not seem unreasonable that the charge injection from the cathode should increase as the number and size of the streamers arriving there increases.

4.1.3b Conduction Current Perturbation

Simultaneously with the large spike in the displacement current record a small perturbation (Fig.4.7) is sometimes seen in the conduction current record. Quite what this represents is an open question, but it is certainly much smaller than it would be if the current pulse responsible for the displacement current feature were located at the needle-end and must have some other explanation.

One possibility is that the theoretical analysis presented in section 3 is not perfectly followed by the practical, real, electrode arrangement. Some induced current could be being picked up by the needle from charges located at the cathode; for example, if E_c^* were not zero everywhere far from the needle. However, even if there were any such contribution, it would at least be continuous with the position of the space-charge, and not vary rapidly far from the point. Therefore the perturbation would have the same shape as the displacement current record, which in fact tails off by far the more slowly of the two. This feature, furthermore, would always be present whenever the streamers

cross the gap, although in fact it is not always seen, ruling out this particular possibility.

The alternative is that an enhanced field, associated with a potential redistribution brought about by a return wave, causes the electrons in the channel base to speed up, resulting in a slightly increased conduction current. Though since the perturbation occurs simultaneously with the peak in i_d (or rather within the 16ns sample window), this implies a propagation velocity in excess of 11Mm/s, compared with a value of ~10Mm/s reported by Marode (1975a) for the speed of the wave during the compensation phase. This velocity is ~100 times that observed by Suzuki)1971) so it seems there is some considerable disagreement regarding the speed of ionizing waves. The wave observed by Marode occurred under the same circumstances as the perturbation discussed here, and so is perhaps the better value for comparison. Thus it seems reasonable to identify this perturbation with the arrival of a return wave - as concluded by Marode.

4.1.4 Attachment Frequency

Once an entire channel has been created, no further increase in electron charge Q_g is expected (unless of course some other electron detaching process occurs). Fitting an exponential curve to the later portion of the Q_g record gives very close agreement, showing that the charge residing on the channel is progressively attached. Attempts to fit exponentials to streamers which do not cross the gap must be treated with caution, for the channel may still be extending although electron density is declining (see e.g. the model in section 3.5.6). The result (e.g. Fig.4.5i shows the result of such a calculation) may indeed be exponential, but does it represent only attachment? The decay of Q_g can only be considered to be attachment after cathode impact, so (e.g.) in Fig.4.5ii the calculation of the attachment frequency based on a fit between the two cursor positions does satisfy the assumption that $\delta Q=0$. This topic will be discussed in the next section. The attachment algorithm is described in the appendix.

4.1.5 Low Pressure Specifically

The results at low pressure are very interesting. Clearly they are of some importance for the questions this work addresses, for a thundercloud may exist in a low pressure regime.

Fig.4.8 shows a low pressure streamer record. It is completely different fro those at high pressure, and one could be forgiven for thinking it to be some new kind of event and not a streamer at all.

η/p for two-body attachment and η/p^2 for three-body attachment depend only on E/p. As the pressure is reduced, the attachment coefficient is predicted to fall, and this is indeed observed to happen. This appears to be the principal effect on the discharge of reducing pressure and is expressed in a number of ways.

4.1.5a Induced Current

The conduction current is due to the electrons produced in the streamer active region drifting along the channel and arriving at the point. The magnitude of the conduction current will thus depend on the number of electrons "added" to the channel, A(x) (section 3.5.5), and upon the attachment coefficient. In this case, the reduced attachment allows more electrons to survive to the point, enhancing the conduction current. Now it is inevitably true that the electron current will also be enhanced by reduced attachment, but for a charge at the base of the channel, $E_c^* \gg E_e^*$ and the increase in i_c due to enhanced current in the channel base will be much greater than the corresponding increase in i_e. The displacement current, essentially a combination of i_c and i_e, will hence be more positive than at higher pressure. This generally explains the novel shape of the i_d records at low attachment rate (pressures).

This can be characterized by plotting the ratio of the positive peak in the displacement current to the negative peak in the displacement current against pressure (Fig.4.9). The correlation is complicated by the difference in streamer arrival times since the velocity is also a function of the pressure but the general trend is clear.

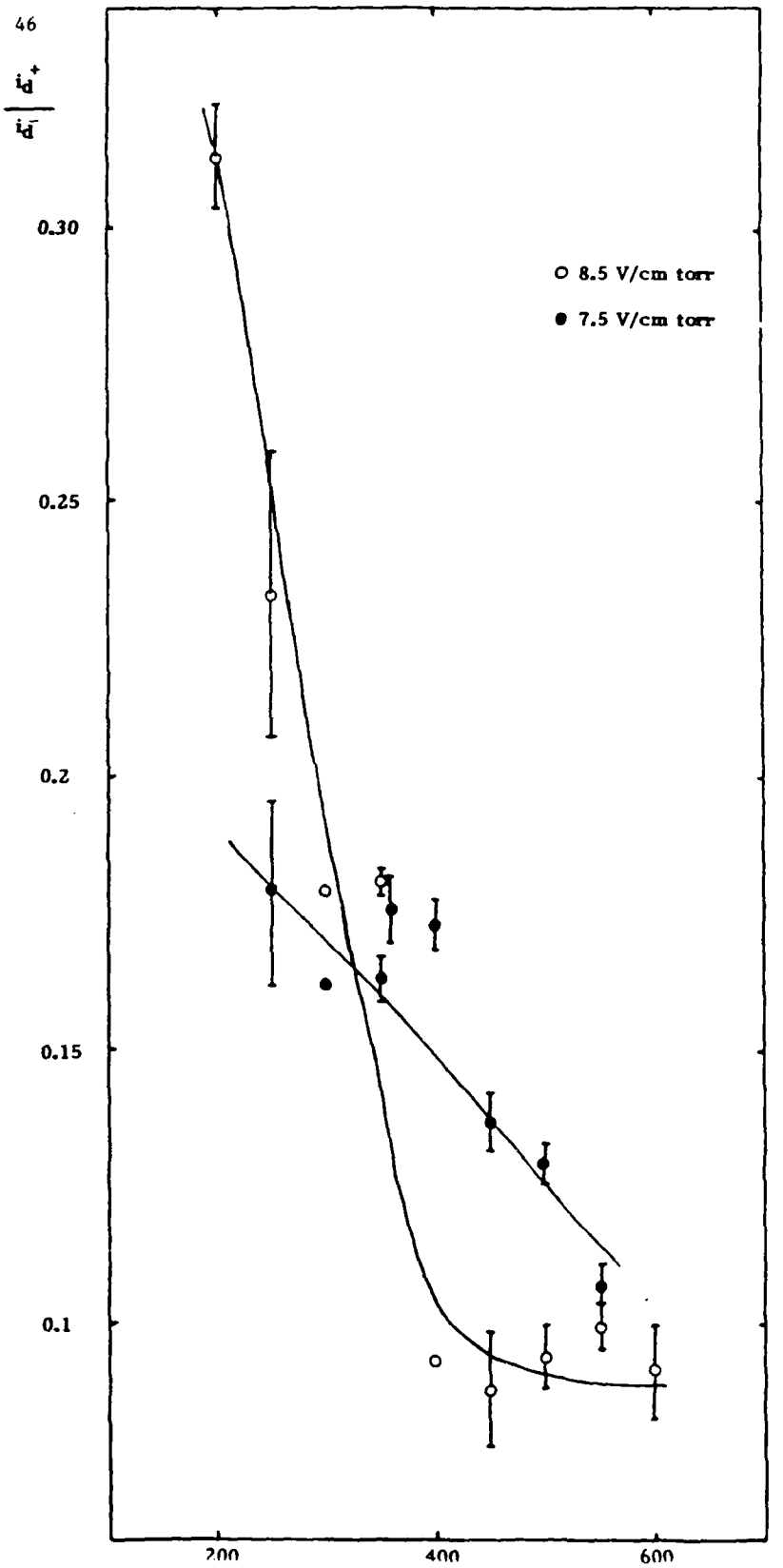
$\frac{i_d^+}{i_d^-}$
0.30
0.25
0.2
0.15
0.1
○ 8.5 V/cm torr
● 7.5 V/cm torr
200
400
600
Pressure (torr)

Fig. 4.13

4.1.5b Time-to-Peak

The balance of attachment and growth influences time-to-peak of the conduction current as well. In fact, Fig.4.10, at extremely low pressure and high E/p, the peak in the conduction current actually occurs after that in the displacement current! This can be explained as follows:- Increased E/p would be expected to cause an enhanced stream growth rate. At higher pressures this would be swamped by the high attachment, but reducing the pressure (attachment) allows more of this increase to survive as far as the needle. The point where attachment dominates over growth occurs later and later in the discharge, ultimately (as observed) producing a time-to-peak longer than the streamer transit time. This process is represented by Eq.3.15; the relationship between the time to peak and the growth rate is discussed later.

4.1.5c δ-like Event

There is evidence (Fig.4.10) for a process somewhat similar to the δ-process described by Marode (1975a): A short almost vertical rise in the conduction current is observed to occur simultaneously with the burst of current already associated with the arrival of the streamers at the cathode (section 3.4). This is occasionally present in measurements of this kind, where the peak in i_c occurs after the streamer transit. But the similarity is not perfect. In Marode's experiment, the δ - event produces the highest conduction current in the discharge, whereas in the present extreme case the conduction current continues rising. This bears on the debate surrounding the establishment of the glow in the channel.

Marode argues that the δ-event accompanies a potential redistribution along the channel, the compensation phase. This is supposed to be due to the difference between the cathode fall voltage and the streamer tip potential travelling down the channel as an ionising, or return wave, after which a resistive phase is entered, where there is current continuity along the entire channel. Marode's measurements indeed support this view. There cannot be current continuity in the present case, as (Fig.4.10) the current rises

following the δ-type event observed, as discussed below.

4.1.5d Current Continuity in the Compensation Phase?

Applying the analysis of section 3, the currents induced to the various electrodes can be found if there is current continuity along an axial channel, for letting the current everywhere be j, one can write for the displacement current:

$$i_d = \int j\, E_d^*\, dr = j\left[\frac{r}{d} + \frac{(d-n)}{d} f(r)\right]_{r=0}^{r=d-n} = j\left(\frac{d-n}{d} - \frac{d-n}{d}\right) = 0 \qquad \text{(Eq.4.1)}$$

And thus it seems, from a fundamental analysis of the induced currents, that for a single axial filament if the current is the same throughout the gap, then there would be identically zero displacement current. The above analysis of course needs extending to a branched streamer system. Considering a segment $r : r_1 < r < r_2$ containing m channels of current j_k where there is continuity of current ($\sum j_k = J$), if one notes that the first term in the integral in Eq. 4.1 does not depend on the radial position in the gap (r is an axial coordinate!), and that the f(r) term will only have an appreciable value near the point where there will be a single discharge channel (and hence the radial variation in f(r) can also be ignored), the displacement curent δi_d^* for the segment involved can be written:

$$\delta i_d^* = \sum_{k=1}^{m} j_k E_d^*\, dr = \sum_{i}^{m_k} j_k \left[\frac{r}{d} + \left(\frac{d-n}{d}\right) f(r)\right]_{r_1}^{r_2} \qquad \text{(Eq.4.2)}$$

With $r_1 \neq 0$, this evaluates to $\sum \frac{r_2 - r_1}{d} j_k = \left(\frac{r_2 - r_1}{d}\right) J$ and $\left(\frac{r_2}{d} - \frac{d-n}{d}\right) J$ for $r_1 = 0$. So it can be seen that for the whole discharge, the increments δi_d^* add up to (d-n)J/d, which nicely cancels the -(d-n)J/d term from the needle-end ($r_1 = 0$). Thus it follows that if there is current continuity, there will be no displacement current whatsoever.

In all the events recorded, there is always appreciable displacement current well after the streamers reach the cathode, and any return wave has long since decayed away. Therefore it can be inferred that current continuity is NOT established along the channel, conflicting with the observations by Marode in small discharges.

So this δ-like event does not establish current continuity along the channel as in

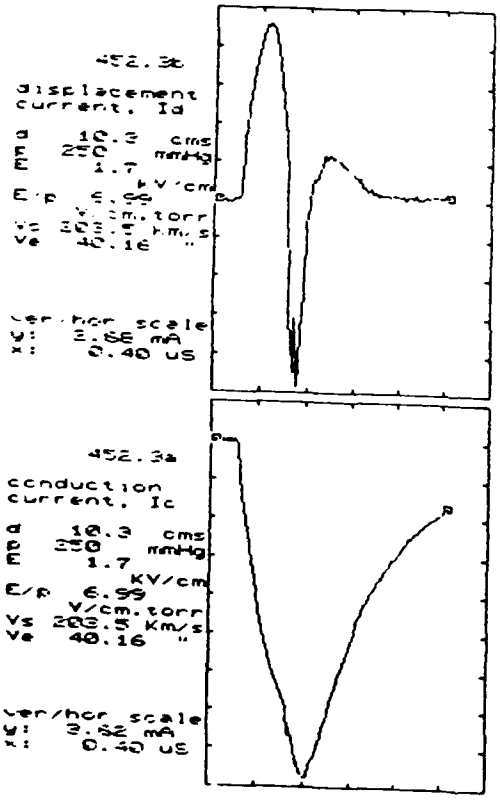

Fig. 4.10

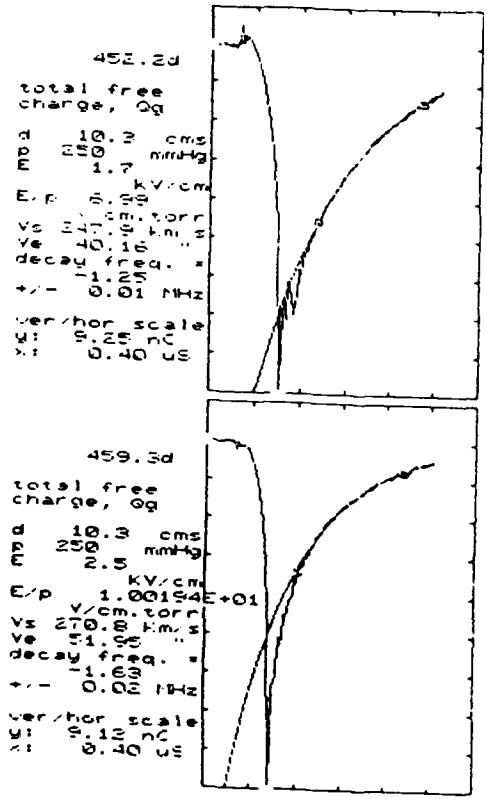

Fig. 4.11(top) 4.12(bottom)

Marode's work, but it does coincide with the cathode impact. A return wave has already been associated with the perturbation in the conduction current (section 4.1.3b). It seems reasonable to argue that this δ-like event is also a return wave, but that the relatively steep rise at these low pressures and high reduced fields is probably due to the greater conductivity of the channel in this case.

4.1.5e Attachment Rate

There is a tendency at low pressure and high E/p to exhibit a slight drop in attachment frequency from the initial value, evident in Fig.4.9, which is exaggerated at higher reduced field and lower pressures (Fig 4.11). It is suggested that the appropriate value of the attachment frequency is the later one, (a) because it is constant for much more of the record than in the very first portion (except in very extreme conditions) and (b) because the charge generation is more likely to be zero in the later portion of the curve.

A possible explanation for the decay in attachment frequency in the early stages of the discharge is that it has been found from the reduction of Q_g. In the early stages, particularly at low pressure where the conduction current is appreciable for longer on account of the reduced attachment rate, there will be an additional reduction in Q_g due to the physical removal of charge from the channel. So Q_g will drop a little more rapidly at the start of the decay of the channel, over and above that expected from the attachment observed later on. An extreme example of this process is shown in Fig.4.12.

Throughout this study, the attachment rate has been found by using a simple least-squares-fit to the Q_g data. In all but the most extreme conditions this is entirely reasonable, for the maximum charge extracted from the base of the channel beween samples might be ~320pC with a 16ns sample time and 20mA peak conduction current. The corresponding value of Q_g can be as high as 800nC, though something more like 50nC is more typical, and might decay at typically 3MHz in 16ns→2.3nC. So except at particularly low attachment rates, where the conduction current persists for a very long time and Q_g decays by less in a sample interval due to this attachment, no difficulty is ex-

pected to arise from the loss of charge from the channel base and the least-squares-fit method is satisfactory.

Many different streamer current profiles are seen, depending on the field, pressure and propagation distance. But it can be seen from the foregoing that the general features of all of them are similar. The variation in the shape of the individual curves is largely due to the different attachment rates and transit times.

4.1.6 Growth Frequency

The first thing one notices about the Q records is the amount of noise. The reason for this is that in calculating Q comparison is made between adjacent samples of Q_g, itself produced from adding "simultaneous" samples of i_c and i_d. The scatter in δQ therefore represents sampling error.

Fig.4.5 shows a sequence of Q_g and δQ records as the streamers first of all just cross the gap and then grow successively more and more strongly. The growth of a large and extremely narrow spike in δQ is very satisfying evidence that the charge injection from the cathode has been very successfully separated from the background of the free charge remaining on the channel.

The general behaviour of Q_g from the simple model outlined in section 3.5.6 is clearly shown in this sequence, and shows up in δQ also. The sub-stability field streamers die all the way to the cathode and this shows up as a reducing δQ. Likewise δQ rises for growing systems. These curves are found by using the attachment frequency calculated in the decaying channel. In this case the loss of charge from the base of the channel has been explicitly taken into account as is plain if the defining equation for δQ is recalled:

$$Q_2 = \left(Q_1 - \int_{t_1}^{t_2} i_c\,dt\right) e^{\nu_a(t_2 - t_1)} + \delta Q \qquad (3.14)$$

Thus the difficulty raised above with the attachment rate at low pressure has been overcome. In this case the correction matters, for in the early portion of the discharge

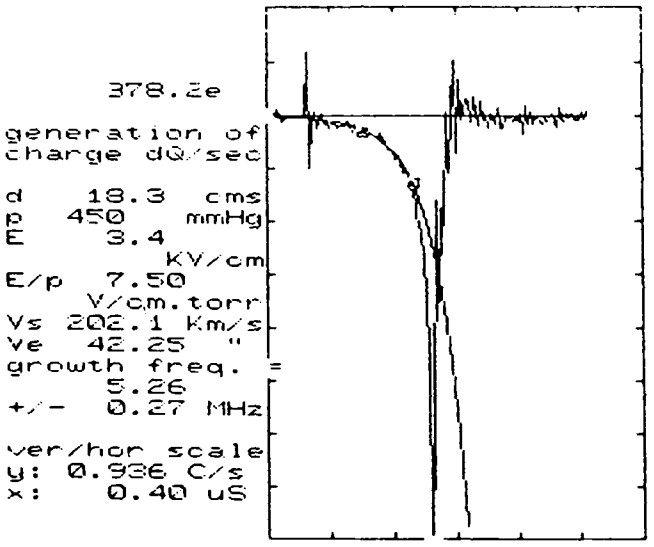
378.2e
generation of
charge dQ/sec
d 18.3 cms
p 450 mmHg
E 3.4
KV/cm
E/p 7.50
V/cm.torr
Vs 202.1 Km/s
Ve 42.25 "
growth freq. =
5.26
+/- 0.27 MHz
ver/hor scale
y: 0.936 C/s
x: 0.40 uS

Fig. 4.13

there is more conduction current than later on when the attachment is found.

The synchronizational error responsible for a single narrow negative spike at the outset of the Q_g record seems to the δQ algorithm to be a sudden injection of charge, followed by a sudden removal of charge. The result is that there is a large negative and then positive spike in δQ. A positive spike in Q_g will produce a positive and then a negative spike in δQ. These correspond to the single spike in Q_g which was an artefact, and (again) are ignored.

Finally, one notes the slight tendency for δQ to edge above the axis right after the streamer transit (Fig.4.13). This is due to the attachment frequency falling slightly from its value immediately after impact with the cathode. As discussed above, this drop is due to residual conduction current making the attachment seem greater early on. The value of the attachment frequency used in calculating δQ is lower than the actual value just after cathode impact. There will be more charge removed from the channel than predicted using the lower attachment coefficient. Since δQ is thought to be zero in this region, using Eq. 3.14 to find δQ will result in a positive value.

The amount of information represented by the δQ curves, information furthermore directly related to the growth of the streamer, and corrected for the removal of charge from the base of the channel; such as the initial decay, take-off of growth or decay depending on the external field, and charge injection from the cathode, shows that of the available quantities, this best represents the growth of the streamer.

4.2 Pre-breakdown Corona Modes

As the breakdown field is approached, new corona modes are observed normally involving a change in the observed current. These phenomena have the appearance of choked-off breakdown processes.

There are a number of different prebreakdown modes; the corona can exist in distinct states, which can be stable over periods of minutes, or can switch intermittently from one state to the other every few seconds or so. In an attempt to elucidate the dif-

ferent conditions under which the various modes were exhibited, a case study was made of the 500torr behaviour and this is presented in section 5.

The general form of the various modes is discussed here. It should be remembered that the discharge current growth is limited by the series resistor.

4.2.1 Terminology

Since some of the mode parameters are peculiar to the present electrode geometry some definitions may prove useful. The classic streamer discussed above is called primary streamer to make plain that this is the usual mode observed (at low reduced field). Secondary streamers as identified by Marode (1975), Hudson & Loeb (1961), etc. are not studied in this section - they properly belong to a discussion of classic streamer development. All the prebreakdown modes involve an increase in the gap current.

Mode i: This has been termed "second corona" and has a large conduction current event growing out of the primary streamer (before the channel has quite decayed).

Mode ii: Called a "delayed second corona" as it has some features in common with Mode (i). As might be expected, there is a distinct period between the primary and the delayed second corona where no current growth occurs.

Mode iii: Called "multiple second corona" or the "multiple" or "high-frequency" mode since this represents the main characteristic of this mode; it is basically several events of type (ii) in rapid succession. Fig. 4.14 summarizes the differences between the various types.

4.2.2 Mode (i): Second Corona

As the field increases, the first new phenomenon observed following the return wave involves a discontinuous jump in the conduction current (Fig. 4.15). This always occurs something like 50 to 100ns after the streamer transit, and cannot therefore be simply a large return wave (see for example Fig.4.15) where a perturbation in the con-

Fig. 4.14 (i) - (iv)

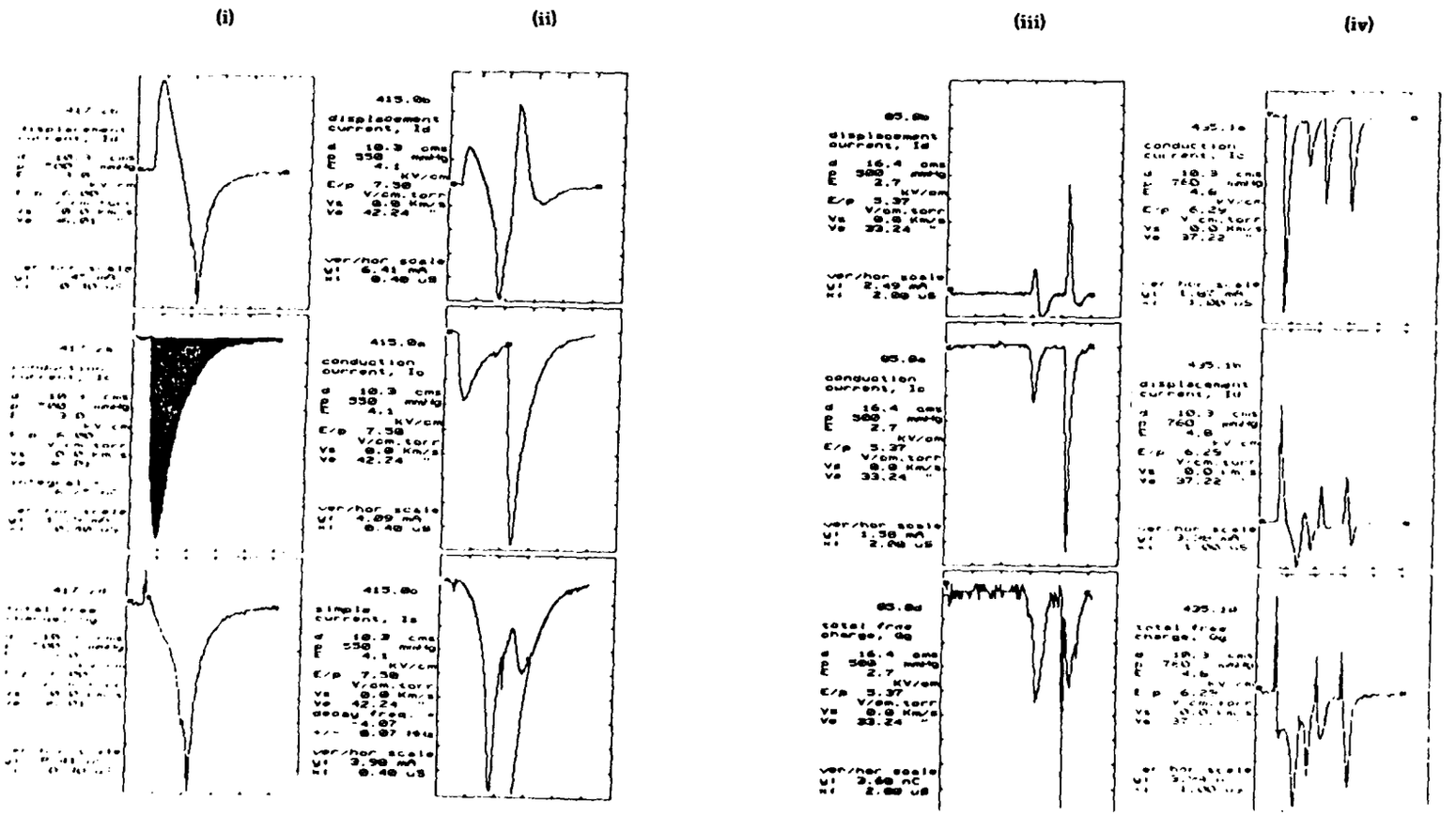

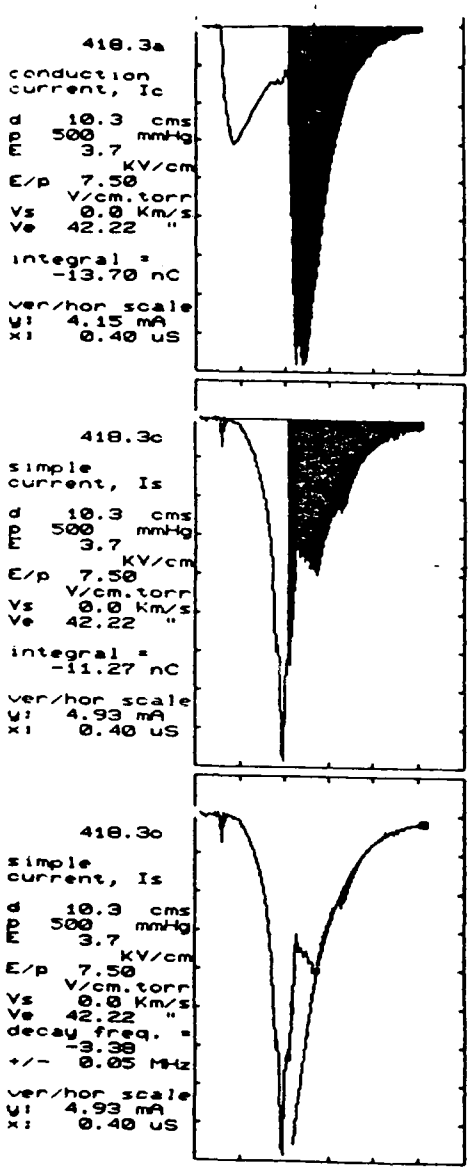

Fig.4.15

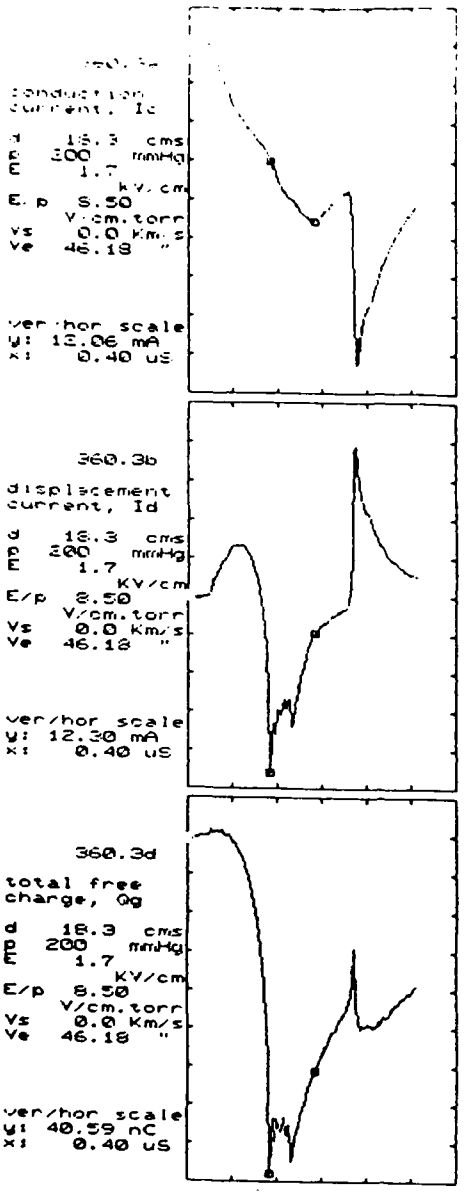

Fig.4.16

duction current, coinciding with the return wave proper, can clearly be seen 80ns before the regeneration of the channel).

4.2.2.a Regeneration of the Channel

The second corona current is large, compared with that of the primary streamer. The first feature of interest in the second corona is that the current undergoes a large and fast regeneration.

Meanwhile the electron current, i_e which was dropping away very rapidly before this regeneration of the channel shows a tiny increase by comparison. Since both i_c and i_d are changing very rapidly, and in opposite directions, even this feature is probably a synchronization artefact.

The displacement current shows a positive excursion simultaneous with the regeneration of the conduction current; as discussed in section 3, this shows unambiguously that this event is confined to the region of the needle-end. Furthermore if such a large i_c record can be obtained, with little or no corresponding signal in i_e, then the spatial extent of f(r) must be quite small indeed, confirming the position taken in section 3.

4.2.2.b Appearance of the second corona

Visual observations of the discharge, when the current records exhibit this feature, show it to contain a single bright channel, in the lower portion of the gap, extending from the point. This regeneration of the channel base clearly represents the early phase of a regeneration of the whole of a single filament in the lower channel (see below under "growth of second corona", section 4.2.2.e)

Qualitative observations suggest that, like return waves, this phenomenon also is more readily expressed at lower pressures. At higher pressures the channel can nevertheless be regenerated, but with lower probability.

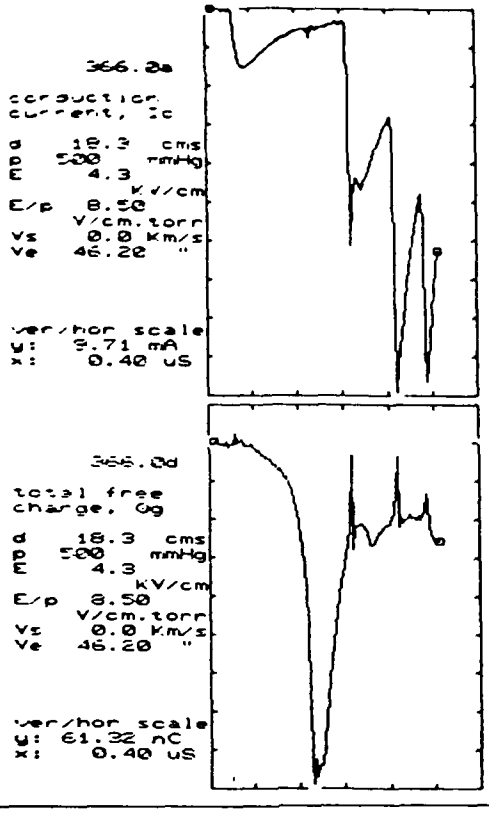

Fig. 4.17

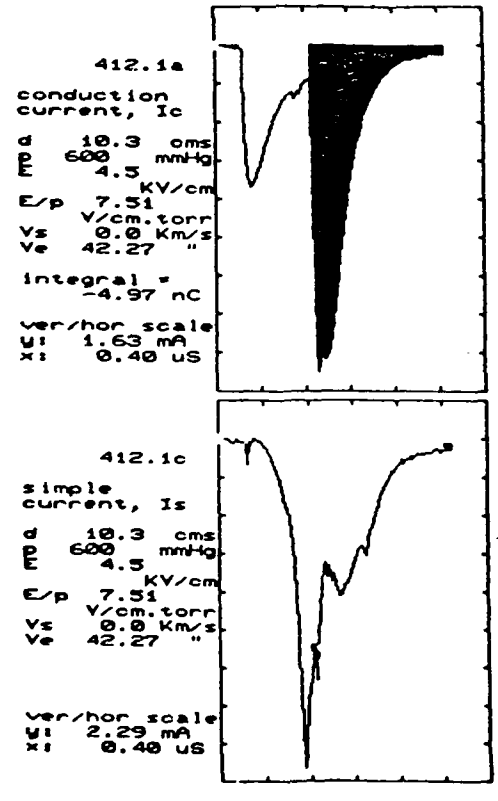

Fig. 4.18

4.2.2.c Attachment rate/heating from the discharge?

It can readily be seen from the G_g curves of such an event that the attachment frequency is lower than before; the slope of the curve is considerably shallower after the second event. Owing to the possibility that the channel has been heated, and therefore that the electron drift velocity (because of the change in pressure) is undefined, the new attachment coefficient cannot be determined from the attachment frequency. Using the old attachment frequency to calculate δQ leads to a negative displacement of the second portion of the curve. The old attachment frequency implies a net negative in-jection of charge - a consequence of the lower real attachment frequency. This feature is shown unambiguously by the low pressure event in Fig. 4.16.

4.2.2.d Detachment or ionization?

A question to be addressed is whether or not this very rapid growth in electron density is associated with a new ionizing regime, or with some process whereby electrons detach from pre-existing negative ions.

Ionization and detachment both lead to an increase in the electron charge. The distinction between the two is rather more subtle, the electrons have been removed from different species and thus the energetics and dependence on gas composition or ionic state become important: detachment from negative ions may proceed by a larger number of routes than the ionization of neutrals, and requires less energy (Elliason & Kogelshatz, 1986).

Neverthless, the peak in the conduction current associated with the regeneration of the channel base is larger than the initial conduction current peak. This difference in size can at times be exceptionally large (see e.g. Fig.4.18) and it seems unlikely that detachment from the negative ions created during the transit of the primary streamer can account for all the electrons freed in the second corona. Hence some fresh ionization must occur to provide the balance of the electrons.

Finally the comparison with secondary streamers must be ruled out categorically;

secondary streamers are entirely a decaying current regime. Spectroscopic evidence (Hartmann, 1974) shows the electron energy is too low for there to be any ionization in the secondary streamer. This feature is associated with a decaying channel from the primary streamer and would always follow primary streamers which crossed the gap. The second corona is not always produced and is an increasing current regime, and cannot, again, be a secondary streamer.

4.2.2.e Growth of Regenerated Channel

After the initial rapid regeneration, confined to the base of the channel i_e then begins to increase, though more slowly, producing a broad peak in the i_e record (Fig.4.15). There is often a time delay of some ns before this occurs and further attachment in the body of the gap reduces i_e in the interim. The attachment frequency during this period does decrease slightly as can be seen in Fig.4.15 by comparing the decay curve before and after the small perturbation (which in this case is probably an artefact as discussed in section 4.2.2.a)

This broad peak in i_e, unrepresented in i_c, shows (section 3.4) that the ionization/detachment processes are occurring beyond the point region and by implication suggests that a new ionizing/detaching regime is developing probably along the single bright channel observed visually. Other evidence for a growing channel is the width of the second corona conduction current pulse. If the current were all confined to the base of the channel - as it clearly is at the outset of this event since thre is no correspondingly large electron current signal - then i_c would contain only an impulsive signal - the electrons would drift to the anode very quickly. In order to provide the electrons to sustain the conduction current (observed in second corona records to last quite as long as primary streamer conduction currents), there must be a channel growing from the point. All this points to the spatial growth of the second corona event.

The delay between the inception of the second corona and the rise of the broad peak in the electron current, already touched upon above, is a very interesting

phenomenon. After the perturbation associated with the synchronizational error when the second corona occurs, the attachment frequency can clearly be seen to reduce slightly. Once the second corona has begun to propagate into the gap, its growth picks up very strongly, indicating that some property of the gap is enhancing its growth. The view advanced here is that the remaining electrons in the "old" channel are responsible. The density of free electrons near the point will be low, as they are most effectively swept out of the gap here. The electrons at the point will have been generated further out in the gap as the time lag between first and second corona increases, and consequently will be more heavily attached. The density immediately near the point will thus increase as the second corona propagates out into the gap. This will explain the enhanced growth as the second corona travels away from the point; the conductivity increases as the point is left behind. The larger free electron density will mean that a streamer tip, for example, will not need to produce secondary electrons, and will propagate very much more vigorously than in a lower electron density.

No information on the speed of this phenomenon is available, as the distance it has *propagated* is not known, and streak or photomultiplier techniques were not used. But visual observations suggest that the length of the new channel could be about half the gap length, occasionally more, and the current records show this occurs in times of about $\frac{1}{2}$ to $\frac{3}{4}$ of a streamer transit time suggesting a speed about the same or slightly less than a classic primary streamer.

4.2.2.f Explanation?

This raises the intriguing possibility that this is in fact a new streamer, forming after a delay much shorter than the $\sim$100μs expected from observations of primary streamers, and guided into a single channel by some mechanism. Certainly the regeneration responsible for it produces a conduction current pulse larger than seen from primary streamers and once these electrons have been neutralized at the needle-end, enough positive charge will be left to produce a streamer tip. Though how concentrated

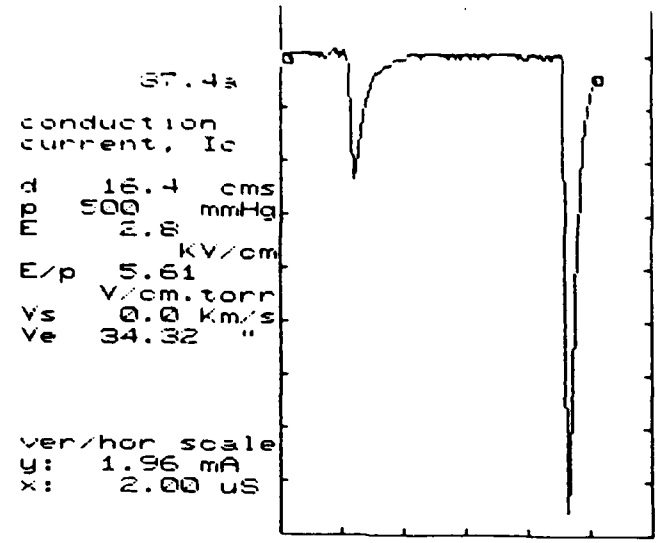

Fig. 4.19

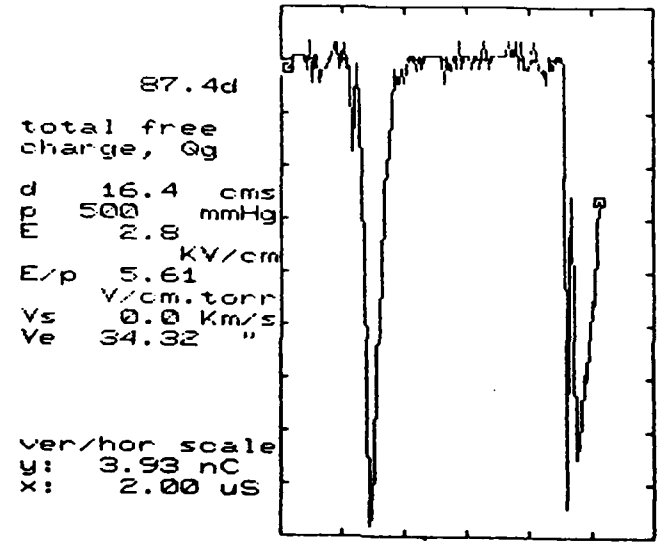

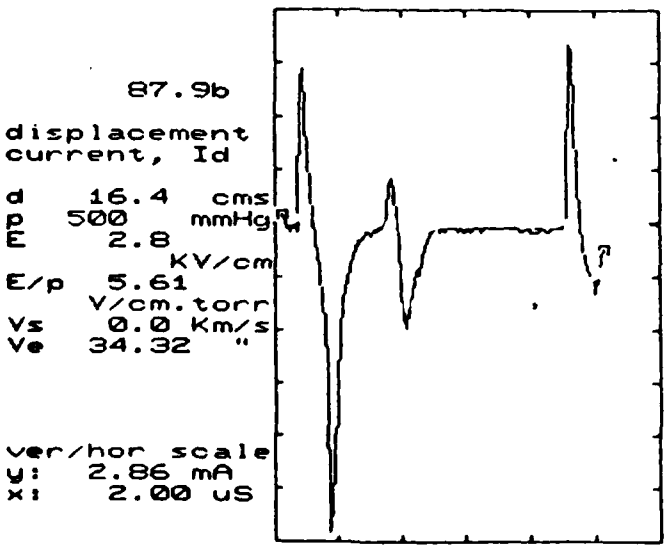

Fig. 4.20

this is, is again left open.

The growth of the regenerated channel, and its propagation into the gap is so similar to the features of primary streamers that this new corona mode has been termed a "second corona", to distinguish it from a secondary streamer and to tentatively associate it with "subsequent corona" in long point-plane gap impulse work. Certainly the sequence of events; (i) a burst of conduction current identified as being near the tip, (ii) free electrons generated in the body of the gap and (iii) a continuing supply of electrons to the point from the discharge; is strongly suggestive of at least an ionizing or detaching event which propagates out into the gap.

As the field and gap length increases (section 5.3.3), successively larger regenerations, or further coronae are seen (Fig. 4.17). This violent growth of conductivity in the gap is strongly indicative of a stifled breakdown. This topic is considered in more detail in section 6.

4.2.2.g Second Corona Reach Cathode?

An intersting feature remains to be discussed. Occasionally a small increase in i_e (Q_g) is seen (Fig.4.18) in the later stages of the propagation of the second corona. This is not present in i_c and so by analogy with primary streamers, can the second coronae possibly have reached the cathode? This feature would then represent electron injection from the cathode.

This is discounted for two reasons, firstly the feature is too small: charge injection from the cathode due to the primary streamer arrival is much greater, and secondly there is no sign of a return wave signature in the conduction current record, as has already been shown to be present when the primary streamer reaches the cathode.

As discussed in section 3 this last feature, having no corresponding increase in the conduction current record cannot be occurring anywhere near the needle-tip, nor as just indicated is it identified with the arrival of the second corona streamers at the cathode and so it is thought that it must be a further ionizing event started entirely in mid-gap.

4.2.3 Mode (ii): Delayed Second Corona

With a low trigger level only the first streamer mode was seen, but by turning up the oscilloscope trigger, on a short time-base, higher current pulses could be observed, suggesting a bi-modal distribution of corona. These pulses had conduction currents which rose on timescales comparable with primary streamers, but were of larger amplitude. The displacement current as a result was more positive-going and less negative-going than its primary streamer counterpart.

Observations with longer timebase showed that rather than there being a bimodal streamer distribution, the second corona (Fig.4.19) was occurring up to 5μs after the primary streamer had completely decayed. In cases where the second corona seemed to be in isolation, it is inferred that the first corona had escaped the oscilloscope "window". The delay variability is discussed below (section 5.3). The visual appearance of the corona in this mode was exactly the same as for classic streamers, and contained none of the bright channels observed in the more rapidly generated second coronae discussed above. The likelihood of observing this delayed second corona was very low compared with that of observing the accompanying classical corona in isolation.

4.2.4 Mode (iii): Multiple second corona

The corona could switch into a third, high frequency mode, where not just a few, but very corona pulse displayed multiple second corona-like pulses. This mode was intermittent and could cut in and out irregularly. A typical current record is shown in Fig. 4.20. The intermittency suggests it is dependent on some gross parameter of the gap, which can stabilize the mode - the discharge had to be running for a while before this mode appeared. This irregularity made observation difficult though.

The visual appearance of the corona in this, third mode was different from that observed when an isolated second corona pulse was present. It appeared exactly the same as normal corona, except now the whole discharge ws much brighter than usual. Isolated trains of subsequent corona were observed right down to onset, though with low probability (see case study, section 5.3). The high frequency mode is clearly just this

phenomena occurring repetitively.

The difference in the appearance of the corona could possibly be attributed to the second corona in this case, being started in an inactive channel. When the event causing the inception of the second corona occurs in a channel with significant electron density, perhaps there is a tendency to guide the corona along the highest current channel, whereas if the channel has decayed so far that there is insignificant electron density, then perhaps the guiding effect is less pronounced.

4.3 Breakdown

Experiments to determine the breakdown field were carried out, with the instruments disconnected, and the charging resistor out of the circuit. Determining the breakdown field is not an easy measurement with a d.c. corona, for the high repetition rate means that very low breakdown probabilities can be detected. Defining the lower limit is virtually impossible. One breakdown in a five minute period was observed at 3.62kV/cm, (6V/cm.torr at 600 torr) well below the usual level of about 7kV/cm (or ~9.2V/cm.torr at S.T.P).

The probability of second corona was also investigated and the results (Fig.4.21) plotted along with the breakdown field. The suggestion is that the formation of second corona would ultimately lead to breakdown, but is prevented from so doing by the series resistor. This is certainly the picture at high pressure.

At lower pressures, a further, interesting observation is that the gap will not break down even when second corona is observed, and the resistor is out of the circuit.

The explanation may lie in the availability of energy in the gap. To obtain a particular reduced field does not require as high a voltage on the cathode at lower pressures as it does at higher pressures. So the stored energy in the gap is less at lower pressure. Since a breakdown event is faster than the 10ns or so required for the recharging of the gap capacitance then the principal source of energy for the breakdown is the stored energy in this capacitance. At very low pressures not enough energy is present at re-

duced field otherwise capable of producing breakdown in the absence of an energy limit.

4.3.1 Energy Limit

In the event shown in Fig. 4.16 (#418.3), the total charge drawn by the external circuit, $\int i_e dt + n/d \int i_c dt$, is ~23.6nC, compared with ~110nC stored on the gap capacitance at this field. This amounts to something like a 20% drop in applied field and is significant enough to explain the failure of the gap to breakdown. Note though that this is not Q_g, which may be a good deal higher than this figure before the applied field begins to drop, depending on $\int i_c dt$.

4.4 Summary

The first section was devoted to classic corona, corresponding in general with the description to be found in the literature of "positive corona streamers". The general features of current observations of these are discussed, in the light of the induced current analysis developed in section 3. The wide variability of the appearance of the streamer currents as the field, pressure and propagation length are varied, is shown to be mainly due to the same phenomena, differences being due to changes in the attachment frequency and transit time.

Thereafter, it was found that as the reduced field increases, different corona modes are seen. Indicative of further current growth occurring after the primary streamer channel has begun to decay these phenomena are associated with pre-breakdown. Close analysis of the induced currents (again following section 3), shows the mode occurring at the highest field to be due to a streamer-like event, born at the needle and subsequently propagating out into the gap. Visually this mode (mode (i)) is associated with the presence in the discharge of discrete bright channels, which are not present at lower reduced fields. This mode appears to depend upon the electron density in the channel. The major difference beween it and the lower reduced field modes (ii and iii)

with longer inception times, is that in the latter case the channel has almost decayed before inception.

Breakdown measurements with the high voltage charging resistor either in or out of the circuit (Bicknell & Shelton, 1985) show that the breakdown is being choked-off by the shortage of energy in the observations just described; the gap would usually breakdown if the resistor were not present.

The next section considers in detail the way in which parameters characterizing the classic discharge are affected by the ambient conditions and particularly by the propagation length. A case study has been made of the many different corona modes in the pre-breakdown regime, to try and elucidate their dependence on these same parameters.

Section 5: Experimental Results

Introduction

In this section the bulk of the data obtained is presented in graphical form. The considered parameters include peak conduction current, streamer velocity, attachment frequency, maximum free charge, electron injection from the cathode and attachment frequency (coefficient). An interactive computer program was used to analyse the data (Appendix **A**) which was stored in a data base reproduced in Appendix **B**. The data refers to what are termed here "classic streamers" or those streamers generated between onset and breakdown. As breakdown is approached the streamer behaviour becomes more complex and this behaviour is considered as a separate item at the end of the section. Where appropriate some discussion is presented but more detailed discussion is reserved for subsequent sections as indicated.

5.1 Treatment of Data

In most cases, four corona events were analysed for each set of experimental conditions; gap length, pressure and field. For consistency, dry air was used throughout. For some combinations of parameters, 10 or more events were analysed. In some cases, not all events recorded could be analysed fully and only some of the derived quantities are available. For example, while all streamers have a velocity, this cannot be measured by time-of-flight for those which do not cross the gap. As a result there is no velocity data for certain ranges of parameters. Because the reduced onset field increases with falling pressure, for certain fields at low pressure there was no corona whatever, and again no parameters are available.

Where a discrete value is obtained, (i.e. all parameters except attachment and growth frequencies, then the mean and standard deviation of the measurements were plotted.

In the case of the attachment and growth frequencies, being obtained from a

least-squares technique, an error σ_i could be obtained for each experimental point, x_i. Plotting these individual measurements, since the range of experimental errors was wide and the values not a little scattered, gives a confusing picture. Hence a weighted mean of the means and standard deviations of the raw derived results are plotted, where the weight is the reciprocal of the fractional error of the point, $w_i = x_i/\sigma_i$. The means and standard deviations then become:

$$\bar{x} \pm \bar{\sigma} = \frac{\sum x_i w_i \pm \sum \sigma_i w_i}{\sum w_i} \qquad (5.1)$$

The effect of this weighting is to emphasize the measurements having the smallest error, without actually eliminating any one point. And since the mean of the individual errors is used, σ represents the range of the observations, not the error of the mean, as for the other (discrete) data. Where the points are so close together that the error bars make the graphs confusing, only the points are plotted. When this is necessary, the spread of the data is generally wider than the accuracy of any one particular measurement and hence the underlying variability is not affected; it is, on the contrary, highlighted.

5.2 Classic Streamers

5.2.1 Conduction Current

Fig.5.1 reports the variation of peak conduction currents with E/p, pressure and propagation length. Data below 400 torr are not plotted, as the δ-event disrupts the measurement.

The data tend to a limiting value after the stability field is attained, except that

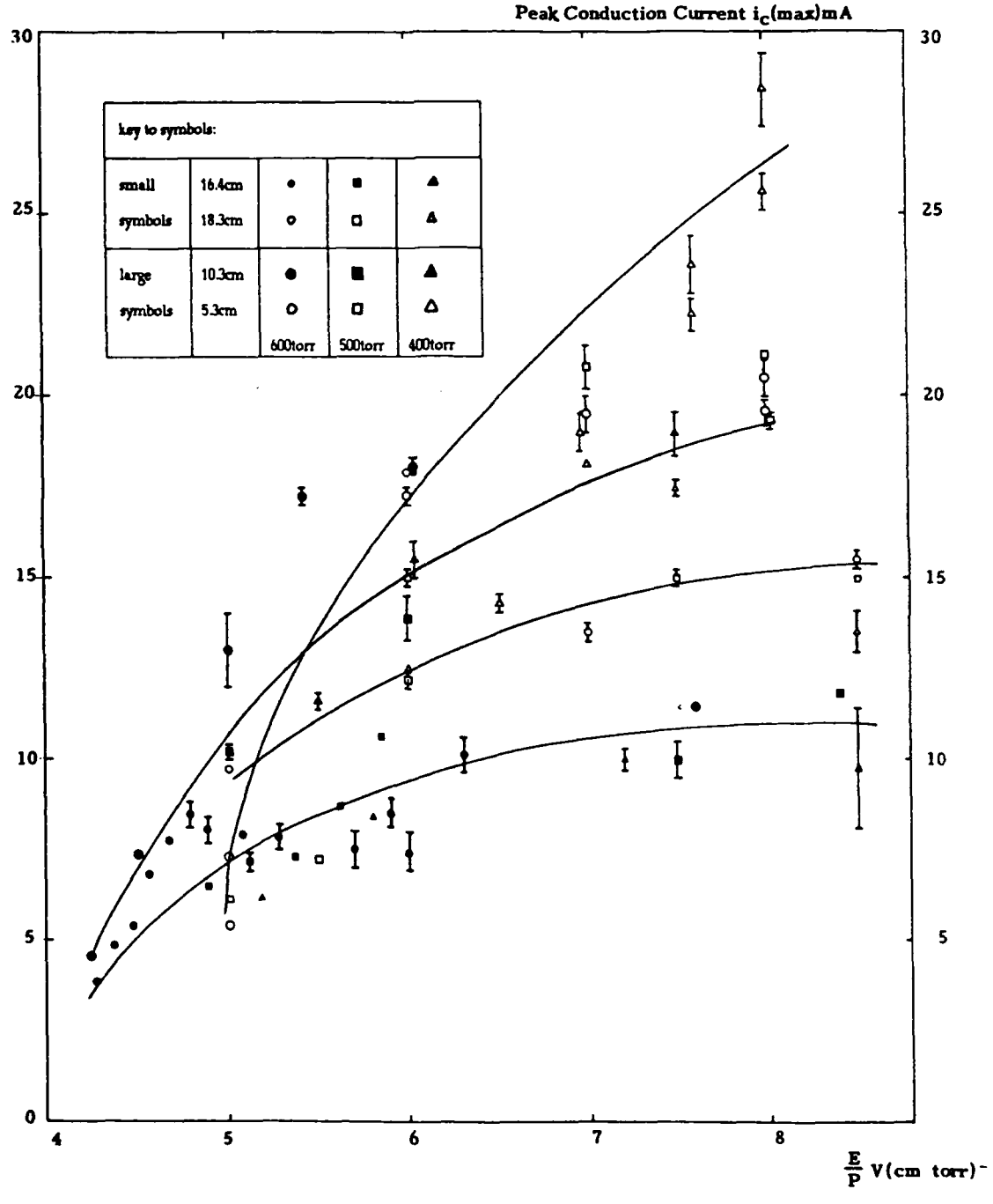
Peak Conduction Current i_c(max)mA
key to symbols:
small symbols
16.4cm
18.3cm
large symbols
10.3cm
5.3cm
600torr
500torr
400torr
30
25
20
15
10
5
0
4
5
6
7
8
$\frac{E}{P}$ V(cm torr)$^{-}$

Fig. 5.1

obtained at 5.3cm, which may not have levelled off at the reduced fields studied. Within it must be stressed an extremely large experimental spread and at 400 torr and above, the limiting value appears not to depend on pressure, but on the propagation length.

Fig.5.2 shows a plot of the limiting value of the conduction current peak against propagation length, d. It shows a minimum at somewhere around 15 to 16 cms. Though is must be observed that the range of currents of between 8 and 20mA is not wide, digital sampling error could contribute significantly to the uncertainty in the maximum value of i_c measured, and the large error involved may mean that the rise in i_c(max) at higher d may not be significant. The increase in the limit at low d though, is too steep to be ignored.

Marode (1975a) reports a typical streamer current maxima of around 50mA or so, for prebreakdown point-plane systems 1cm or so in extent. Though the influence of vibrational states may be invoked to explain some of this increase (from enhanced ionization, or other mechanisms), the magnitude of the increase does in general confirm the trend to higher maxima at lower gap length.

The difference compared with the point-plane work of Marode is particularly interesting, since in point-plane work it is considered that the corona current is dependent on the potential of the tip, rather than the average field. So it might be argued that the three electrode system used is sufficiently similar to point-plane geometry that the actual voltage on the needle is crucial. The gap in the present study is "inverted" with the voltage applied to the cathode, but nevertheless the voltage difference to establish a particular field will increase with the separation of the electrodes. Analogy with point-plane geometry would imply a uniformly increasing streamer current at the same field as the gap length goes up. The distinct fall in current as distance increases very clearly shows this analogy to be groundless. (It can also be argued that at a given E/p and d the voltage point above the cathode voltage must drop as the pressure drops, to maintain E/p. This would imply a lower value of i_c(max) using the analogy with point-plane findings - again this is not seen in the Figure.)

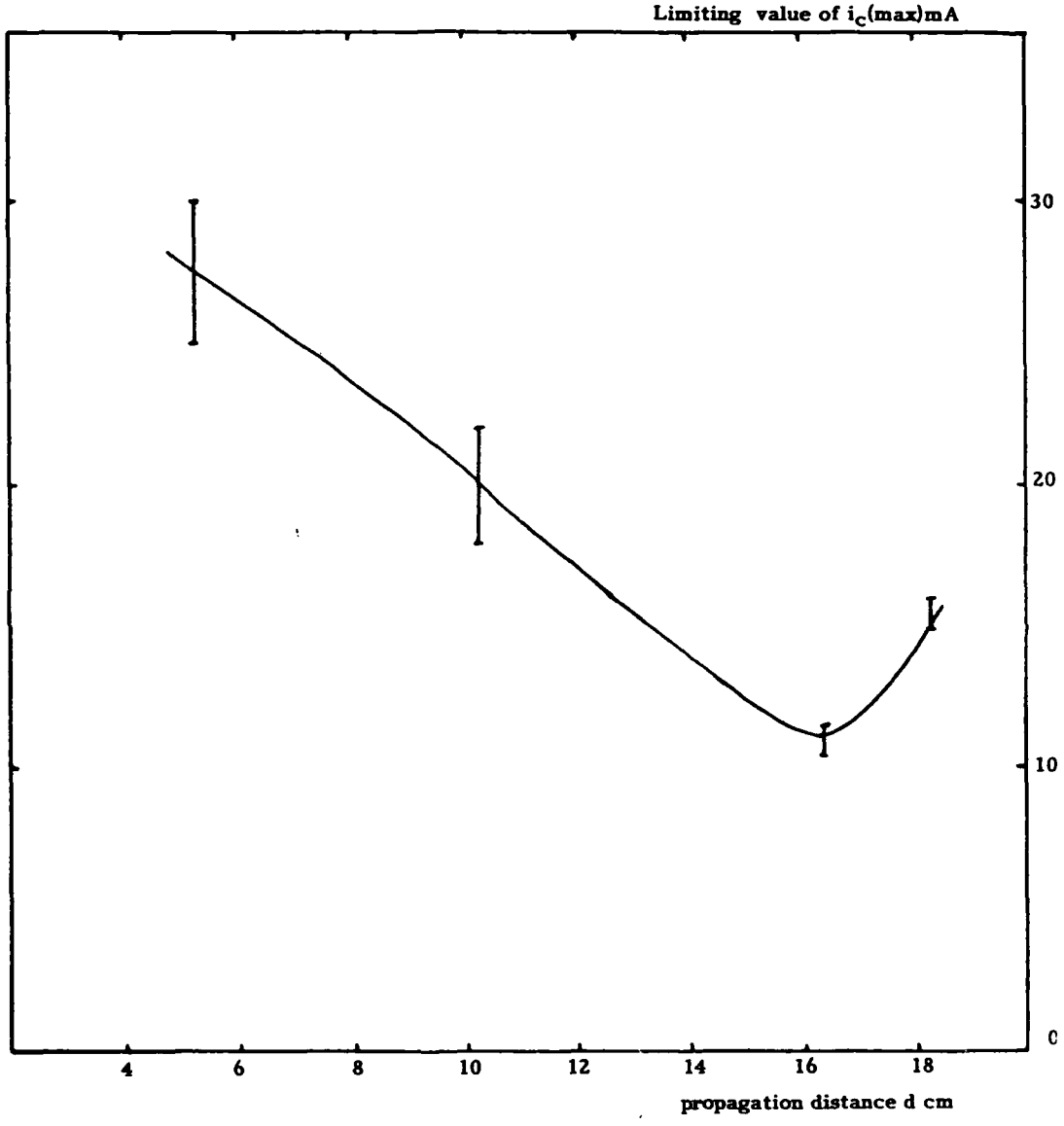
Limiting value of i_C(max)mA
30
20
10
0
4
6
8
10
12
14
16
18
propagation distance d cm

Fig. 5.2

The topic of the conduction current maximum is taken up in the discussion, and while the low gap length arm of the curve (Fig.5.2) might be explicable as a geometric factor, the possibility that it can subsequently increase with distance cannot be explained by supposing residual current to reach the point from the rest of the enlarged streamer system, for the peak occurs in some 100 to 200ns at most. Electron drift speeds of even 50km/s mean that at most the first cm of channel only can be responsible for determining the peak in i_c. Thus the suggestion of a variability with length over and above the first few cm is quite extraordinary.

5.2.2 Streamer Velocities

Fig.5.3 shows plots of streamer velocities against E/p, for various propagation lengths and pressures, found by time-of-flight. With the exception of the 5.3cm data, all the 600 torr velocities lie on the same curve. At 500 torr, the story is the same, except that the tendency to lower streamer velocity at 5.3cms is also shown, though less strongly, by the 10.3cm data.

Fig.5.4 shows a family of curves, each at a different value of E/p, showing v_s as a function of pressure, for the 18.3cm data. There is a very interesting minimum at around 400 torr, but only for an E/p of 8.5V/cm.torr; at lower E/p there is only a point of inflexion here.

Streamer propagation velocity is an easily measured but clearly very complex parameter, and no satisfactory theory of streamer velocity exists. The rise in streamer velocity with reduced field is self-evident, for the electron drift velocity will be higher. Explaining the minimum in velocity when plotted against pressure at a given reduced field is not easy, but it may be possible to show qualitatively how the minimum comes about by considering the time to create a secondary avalanche.

A particular property of this minimum is that it occurs only at high reduced field. The curves might be considered to be a general reduction in streamer velocity as pressure increases, with an E/p-dependent enhancement which increases strongly with

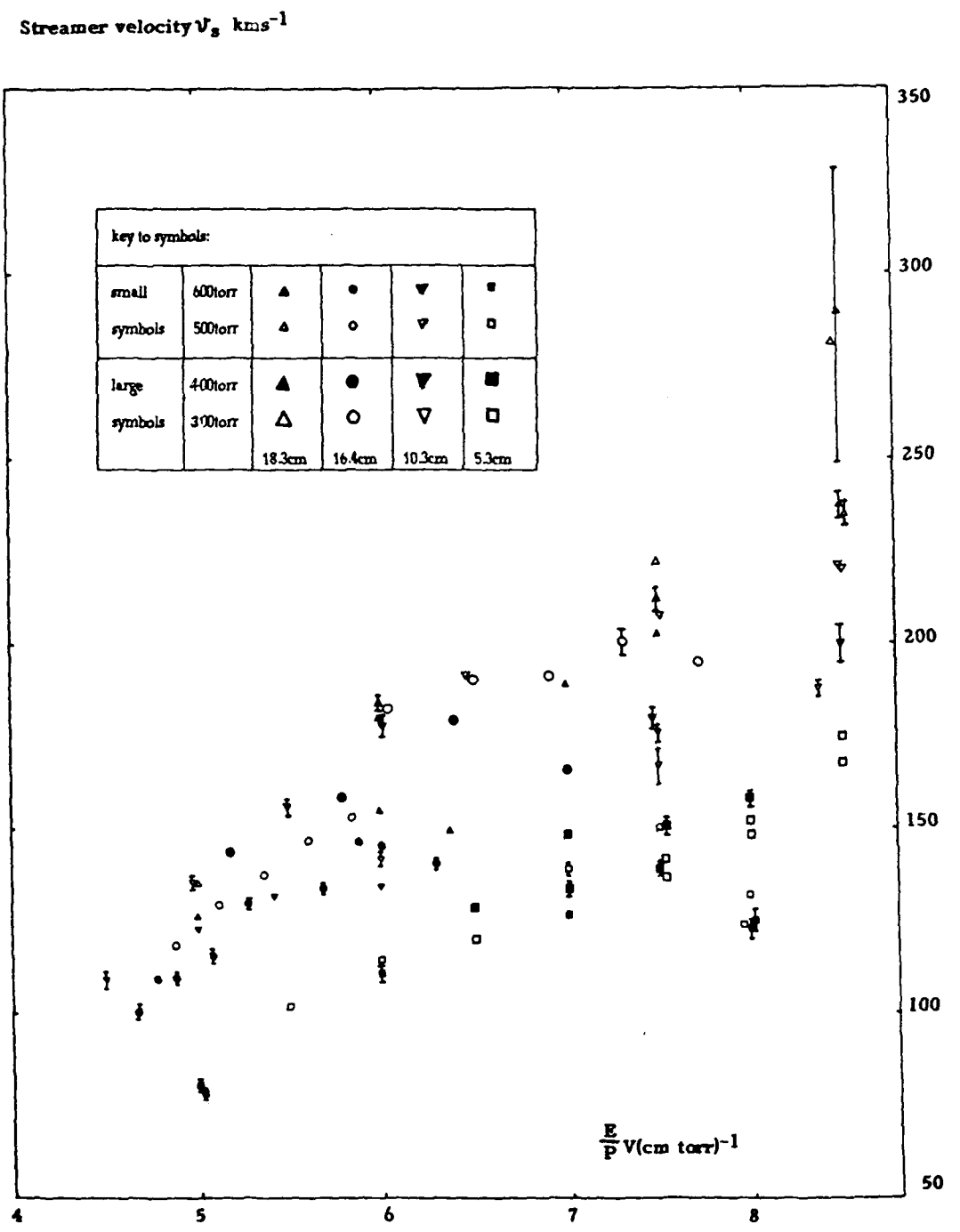
Streamer velocity v_s kms^{-1}
key to symbols:
small symbols
600torr
500torr
large symbols
400torr
300torr
18.3cm
16.4cm
10.3cm
5.3cm
350
300
250
200
150
100
50
4
5
6
7
8
$\frac{E}{p}$ V(cm torr)$^{-1}$

Fig. 5.3

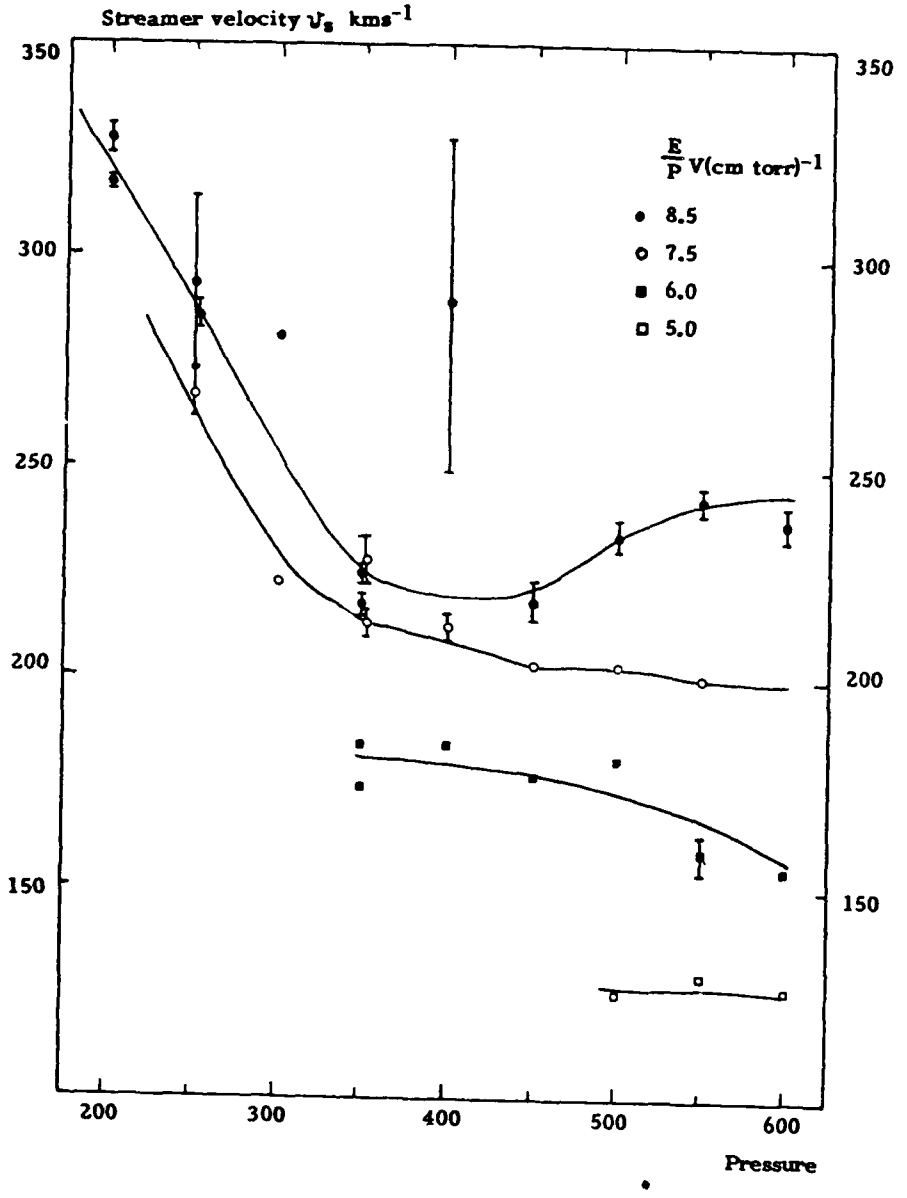
Streamer velocity v_s kms^{-1}
350
300
250
200
150
$\frac{E}{P}$ V(cm torr)$^{-1}$
8.5
7.5
6.0
5.0
200
300
400
500
600
Pressure

Fig 5.4

pressure above 500 torr.

5.2.3 Free Charge

To provide an easily defined parameter to characterize the streamer growth, the maximum free electron charge, $Q_g(max)$ was measured. This parameter does not appear to have been measured in this way by any other investigator and hence the way it varies is of interest.

The maximum in Q_g, however, is something of a hybrid, representing as it does the free charge residing on the channel and from cathodic injection. It is no easy task to separate the cathodic injection by sight from the background of the growing streamer system, and so the easier-to-identify-parameter, the maximum, was measured. This is something of a compromise, but the unambiguous definition of the maximum was preferred to the more subjective measurement which would have arisen from trying to define the separation point between the growth in Q_g and the charge injection from the cathode. Anyway, the charge injection can, in principle, be more satisfactorily measured from the size of the narrow spike in the δQ records. (see below section 5.2.4).

Fig.5.5 shows the variation of $Q_g(max)$ as a function of E/p at various propagation lengths and pressures. In the figure it can be seen that after the stability field is passed the gap charge rises exponentially through a decade for an 0.1V/cm.torr increase in E/p. Except for the 5.3cm data this seems to be independent of propagation length: all the data lie roughly on the same curve. This shows the strong increase in charge once the system begins growing.

Beyond 5V/cm.torr the data separates and a strong propagation distance dependence sets in, with weaker growth as a function of E/p. Replotting the data as a function of propagation length results in an (almost) exponential increase in Q_g with distance (Fig.5.6). The strong growth of $Q_g(max)$ with distance would suggest either that the charge on the channel, Q_g, is considerably larger than that injected from the cathode, or else that the charge injected from the cathode is proportional to Q_g. This might be

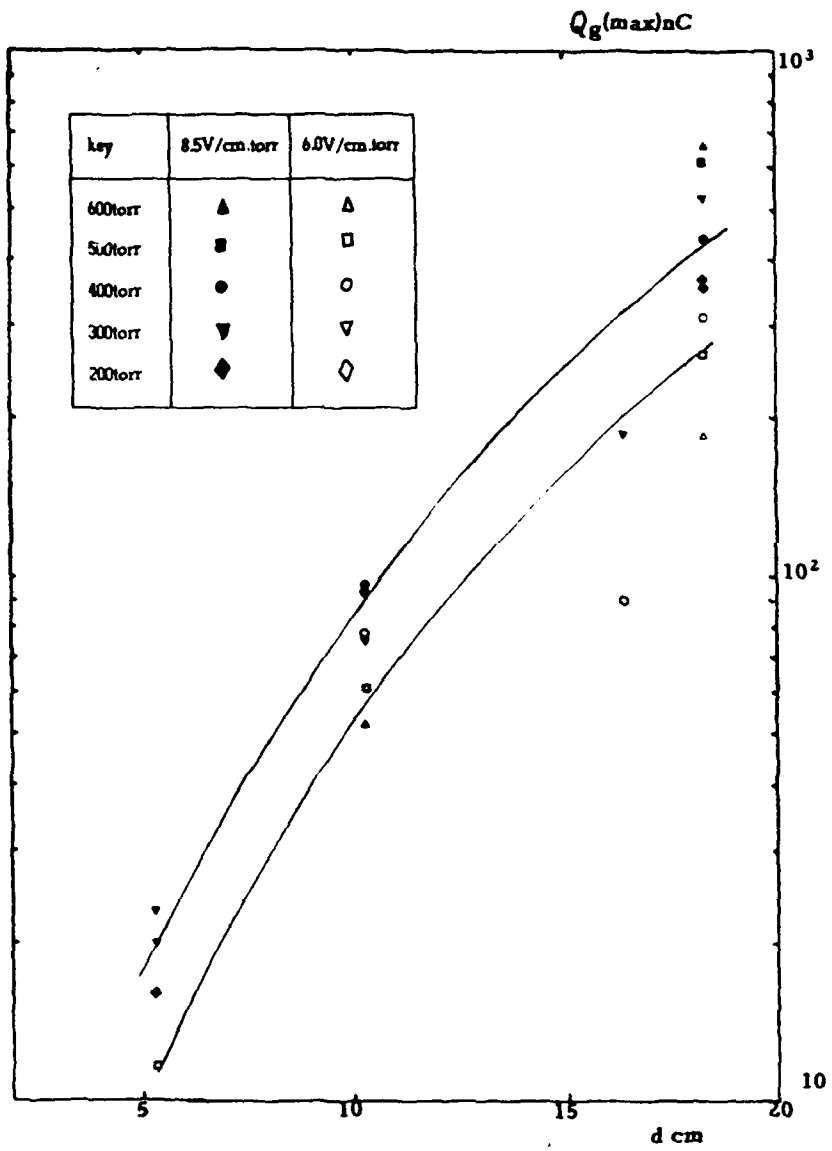
Q_g(max)nC
key
8.5V/cm.torr
6.0V/cm.torr
600torr
500torr
400torr
300torr
200torr
10^3
10^2
10
5
10
15
20
d cm

Fig. 5.6

Fig. 5.5

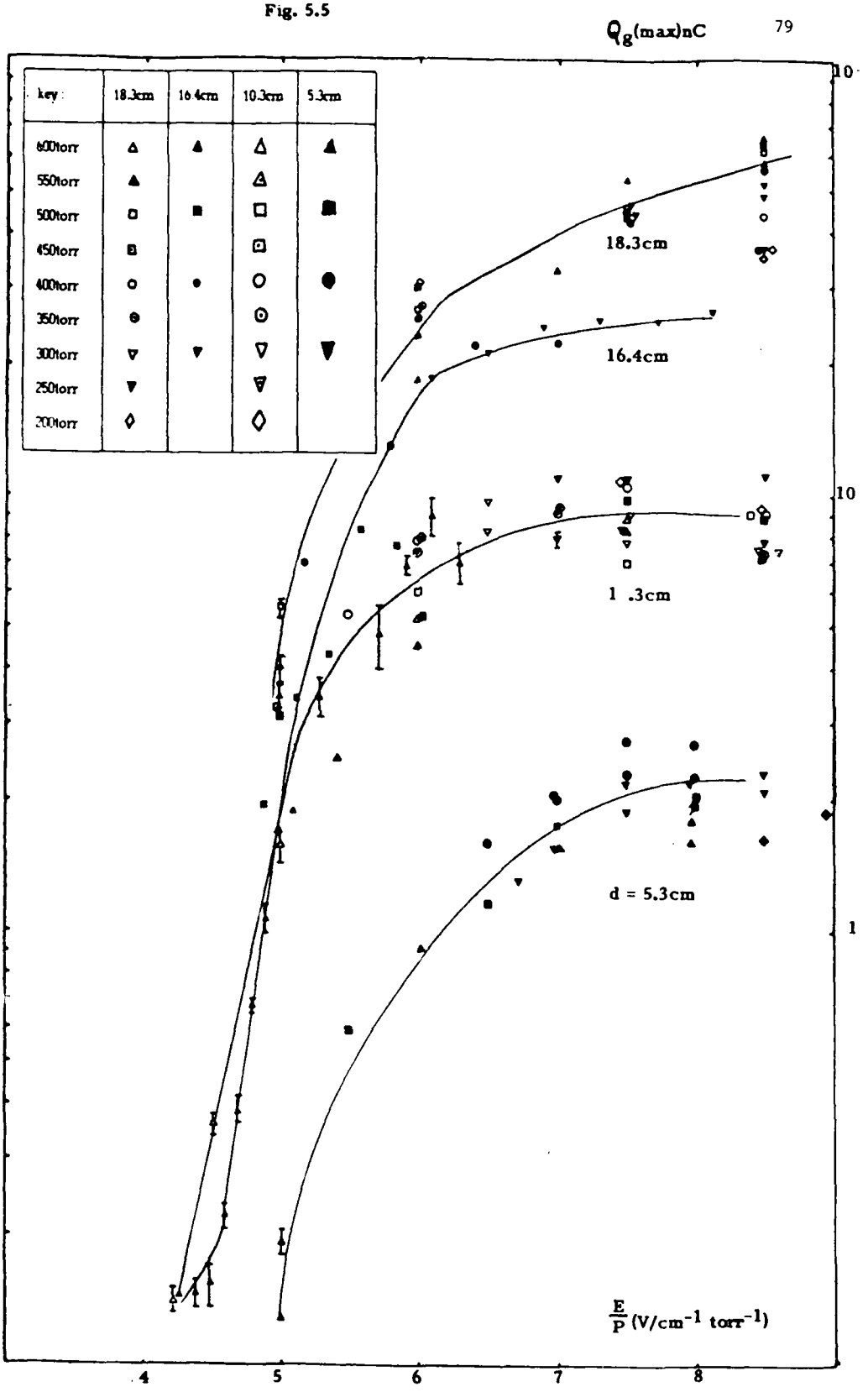
Q_g(max)nC
key :
18.3cm
16.4cm
10.3cm
5.3cm
600torr
550torr
500torr
450torr
400torr
350torr
300torr
250torr
200torr
18.3cm
16.4cm
1 .3cm
d = 5.3cm
10
10
1
4
5
6
7
8
$\frac{E}{P}$ (V/cm^{-1} torr^{-1})

accounted for as follows.

5.2.3.a Tip/Channel Charge Ratio

Redefining the coordinate frame such that the end of the streamer is at y=0 (Fig.5.7), and considering the electrode to be an infinite distance away (i.e. that all electrons attach before reaching the anode), the channel function, $\lambda(y)$ can be written:

$$\lambda(y) = A(y')\exp[-\eta(y-y')] . \qquad y' = y(1-\frac{V}{V_s}) .$$

$$\therefore\ Q_g = \int_0^\infty A(y')\exp[-\eta(y-y')]dy = \int_0^\infty A\{(1-\frac{V}{V_s})y\}\exp[-\eta y\frac{V}{V_s}]dy \qquad (5.2)$$

which can easily be evaluated for a particular form of A(y). This will hold for a branched streamer system, as well as for a single channel; for considering a horizontal slab through the discharge, and taking the idealized view of the per-unit-field distribution outlined in section 3 the induced current is just that from adding the currents induced from the individual filaments. G_g is just the total charge in all these filaments and the attachment will always be proportional to it. The growth will depend on the size of the individual streamer tips, but this will affect the situation by changing the growth function A(y), which is what one hopes to measure - hence there is no need to build into A(y) the influence of the tip potential distribution.

The principle question is whether this integral will give a result proportional to A(y=0), that is to the size of the tip. Assuming the charge injection from the cathode to depend at least on the size of the tip also, the maximum in G_g evaluated at some particular reduced field would then be proportional to the total streamer tip charge even taking the channel in to account. With a constant growth rate, $A(y)=\Lambda$ this evaluates to Λ/β (writing $\beta=\eta V/v_s$). With an exponential growth rate, $A(y)=\Lambda\exp\gamma(d-y)$ (y is defined backwards along the channel: $A(x)=\Lambda\exp\gamma x$; $x=d-y$ where d is the length of the channel). This evaluates to:

$$\Lambda\int_0^\infty \exp\gamma(d-y')\exp(-\beta y)dy = \Lambda\int_0^\infty \exp\gamma(d-(1-\frac{V}{V_s})y)\exp(-\beta y)dy \qquad (5.3)$$

$$= \Lambda\exp\gamma d/(\gamma(1-\frac{V}{V_s})+\beta).$$

(i) $y=y'$: charge deposited is $A(d-y')dy$

(ii) $y=0$ streamer arrives at time $t=y'/v_s$

(iii) y: electrons drift to y in time $(y-y')/v_e = t$

charge $\Rightarrow$

$A(d-y')dy\ e^{-\eta(y-y')}$

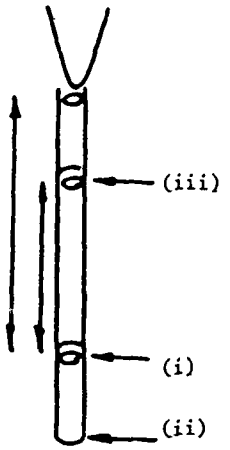

Equating times

$y'/v_s = (y-y')/v_e$

or

$y' = (1-V/v_s)y'$

Fig.5.7

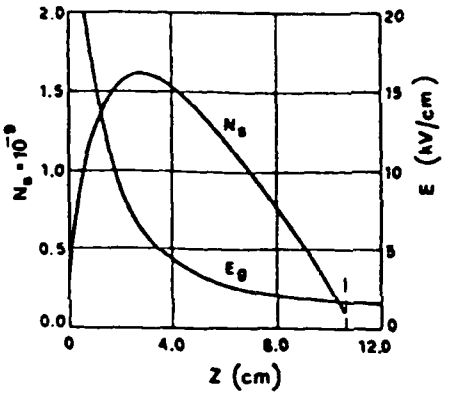

Fig.5.8

Variation of positive ion number N_s into field E along the streamer path (after Gallimberti)

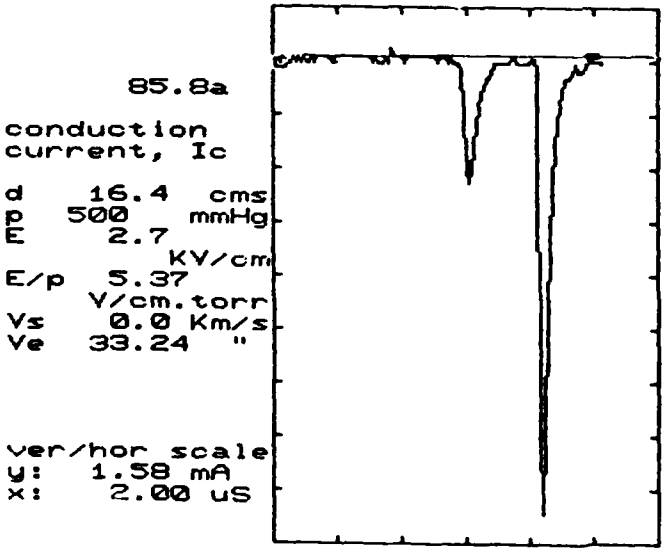

Fig.5.16

Showing a small dark current between the two corona events.

Using a power function is not as tractable a problem, substituting $A(y')=\Lambda(d-y')^n$ into Eq.5.2 ($x=d-y'$, as above) and integrating by parts yields:

$$\Lambda\int_0^\infty (d-y')^n \exp(-\beta y')\,dy = \Lambda\int_0^\infty \left(d-(1-V/v_s)y\right)^n \exp(-\beta y)\,dy$$

$$= \left[\frac{-\Lambda\left(d-(1-V/v_s)y\right)^n}{\beta}\exp-\beta y\right]_0^\infty - \Lambda\int_0^\infty \frac{(1-V/v_s)n\left(d-(1-V/v_s)y\right)^{n-1}}{\beta}\exp(-\beta y)\,dy$$

Writing $U_n = \int_0^\infty \Lambda\left(d-(1-V/v_s)y\right)^n \exp(-\beta y)\,dy$

the above gives the recurrence relation:

$$U_n = \frac{\Lambda d^n}{\beta} - \frac{n(1-V/v_s)U_{n-1}}{\beta} \quad ; \quad U_0 = \frac{\Lambda}{\beta} \tag{5.4}$$

If $U_n \propto A(y'=0)$, the size of the streamer tip charge, then this implies $U_n \propto d^0$. Clearly Eq. 5.4 is inconsistent with this even for n=1, as then $U_1 = \frac{\Lambda d}{\beta} - \frac{\Lambda(1-V/v_s)}{\beta^2}$. In SI units typical values are: $d \sim 0.1$m and $\beta \sim 20 m^{-1}$.$(1-V/v_s) \sim 0.9$, and so these terms are of nearly equal size. U_1 is not even approximately $\propto d$, as would be required if the tip charge were to be proportional to the channel charge.

So the maximum gap charge and the system size prior to impact will be proportional if a constant, or an exponential growth is assumed, but not if a power-law is used for the streamer function, A(y). The almost exponential growth in $Q_g(max)$ with distance suggests an exponential growth function, A(y) as the two would then be self-consistent. This analysis depends on the channel having decayed to zero free charge at its base by the time the cathode is reached. This is clearly not the case for the 5.3cm systems studied (see e.g. Fig.5.5), and so this analysis breaks down at 5.3cm. This will explain the fact that the 5.3 data do not coincide with the rest at fields slightly above stability field and will also explain the apparently steeper growth of the spatial $Q_g(max)$ curves (Fig.5.6) in the early stages.

The almost exponential spatial growth (Fig.5.6) underscores the difference between point-plane and uniform field corona. In this study, the streamer growth seems to

be exponential with distance, implying for constant velocity a growth rate proportional to the system size. This can be compared for example with the calculated tip size obtained by Callinberti (1972c) (Fig.5.8) which rises and then falls in the highly non-uniform rod-plane field.

5.2.4 Charge Injection

The charge injected by secondary processes when the streamer reaches the cathode results, as discussed above, in a large, narrow spike in the δQ curves. This appears to be a well-defined parameter and its size has been measured. But a slight warning ought to be attached to this data, the records are digital and the peak in δQ is very narrow - a few samples. So whilst it is fair to say that only one experimental parameter (i_c) is varying at all rapidly when δQ is found, the error in the maximum may still be fairly large.

Fig.5.10 shows the variation of this parameter with pressure, E/p and propagation length. The behaviour of δQ is broadly similar to that of G_g, though this similarity really shows how strongly both depend on the system growth. The magnitude of the charge injection rate is very high, ~ amps, but of a short duration, ~10's of ns. A 1 amp pulse of current lasting (typically) 32 to 48nS will inject 32 to 48nC of negative charge into the gap.

Even 100 streamer tips will have a total charge of perhaps 1nC (10^{-11} coul. each). Thus it can be seen that the electron injection of some ~50nC from the cathode is very efficient by comparison with the streamer active region. This is not very surprising if it is considered that the ionization potential of oxygen is ~16eV, compared with a work function of ~4.2eV for aluminium, and that the collision frequency for production of a photo-electron from the cathode is many orders of magnitude higher than that for ionization of a gas molecule.

In fact, the removal of electrons from the base of the channel will result in a net positive charge on the channel, and integrating the conduction current yields a value

of ~20 to 30nC at most for the conduction charge. The injection of electrons from the cathode then results in a change from a net positive to a net negative charge on the channel.

In summary, the charge in the streamer active region may be a little below ~1nC, but results in ~50nC being injected from the cathode due to the greater photo-efficiency. The free charge in the gap, Q_g, is ~500 to 1000nC in extreme cases but the net positive charge on the channel is only ~20 to 30nC at most, and the injection from the cathode reverses the polarity of this net charge. The charge injection from the cathode is so small by comparison with Q_g that the value of $G_g(max)$ will be but little altered by this. This explains the difficulty observing the injection of charge from G_g records except at low E/p.

5.2.5. Attachment Frequency

An exponential fit routine was used to analyse the G_g data. The end-points could be varied in real-time, and a fit obtained over any desired portion of the record. Whether the data actually follows an exponential form is immaterial to the fit routine, which happily calculates a decay or growth frequency for the data selected. The routine, though, does find an accuracy figure, following the method outlined by Barford (1967). The appropriateness of the calculated values, therefore, depends to no small amount on the portion of the curve selected, but is represented by the calculated error.

The selection of data is important because the derivation of the attachment frequency requires there to be no generation of free charge in the gap and that the electron drift speed be known. The data, plotted in Fig. 5.11, were not calculated after any secondary phenomena (like regenerations), for the possible channel heating might affect the local pressure, and hence the electron drift speed. At low pressure, where there is apparently a marked drop in attachment early in the mature stage of the discharge resulting from significant removal of charge from the gap at the needle-end, the end portion of the G_g record, where the conduction current has most fully decayed, is preferred

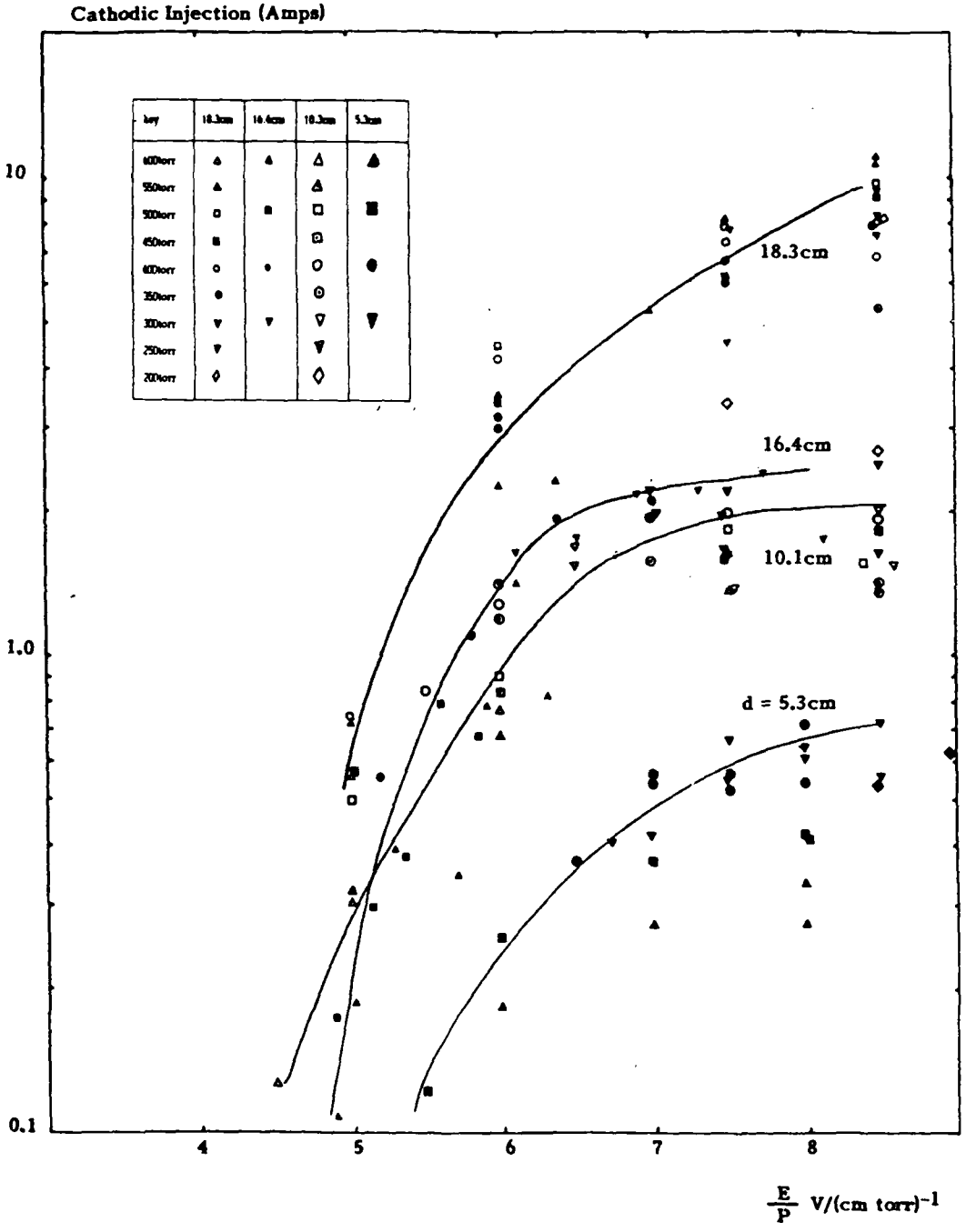
Cathodic Injection (Amps)
10
1.0
0.1
4
5
6
7
8
18.3cm
16.4cm
10.1cm
d = 5.3cm
E/P V/(cm torr)-1

Fig.5.10

for the calculation of attachment frequency. In cases where the channel was regenerated this is not possible, for a secondary process has intervened, but these data might be intercomparable and so have been included. The attachment frequency sought is a lower bound on the low pressure values.

In general, the calculation was extended to as much of the discharge as possible whilst maintaining a satisfactory fit. The selection of the portion of the decay for the fit was not normally a problem since usually the decay in G_g was satisfactorily exponential over the whole of the record.

The low E/p data at 600 torr warrant discussion. Approaching the stability field, it would seem that the attachment rate falls steeply as the reduced field approaches this value, at which the attachment rises abruptly to a very high level. The key is that this occurs at the stability field - at which the channel is only just sustaining itself and so below this decay of G_g sets in before the channel is dead. The generation of charge is not zero and a true attachment rate is not found. This data has been included in the figure to illustrate this process.

The data have been converted from attachment frequencies into attachment coefficients as this is still the more widely used parameter. Further, the reduced attachment coefficient is plotted, for this removes the inverse pressure dependence resulting from the greater mean free path. If a purely two-body attachment process operates, then all the curves should coincide if η/p is plotted against E/p.

This is almost the case, as it can be seen from Fig.5.11 that η/p is only lower at greatly reduced pressure. It would seem that no clear distinction can be made from this data as to the nature of the attachment process; it clearly involves mainly two body processes but is not exclusively so.

The range of attachment coefficients measured corresponds to those found by other workers, as does the scatter of experimental points, Figure 5.12(a) showing a compilation of reduced attachment coefficient measurements is reproduced here, with the range of observations covered by the scales in Fig.5.12 indicated by the small rectangle.

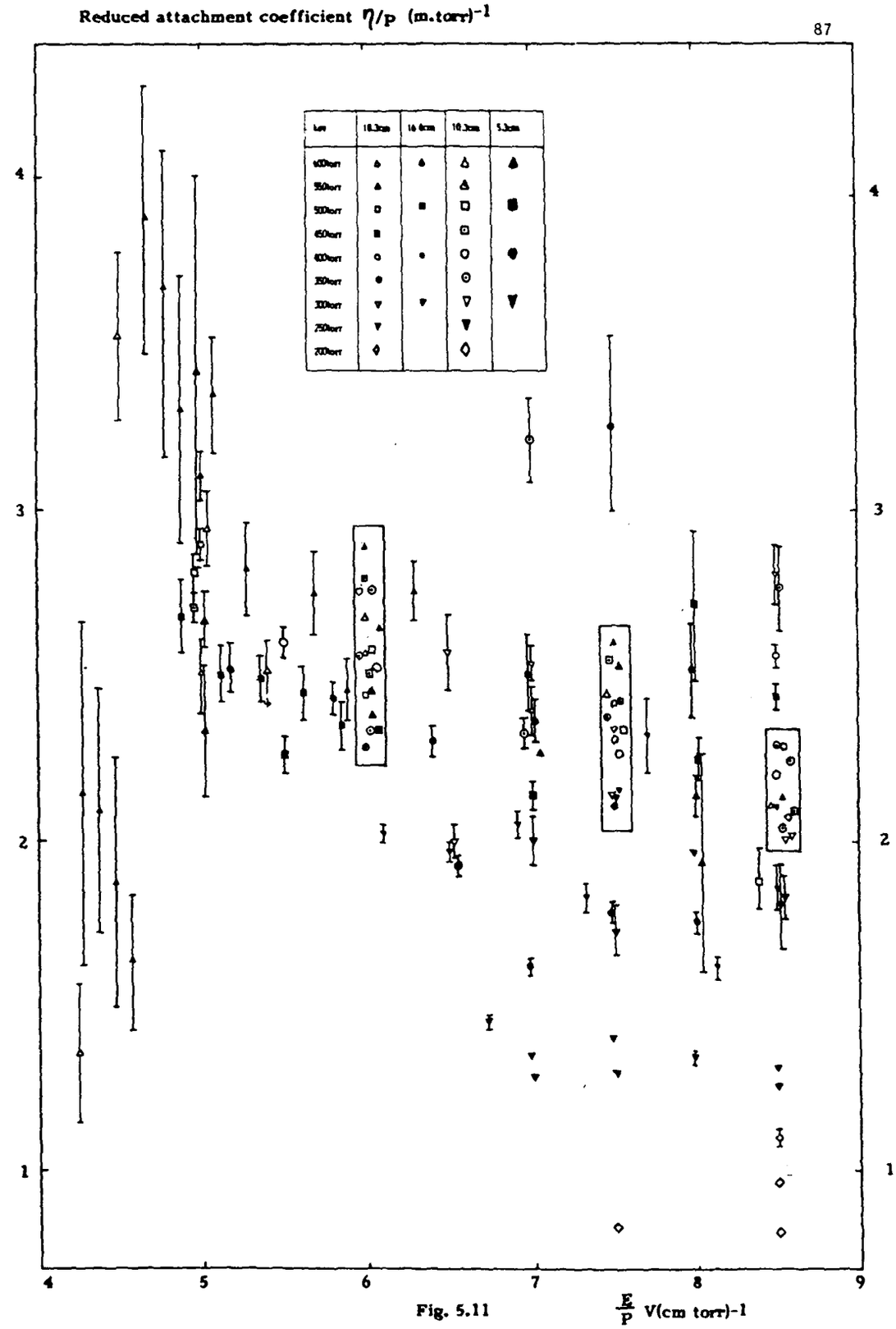
Reduced attachment coefficient η/p (m.torr)$^{-1}$
4
3
2
1
4
5
6
7
8
9
$\frac{E}{p}$ V(cm torr)-1

Fig. 5.11

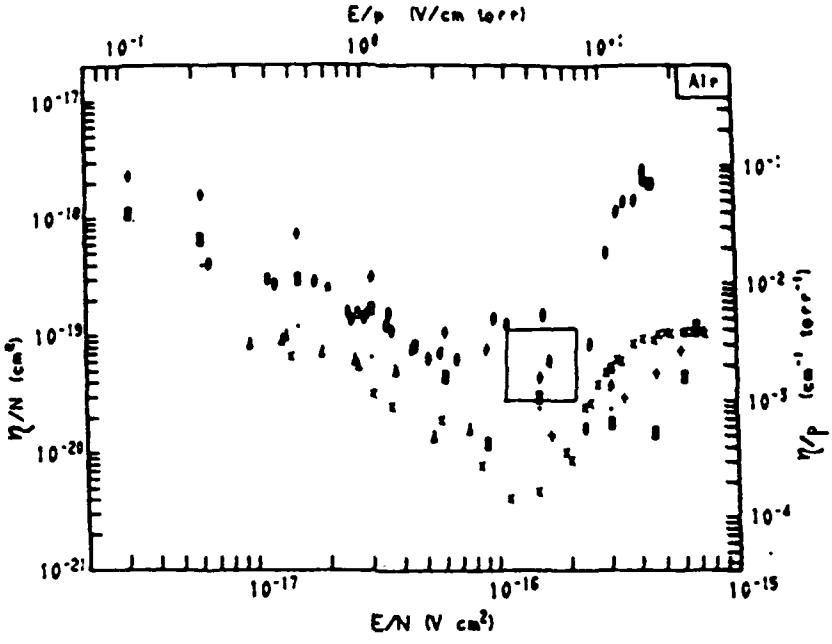

Experimental: θ Bradbury(1317); Δ Bailey(1332;2953);
x Kuffel(1433) ♦ Chatterton(2408);
•,□,◊ Hessenauer(3165).

Experimental values of the attachment coefficient for air for $E/N < 68 \times 10^{-17}$ V cm².

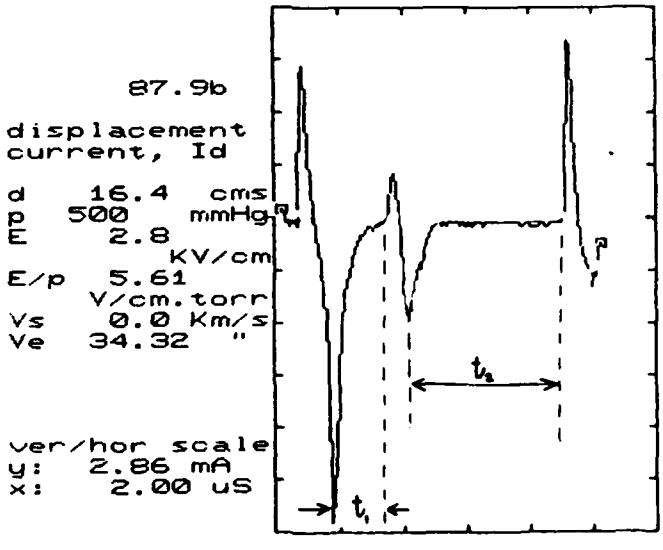

Fig. 5.12 (top)

Fig. 5.15 (bottom)

The published data are evidently scarce, but the range of measurement is within the range of measurement reported by other authors.

5.2.6 Charge Injection Rate

As discussed above (section 3), applying charge conservtion to the gap yields the parameter δQ, the charge generation, or injection rate. Since the data was very noisy and almost any rapidly growing function could be used to characterize the data with equally good (bad) accuracy, for simplicity and computational convenience the exponential fit routine used to obtain the attachment frequency was also used to find a growth frequency, Γ, for the charge generation rate, defined from the equation:

$$\delta Q = Be^{\Gamma t} \qquad 5.5$$

This may prove to have been an unfortunate choice, considering the remarks in section 6.1 concerning the unsuitability of an exponential for the streamer growth. The alternative: a polynomial, contains a great many degrees of freedom and considerable thought must go into deciding the form of equation to use in the fitting routine, if meaningful results are required. As a first attempt at characterizing the behaviour of this entirely new parameter, δG, an exponential fit is on balance as adequate as any other. Furthermore, it has the advantage of providing the instantaneous growth rate directly.

Since the charge generation rate depends on the size of the active region, the growth frequency of this parameter also represents the temporal growth rate of the streamer tip charges.

Plotting this very secondarily derived parameter (Fig.5.13) shows no clear trend with pressure, or system size, but a broadly linear growth against E/p.

Considering the strong influence of pressure on streamer velocity and streamer diffusion radius, it is by no means clear that the streamer growth will be independent of pressure.

5.3 Pre-Breakdown: A case study

Turning from straightforward, classic streamers to the various pre-breakdown modes discussed in section 4, the data is fragmentary, and difficult to synthesize. Accordingly, to try and clarify the relativity of the processes, a particular set of experimental conditions was selected for closer study. All the 500 torr data were selected for the low onset field at this pressure means that low reduced field measurements are available.

5.3.1 Low reduced field/multiple streamers

Fig. 5.14 shows a multiple streamer event, obtained at just above onset. The current pulses are distinct; they do not run into each other. The repetition frequency is much higher than is normal for streamers (usually kHz). Records of this character were difficult to obtain as they are seldom observed at low field.

The displacement current record displays the tell-tale character of this type of corona (Mode (ii)): as the discharge progresses the pulses have successively larger positive-going peaks in the i_d record, the negative-going ones being successively smaller. This, as discussed in section 3, indicates that the discharge is located progessively closer to the needle-end. Visually though, the corona is similar to classic corona as might be expected since the multiple mode occurs with such a low probability. The current records, furthermore, are indisinguishable from those of the high frequency modes (Mode (iii)), where the streamers are again visually similar but on the whole brighter than classic streamers. Again, this is probably due to the probability of the multiple streamer event being greater in this mode.

To try and characterize the behaviour of this mode, a "dark-time" t_{dk} was defined (Fig.5.15) in analogy with long gap impulse studies (e.g. Gallimberti, 1979). Either the transit of the first streamer, or the negative peak in a subsequent corona is taken as the start of the dark period, the end as the beginning of fresh current growth. In Table 5.1 these dark times, the positive and negative i_d peaks, the maximum value of G_g and the

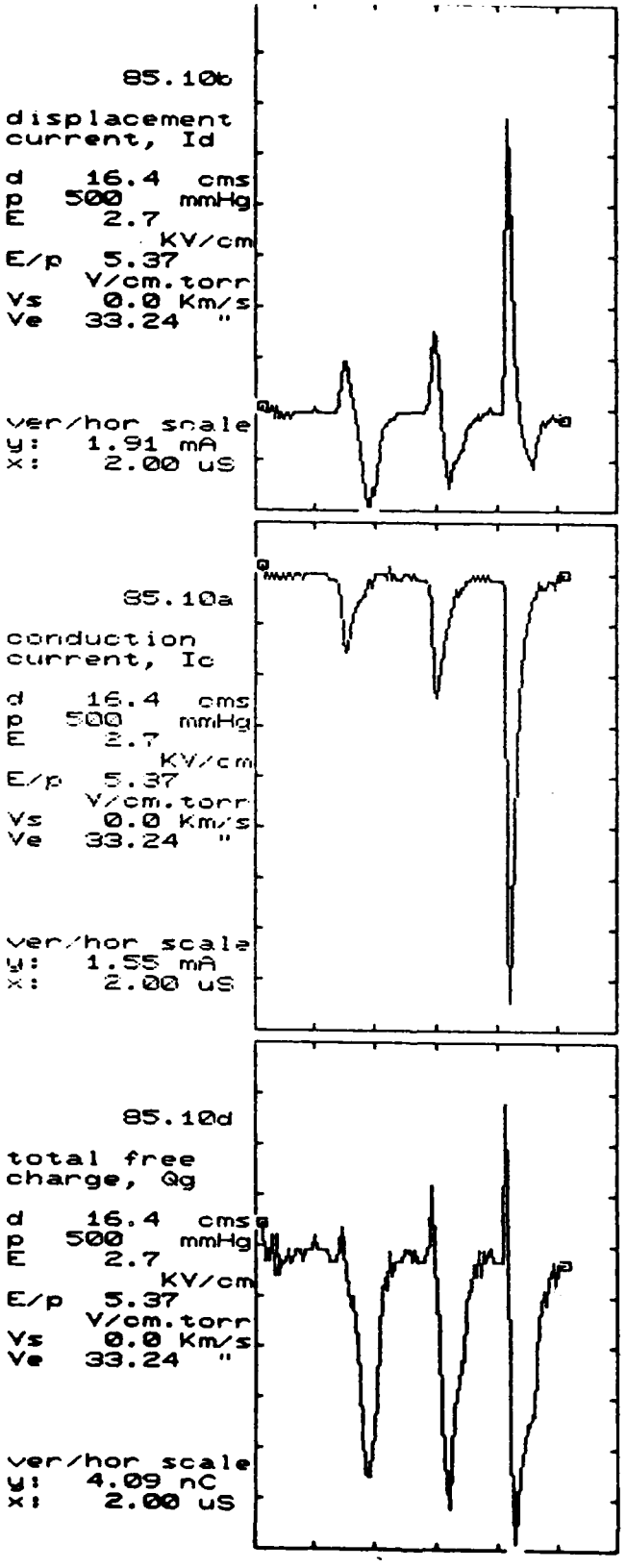

Fig. 5.14

A multiple corona (streamer) event near onset at a low reduced field

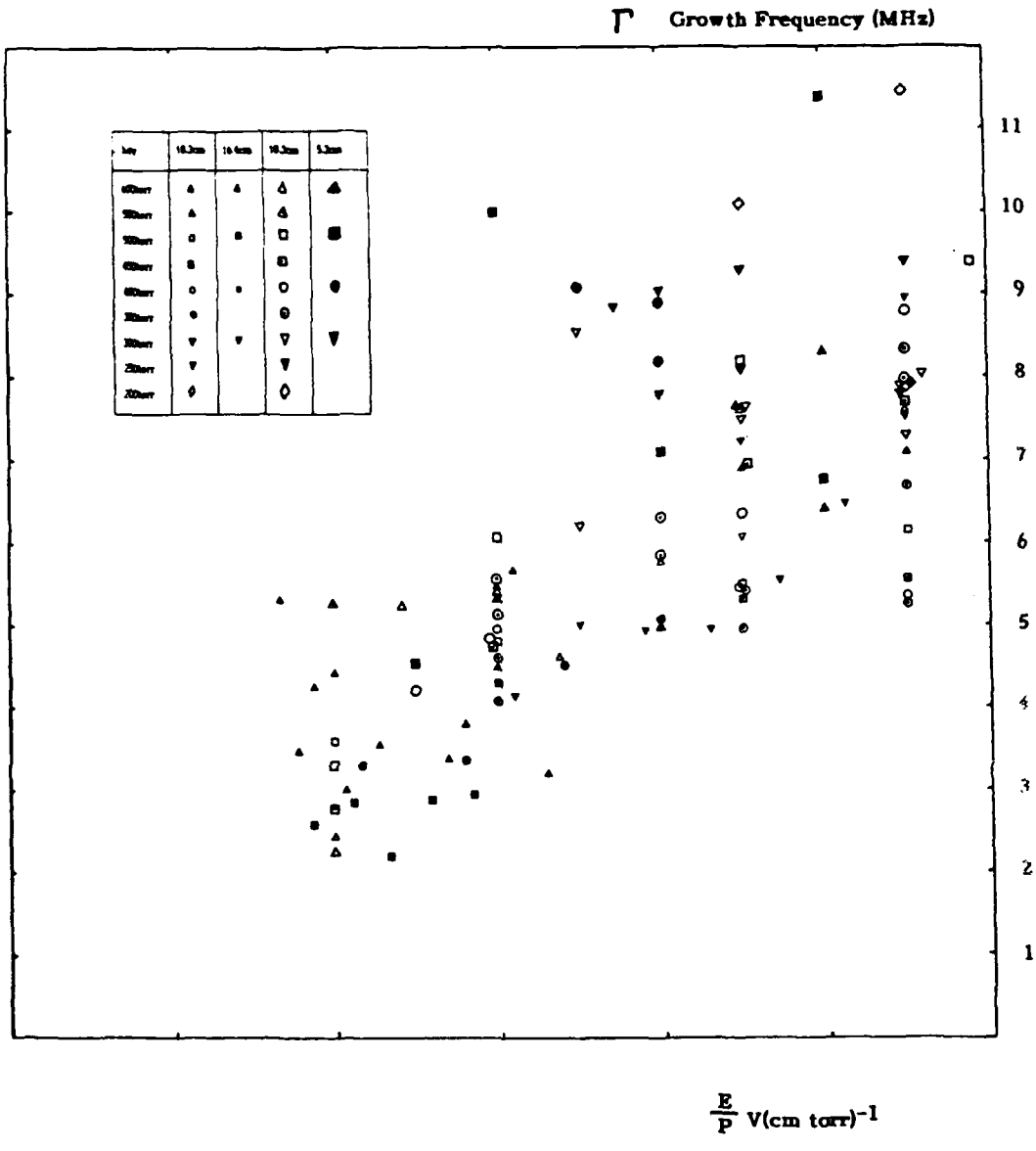

Fig. 5.13

integral of the corresponding conduction current pulse are given, for all the corona of this type observed at 500 torr.

The total number of pulses observed is small, but it becomes clear that for most records, the second corona has a larger conduction charge ($Q_c = \int i_c dt$) than the first. The dark time is less between the second and third, than between the first and second coronae. Event number 87.9, however, has a smaller second corona conduction charge, Q_c, and has a longer dark time after it. An inverse relationship then appears to hold in nearly all cases: other factors being constant, the dark time is reduced and the conduction charge increases as the discharge progresses.

In general,also, the electron charge, Q_g, decreases with each subsequent corona event (the exceptions being events 85.10 and 418.0, which have the longest dark times, during which it is possible that the cathode has recharged a little more, permitting a stronger growth in the subsequent corona).

A further, interesting observation is that there is a "dark current" in the conduction current records, of between 180 and 280μA (Fig.5.16), though this feature is not always present. Not enough data exists to make out any clear trend.

5.3.2 High reduced field/Mode (i)

At higher reduced field, the prebreakdown current records (Fig.5.17) look completely different. The second corona occurs much sooner than at lower E/p and may repeat on very short timescales. The events run into each other, rather than being distinct, as observed at low field. And it will be recalled, the discharge is concentrated into a single channel.

The same parameters as for the multiple mode are shown in Table 5.2. Defining a second dark time, t_{dk2}, is difficult for this data, as the end of the second corona is difficult to make out. Looking at Table 5.2 one first notes that the dark time, t_{dk1} is on the whole shorter than at the lower reduced field in Table 5.1. Between the lines of Table 5.2 (excepting 764.3), the trend is the other way, the dark period increasing

parameters of prebreakdown modes ; 500torr, low reduced field

#	d	E/p	I_{d1+}	I_{d1-}	t_{1x}	t_{2dk}	I_{d2+}	I_{d2-}	t_{2x}	t_{2dk}	Q_{1c}	Q_{2c}	Q_{1g}	Q_{2g}
	cm	V/cm.torr	mA	mA	μs	μs	mA	mA	μs	μs	nC	nC	nC	nC
85.10	16.4	5.37	1.953	3.473	1.088	2.199	3.093	2.822	0.750	1.688	1.264	2.047	18.359	20.915
85.8	16.4	5.37	2.081	>2.490	0.938	1.500	11.743	1.443	1.069	_	1.594	4.827	16.773	14.727
85.6	16.4	5.37	1.861	2.606	0.947	1.114	9.896	1.613	0.891	1.114	1.455	4.412	16.065	13.427
85.4	16.4	5.37	2.509	3.127	0.844	1.125	5.527	2.473	1.013	0.844	0.786	2.380	18.348	14.911
87.9	16.4	5.61	8.450	16.575	0.919	1.781	2.600	5.688	0.656	4.875	3.297	1.735	82.573	31.631
87.4	16.4	5.61	3.631	6.245	0.750	6.188	12.102	2.905	0.938	_	2.245	>6.838	32.601	29.922
418.0	10.3	7.5	6.396	7.766	0.563	2.719	19.186	2.284	0.516	_	2.95	7.48	22.527	24.136

Table 5.1

parameters of prebreakdown modes ; 500torr, high reduced field

#	d	E/p	I_{d1+}	I_{d1-}	t_{1x}	t_{2dk}	I_{d2+}	I_{d2-}	t_{2x}	t_{2dk}	Q_{1c}	Q_{2c}	Q_{1g}	Q_{2g}
	cm	V/cm.torr	mA	mA	μs	μs	mA	mA	μs	μs	nC	nC	nC	nC
764.3	5.3	8.0	17.250	5.646	0.338	0.150	12.232	0.941	0.469	_	6.742	4.029	17.696	5.725
764.2	5.3	8.0	18.213	9.396	0.375	0.150	12.648	0.524	0.488	_	7.347	5.050	23.209	4.709
764.1	5.3	8.0	17.715	5.061	0.394	0.124	12.207	0.596	_	_	7.266	4.881	18.682	6.072
764.0	5.3	8.0	18.269	7.721	0.338	0.131	14.902	1.122	_	_	7.024	6.619	21.946	5.809
366.2	18.3	8.5	14.222	120.893	0.713	0.263	50.965	_	_	_	6.806	21.586	486.841	232.437
366.0	18.3	8.5	14.213	130.497	0.713	0.319	18.089	5.169	0.263	0.113	7.500	14.625	536.550	167.236
418.3	10.3	7.5	10.799	38.749	0.506	0.113	15.246	3.811	0.506	_	4.93	13.78	106.452	47.925
418.1	10.3	7.5	10.214	29.522	0.488	0.113	11.916	3.405	0.458	_	4.52	13.06	82.305	44.943
419.2	10.3	8.39	10.701	32.852	0.488	0.161	31.163	_	_	_	4.94	11.84	86.182	73.091
419.0	10.3	8.39	10.409	36.432	0.469	0.135	46.841	_	_	_	4.82	21.71	96.051	96.747

Table 5.2

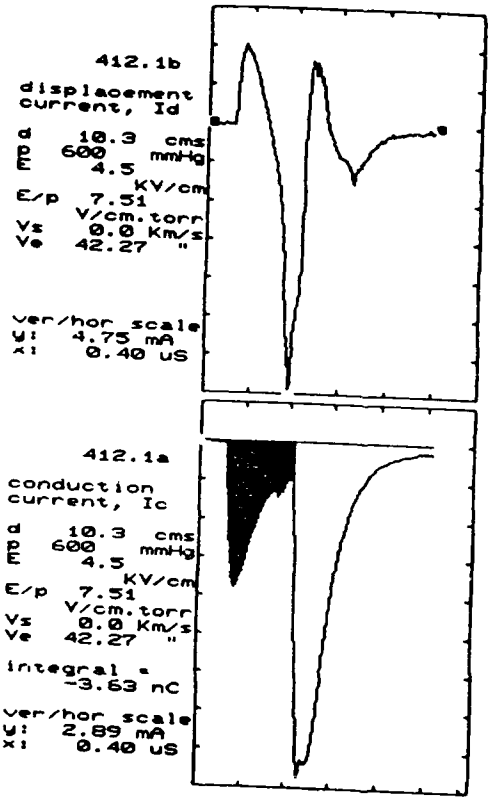

Fig. 5.17

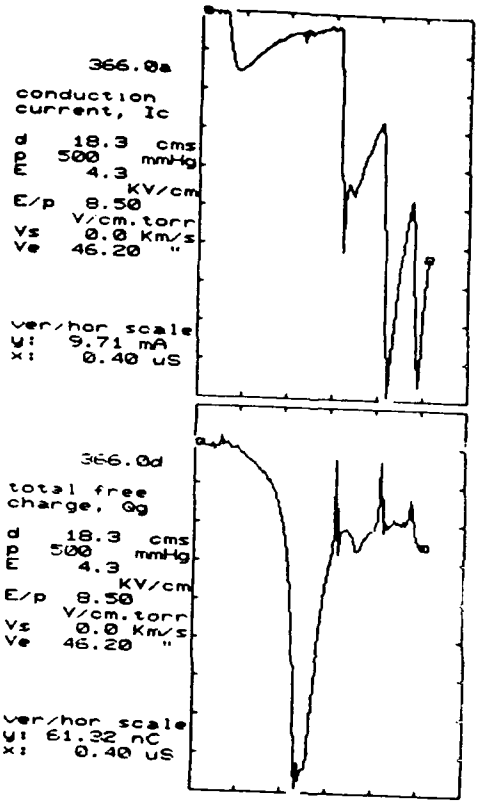

Fig. 5.18

slightly with increasing reduced field. But this may be just a reflection of the following:

It was suggested in section 5.3.1 above that an inverse relationship exists between Q_c and t_{dk}. In this case the conduction charges measured increase very roughly with E/p and this may contribute to reversing the gross trend toward lower t_{dk} at higher E/p which, it must again be stressed, is large and unambiguous. The influence of Q_c is very much a secondary effect by comparison.

No clear influence of electron charge on dark-time is evident. One notes, however, that Q_g is generally reduced for each subsequent corona, while Q_c increases. Listing the reference numbers of the records in order of increasing Q_g and then in order of increasing t_{dk} one gets (764, 419, 418, 366) for Q_g and (418, 764, 419, 366) for t_{dk}. The electron charge is a measure of the size of the streamer system and this lack of any correlation with T_{dk} indicates that the second corona inception is independent of the scale of the streamer system.

In fact, the suggestion from all this data is that the gross dependence of the dark-time on the applied field arises because the mechanism responsible for the formation of the second corona is the drift of space-charge accumulated near the needle tip, and this will clear faster in higher applied reduced Laplacian fields. This also explains the secondary trend toward longer dark time at higher conduction charge in the high field data set; there is more charge to clear from the point.

But at low field, successive corona pulses occur with lower [illegible] size of the conduction charge. This is suggestive of the [illegible] states. Being current dependent, the greater density of [illegible] conduction charges will increase the effective [illegible] corona possible at an earlier stage in the drift [illegible]

The difference between the visual appearance [illegible] being much like a high frequency [illegible] bright channel, extending some way [illegible] channel when the regeneration [illegible]

AD-A190 507 THE GROWTH POTENTIAL OF CORONA DISCHARGES FROM AIRCRAFT FLYING IN PRECIPI..(U) UNIVERSITY OF MANCHESTER INST OF SCIENCE AND TECHNOLOGY (ENGL.. J A BICKNELL 12 NOV 87 2/2

UNCLASSIFIED AFOSR-TR-87-1781 AFOSR-83-0003 F/G 4/1 NL

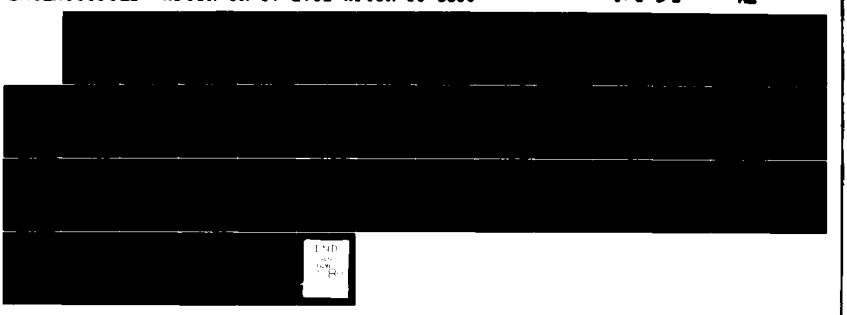

END

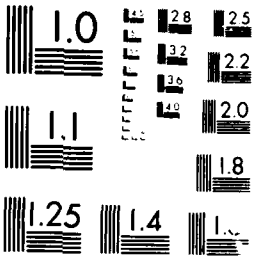

that the channel is still active. The effect of this may be to guide the second corona axially along the highest conductivity path; along the main branch of the streamer system, that is. That this channel is so very intense makes sense considering the existence of free electrons along it: when the streamer arrives at a point in the channel, it does not have to generate secondary electrons, there are plenty there already. The streamer growth would be that much more vigorous as a consequence.

A question remains: if the space charge can clear from the point in time to produce corona only a few μs after the primary streamer, why does this happen only occasionally, the normal interstreamer time being of the order of ms? The suggestion is that the decay by lateral diffusion, or whatever of the vibrational states decreases the effective ionization coefficient, to such a level that the space-charge has much further to travel away from the point before ionization is again possible there.

It may also be argued that the streamer channel, if still active, may generate a more efficient source of starter electrons for the discharge than would normally be available to an avalanche developing in virgin air (by photodetachment, or by detachment from negative ions which would otherwise diffuse away). Hence some critical time exists, beyond which second corona cannot form, and the usual ion clearing time (~ms) determines the corona frequency.

5.3.3 Growth and Magnitude of Second Corona

As already shown, the electron charge, Q_g, is very strongly related to the scale of the discharge. A question being addressed is how the discharge scale influences breakdown and streamer growth. Though no two measurements in this data set has been made at comparable reduced field, looking at the higher reduced field data reveals a very clear trend.

Taking the second corona conduction charge as a measure of the size of the second corona, and considering the influence of electron charge from the first corona, it seems the larger the electron charge, Q_{g1}, the larger the second corona conduction charge, Q_{c2}, whatever the reduced fields. Looking at the current records visually confirms this general behaviour (Fig.5.18). The records in longer gaps are, on the whole, more energetic, the second corona growing more vigorously than in shorter gaps. This is a very distinct trend, and the influence of Q_g is very large indeed, the second corona conduction charge can range between ~5 and 20nC as a result of the enhanced Q_g, in fact ranging from being larger or smaller than the first conduction charge as a result.

Summary

The trends in the data studied suggest that (a) the scale of the discharge has little influence on the second corona inception; (b) the dark time before the second corona inception is reduced as E/p increases, indicating that the clearing of the ions from the needle-tip region controls the second corona inception; (c) since a large conduction charge can reduce the dark time, it is suggested that vibrational states created in the primary discharge will increase the effective ionization coefficient, leading to quicker second corona inception. This is advanced as the controlling process - if no second corona has been produced before the vibrational states diffuse out of the channel (after 30μs), the ions have to clear in the usual ms time interval. Finally the difference between Mode (i) and Modes (ii) and (iii) is suggested to be due to the channel still being active for mode (i). With a non-zero residual free electron density in the channel, a second streamer would have a reservoir of starter electrons, would grow more strongly than usual and, furthermore, would be guided down the old channel, producing a single bright unbranched discharge.

Section 6. Discussion

6.1 Propagation in uniform field

6.1.1 Conduction Current Characteristics

To explain the time-to-peak and peak value of the streamer conduction current is a more interesting problem than it would at first seem. Differentiating Eq. 3.15 for the conduction current yields:

$$\frac{di_c(t)}{dt} = V^2 e^{-\eta tV}\left\{\frac{d}{d(tV)}A(tV) - \eta A(tV)\right\} \qquad \text{Eq.6.1}$$

6.1.1.a Problems with an Exponential Model

If A(x) is an exponential, $A(x) = Be^{\gamma x}$, $dA(tV)/d(tV) = \gamma A(tV)$, and solution of Eq.6.1 to find the maximum of i_c, requires that $\gamma = \eta$. In other words, an exponentially growing generation function A(x) would lead to the current surviving to reach the point always either outstripping the attachment, or be overtaken by it, according to whether γ is $>$ or $<\eta$, respectively. This is apparently in conflict with the choice made earlier to fit an exponential to the charge generation rate curves, δQ and suggests that the exponential growth rate assumed throughout the discussion of δQ cannot be correct.

In fact the measured (assumed exponential) growth frequency of δQ is ~5 to 10MHz, greater than the attachment frequency, on the whole. Consequently, run-away growth in i_c might be indicated. But note that (Eq.3.16), $\delta Q(t) = A(v_s t)v_s$. The measured values, Γ, of the growth frequency of δQ are obtained by fitting an exponential relationship, $\delta Q(t) = Be^{\Gamma t}$ (Eq. 5.5) to the data. Substituting in Eq. 3.16, and putting $x = v_s t$, yields:

$$A(x) = (B/v_s)e^{\Gamma x/v_s} \qquad \text{Eq.6.2}$$

which corresponds with the assumed exponential growth in A(x): $A(x) = \lambda e^{\gamma x}$ (section 5.5.6) given that $\lambda = B/v_s$ and $\gamma = \Gamma/v_s$. Hence γ, the (spatial) growth coefficient for A(x) ($\sim 25m^{-1}$) is below the attachment coefficients ($\eta \sim 100m^{-1}$) measured at the same time, and

the tail of the conduction current will be predicted to be a strongly decaying current regime, as is indeed observed.

6.1.1.b Time-to-Peak/Power-Law Model

The behaviour of i_c, as defined by Eq.3.15, can easily be made to peak by using any function growing more slowly than exponentially. For example, as discussed by Bicknell & Shelton (1986), a simple power law of the form:

$$A(x) = \Lambda x^n \qquad \text{Eq.6.3}$$

yields a time-to-peak, $t_{pk} = n/\eta V$ and the value of this,

$$i_c(max) = \Lambda V (t_{pk})^n e^{-\eta t_{pk} V} = \Lambda V (n/\eta)^n e^{-n} \qquad \text{Eq.6.4}$$

Though this still cannot explain the clear levelling-out of $i_c(max)$ as E/p increases (Fig.5.2, section 5.2.1), for it is clear that if A(x) grows more strongly, that is if Λ or n increase, then $i_c(max)$ will increase also, a prediction of this simple model completely at odds with observations. (Though at least a peak of some kind is indicated; an improvement over the exponential model.)

6.1.1.c Timescales

The behaviour of the peak in the conduction current is consdierably complicated by the timescales involved. The peak occurs within ~200ns at most and ignoring the more rapid drift in the tip region, this corresponds to a distance of ~8mm at electron speeds of 40km/s. Hence the portion of channel which contributes to the peak is close enough to the needle-end for the conditions there to determine the magnitude of the peak.

The proposition that it is the larger scale of the streamer systems which is responsible for the dependence of the conduction current maximum on the electrode spacing is completely ruled out by the foregoing, as by the time the conduction current has peaked, the streamer will, on the whole, have advanced just 4cm (at 200km/s) and the remaining portion of the channel, not having been formed cannot possibly contribute to the size of the peak in the conduction current. This ignores, of course, low pressure stream-

ers, where the low attachment rate causes the peak to occur after the streamer transit. Even than, for electrons to tavel the shortest channel length of 5.3cm requires ~1.3μs.

Whatever the pressure, from the above discussion it can be categorically stated that a mature channel does not bear on the conduction current peak, just its lower portion, and generally only the first cm or so is involved. In thundercloud streamer systems, this argument is more forceful: the part of the channel deciding the peak in i_c is decoupled from the remainder of the streamer system.

6.1.1.d Laplacian Field

How then can there possibly be the obseved dependence of $i_c(max)$ on propagation distance reported in section 5.2.1? Or even a peak of any kind, since the streamer growth seems to be at least roughly exponential (section 5.2.3)? Worse still the simple power-law model, Eq.6.3 for A(x) implies that $i_c(max)$, whilst at least defined, will not depend on the scale of the discharge since this is not taken into account, nor can it explain the levelling-out as E/p increases.

Returning to the variation of the maximum in i_c with electrode spacing, this has already been shown not to be a result of the longer propagation in the longer inter-electrode gaps, and it is inferred that the Laplacian field distribution is somehow different near the point in such situations.

The les Renardieres Groupe (Resultats de 1973) have calculated point-plane per-unit fields for a 5m and 10m electrode spacing with the same conical point (Fig.6.1). The general conclusion is that the enhanced field region extends further out from the point in the small-gap case. Hence it can at least be inferred that the small gap stramers get off to a better start and on account of the extended tip-region will tavel into the remainder of the gap with a larger initial tip potential. The smallness of the region of channel contributing to the peak in i_c means that effects such as this, operative near the needle-end, can have a large influence on the value of the peak. This, at least in principle, explains the low gap-length arm of the minimum in Fig.5.2.

In fact, the measurements of Sadik(1980) show that streamers launched from a

needle at a few kV above the anode potential grow initially as they propagate into the gap. In this case, the needle is at earth potential, but the ambient potential in the gap at the location of the needle-end were it not there would have been ~ En, where n is the height of the needle-end. This will drop away in a distance (see the le Renardieres Groupe results) which increases as the electrode spacing falls. So the potential gradient at the end of the needle is broadly independent of the gap spacing, but falls off more slowly the closer the electrodes are. This is the effect sought. The enhanced growth initially will lead to an increasing conduction current, falling thereafter as attachment takes over from the (comparatively) weaker growth further into the gap once the needle has been left behind. By then the maximum has been determined, as the first cm or so only of the channel contributed to the maximum and the maximum will not depend on the applied reduced field.

The growth observed in conduction current peak as gap length increases cannot continue indefinitely and so, given the large spread in the data, this is ignored as not being significant. An idealized distribution would decrease from some high value reaching a constant level as the gap passed some critical length.

6.1.2 Streamer Growth

The investigation of streamer growth, which was the main object of this study, has most often been undertaken in non-uniform point-plane geometry. So the slant of this discussion must necessarily be rather different from that normally encountered in streamer physics literature.

Studies in point-plane geometry have tended to concentrate on the range of the streamers, for the monotonic, steep fall in the Laplacian field leads to streamers dying throughout their life under these conditions. By contrast the streamers can be expected to grow at a uniform rate in the (quasi-)uniform applied fields used in this investigation. This is dramatically exemplified by the experimental electron charge curves (Fig.5.5), which show that Q_g increases by an order of magnitude as a function of the discharge scale, indeed increasing exponentially with streamer propagation length.

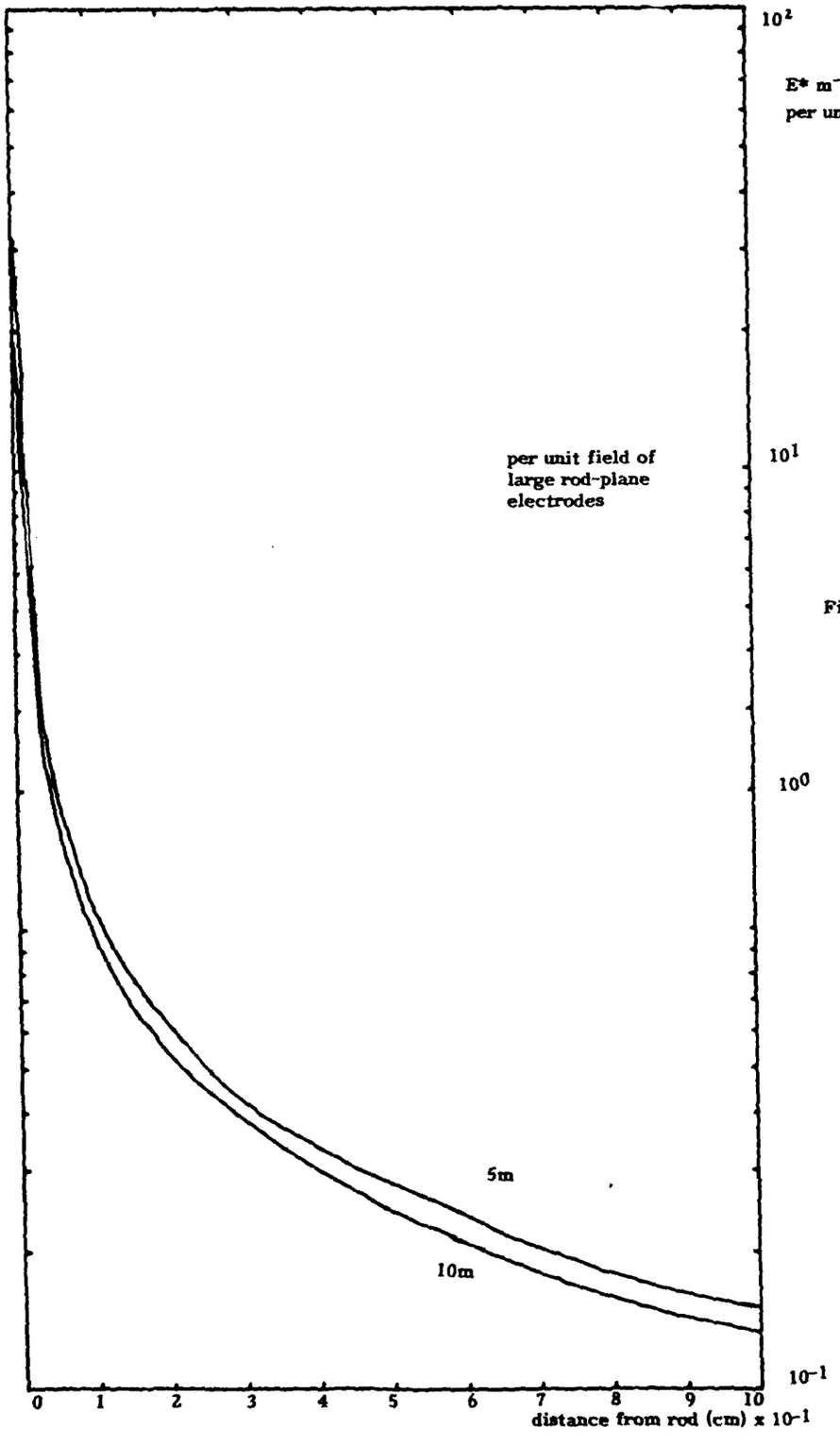
10^2
E* m^{-1}
per unit field
per unit field of
large rod-plane
electrodes
10^1
10^0
5m
10m
10^{-1}
0 1 2 3 4 5 6 7 8 9 10
distance from rod (cm) x 10^{-1}

Fig. 6.1

6.1.2.a Growth Frequency,

In an attempt to characterize the growth of the streamer system, the parameter δQ was defined (section 3.5.1), the charge generation or injection rate and it's growth frequency, , measured (section5.2.6,Fig.5.13). Conceptually this is a little difficult to visualize at first, but consider that the charge injection (or generation) rate is just the charge generated in the discharge (allowing for attachment) needed to satisfy charge conservation per unit time. It is hence representative of, if not actually equal to the current in the streamer active region. Thus the growth frequency, , of this parameter can be thought of as the growth frequency of the charge in the streamer tip region. This is what has beren measured.

It will be recalled that Γ was found, within a large experimental spread, to be roughly linearly dependent on E/p, and independent of pressure and gap length. Actually a better formulation for Γ is a square-root function, for it must fall-off to zero at the stability field. Undue significance should not be attached to the particular form given: *the spread of the data is such that many different formulations may be compatible with the measurements.*

6.1.2 b Spatial Growth of $Q_g(max)$

Plotting the spatial growth (Fig.5.6) of $Q_g(max)$ fleshes out a problem already implied by the above: how can the spatial growth apparently not depend strongly on the applied reduced field, when the growth rate (Γ) increases broadly linearly with the same parameter? Especially considering that the possibility of a charge or energy availability mechanism limiting $Q_g(max)$ is thought (section 5.2.3) to be incompatible with the phenomena, and that the cathodic injection and charge along the channel are both thought to be proportional to the system size (in the case of exponential growth), and so high charge injection from the cathode cannot be invoked to explain the phenomena either - a weakly growing streamer system will have less charge injection from the cathode and less charge residing along the channel: the process cannot be separated. In any case, the charge in-

jection is small compared with the free charge residing on the channel.

The weak spatial growth in $Q_g(max)$, then, is not an experimental construct but a genuine property of the discharge. In attempting to show how this can be consistent with an exponentially growing streamer function, A(x), it is advantageous to collect together the results derived earlier for the free charge in the gap.

6.1.2.c Channel Model; Summary

A channel function, $\lambda(x,t)$ and streamer function, A(x) were introduced, $\lambda(x,t)$ being the instantaneous linear charge density along the channel, A(x) being the charge density added by the streamer active region at a particular positon, $x=v_s t$. They are related, in a coordinate system where the charge produced at X drifts to x at time t, by the relation:(Fig.5.7)

$$\lambda(x,t) = A(X)e^{-\eta(X-x)} \qquad X = \left(t+\frac{x}{v_e}\right)V \tag{3.17}$$

The charge on the channel as a whole can be found by integrating Eq.3.17 for specific forms of A(x). In the case of an exponential, $A(x)=\Lambda e^{\gamma x}$

$$Q_g(d) = \int_0^d \lambda(x)\,dx$$

$$= \Lambda \frac{v_e}{\gamma V-\eta(V-v_e)} \left\{\exp\frac{dV(\gamma-\eta)}{v_s}\right\}\left\{\exp\left(\frac{\gamma V-\eta(V-v_e)}{v_e}\right)d-1\right\} \tag{3.18}$$

This is plotted in Fig.3.14 for typical values of the parameters, providing at least qualitative agreement with the phenomena. In the case where the current in the channel base has decayed to zero, Eq.3.18 can be integrated backwards along the channel to ∞, yielding the free charge in the gap in the limit where the conduction current is zero:

$$Q_g = \int_0^\infty A\left(\left(1-\frac{V}{v_s}\right)y\right)\exp\left(-\eta y V/v_s\right)dy . \tag{4.2}$$

This evaluates to the following for different forms of A(x):

$A(x)=$	Λ	$\Lambda e^{\alpha x}$	Λx^{n}
$Q_g(d)=$	$\frac{\Lambda}{\beta}$	$\frac{\Lambda e^{\alpha d}}{\alpha(1-V/v_s)+\beta}$	U_n where $U_0=\frac{\Lambda}{\beta}$; $U_n=\frac{\Lambda d^n}{\beta}+\frac{n(1-V/v_s)U_{n-1}}{\beta}$

$$\left[\beta=\eta V/v_s.\quad V=\frac{v_s v_e}{v_s+v_e}.\right]$$

6.1.2.d Experimental values of Parameters

In trying to relate these formulations to the experimentally determined parameters, one first notes that the growth frequency, Γ, of δQ defined by

$$\delta Q = Be^{\Gamma t} \tag{5.5}$$

can be related to A(x), according to the discussion above:

$$A(x) = \left(B/v_s\right)e^{\Gamma x/v_s} \tag{6.2}$$

Experimentally, the observed variation of the parameters can be represented by:

$$\Gamma = a_1\left(\frac{E}{p}-a_2\right)^{1/2} \quad \text{(MHz), E/p in V/cm.torr} \tag{6.5}$$

$$\frac{\eta}{p} = a_3 - a_4\left[\frac{E}{p}-a_5\right] \quad \text{(m.torr)}^{-1}\text{, E/p in V/cm.torr} \tag{6.6}$$

$$v_s = a_6 + a_7\left[\frac{E}{p}-a_8\right] \quad \text{(km/s), E/p in V/cm.torr} \tag{6.7a}$$

$$v_e = a_9\left(E/p\right)^{a_{10}} \quad \text{(km/s), E/p in V/cm.torr} \tag{6.7b}$$

Where a_1=4 MHz(V/cm.torr)$^{-\frac{1}{2}}$. a_2=4.5V/cm.torr, a_3=0.3(m.torr)$^{-1}$, a_4=2x10^{-4} /V, a_5=4V/cm.torr, a_9=10(km/s), a_{10}=0.715 and in Eq 6.7 the values of the coefficients are as follows:

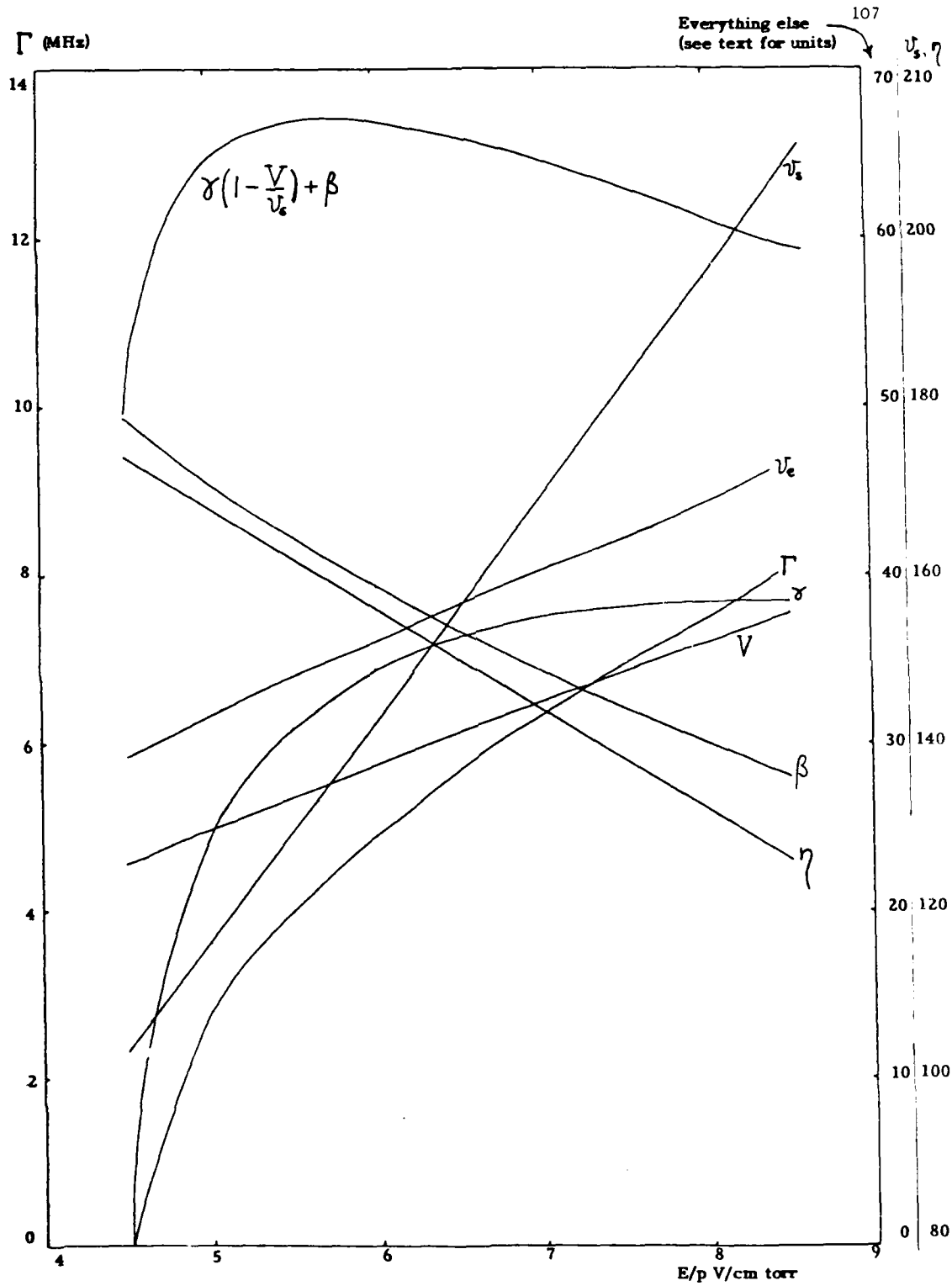
Γ (MHz)
Everything else
(see text for units)
ν_s, η
14
12
10
8
6
4
2
0
70 210
60 200
50 180
40 160
30 140
20 120
10 100
0 80
$\gamma\left(1-\frac{V}{\nu_e}\right)+\beta$
ν_s
ν_e
Γ
γ
V
β
η
4
5
6
7
8
9
E/p V/cm torr

Fig. 6.2

P torr	a_6 km/s	a_7 km/s(V/cm.torr)$^{-1}$	a_8 V/cm.torr
600	90	26.3	4
500	95	30.0	4
400	104	38.3	4

These are only a crude numerical fit to the data and are shown in Fig.6.2 superimposed on the appropriate graphs. No particular claims are being made about the particular form of Eq.6.5 to 6.7 above, the intention is to provide a simple characterization of the gross variability of the experimental parameters.

6.1.2.e Predictions of Channel Model

To see if the simple model presented above can explain the observed behaviour of Q_g, Eq. 3.18 can be rearranged by substituting $V=v_s v_e/(v_e+v_s)$ and $\gamma = \Gamma/v_s$, yielding

$$\frac{Q_g(d)}{\Lambda} = \frac{v_s+v_e}{\Gamma+\eta v_e}\exp\left\{\frac{d\,v_e}{v_s+v_e}\left(\frac{\Gamma}{v_s}-\eta\right)\right\}\left\{\exp\left(\frac{\Gamma+\eta v_e}{v_e+v_s}\right)d-1\right\} \quad (6.8)$$

which is expressed entirely in terms of parameters measured experimentally and which agree roughly with the range of values found by other experimenter (except v_e, which is calculated from a fit (Gallimberti, 1971a) to other worker's results). The form of this variation can be seen to be compatible with the stability field requiring $\Gamma=0$ for

differentiating with respect to d,

$$\frac{1}{\Lambda}\frac{dQ_g(d)}{dd} = \left(\frac{v_s+v_e}{\Gamma+\eta v_e}\right)\exp\left(\frac{d\,v_e}{v_s+v_e}\left(\frac{\Gamma}{v_s}-\eta\right)\right)\left(\frac{\Gamma+\eta v_e}{v_e+v_s}\right)\exp\left(\frac{\Gamma+\eta v_e}{v_e+v_s}\right)d$$
$$+\left(\frac{v_s+v_e}{\Gamma+\eta v_e}\cdot\frac{v_e}{v_s+v_e}\right)\left(\frac{\Gamma}{v_s}-\eta\right)\exp\left(\frac{v_e d}{v_s+v_e}\left(\frac{\Gamma}{v_s}-\eta\right)\right)\left(\exp\left(\frac{\Gamma+\eta v_e}{v_e+v_s}\right)d-1\right) \quad (6.9)$$

and equating to zero to find d_{max} yields:

$$d_{max} = \left(\frac{v_s + v_e}{\Gamma + \eta v_e}\right) \ln\left(V\left(\frac{1}{v_s} - \frac{\eta}{\Gamma}\right)\right) \qquad (6.10)$$

which is undefined for $\Gamma=0$, as required at the stability field. With positive values of Γ, d_{max} will be undefined for all realistic values of v_s, η and Γ. Furthermore, substituting in Eq. 6.8 yields $Q_g(max)$ corresponding to this value of d_{max} when the streamers are below stability:

$$\frac{Q_g(max)}{\Lambda} = \frac{v_s + v_e}{\Gamma + \eta v_e} \exp\left\{\frac{v_e}{\Gamma + \eta v_e}\left(\frac{\Gamma}{v_s} - \eta\right) \ln\left[V\left(\frac{1}{v_s} - \frac{\eta}{\Gamma}\right)\right]\right\}\left(V\left(\frac{1}{v_s} - \frac{\eta}{\Gamma}\right) - 1\right) \qquad (6.11)$$

Dependence on E/p

Using the values of Γ, η, v_e, v_s (and $\therefore$ of V), reported above, and plotted in Fig.6.2, $Q_g(d)/\Lambda$ has been evaluated for various values of E/p and d at 600 torr and the result is plotted in Fig.6.3. The stability field corresponds to $\Gamma=0$; this is artificially imposed on the numerical fit and corresponds to E/p=4.5V/cm.torr. It is clear that the interplay of the variation of Γ, η and v_s results in a fairly flat growth in Q_g(max), except near the stability field, when the curves for all distances considered, d, plunge downward. This simulates the behaviour of the experimentally determined plots of Q_g(max), Fig.5.5 (reproduced for comparison). The levelling-off of this plot has been shown not to be the result of some external parameter and is a real property of the discharge.

Long Discharges

This level growth in Q_g(max) is somewhat at odds with the expected form at large distances from the anode (Table 6.1 above). For exponential growth in A(x),

$$Q_g(d) = \frac{\Lambda e^{\alpha d}}{\alpha(1 - V/v_s) + \beta}$$

and this relation is plotted in Fig.6.4. It can be seen that there is indeed extremely strong growth in Q_g as the discharge propagates, Q_g/Λ reaching $\sim 10^{31}$ for d~2m and E/p~8.5V/cm.torr

Fig. 6.3

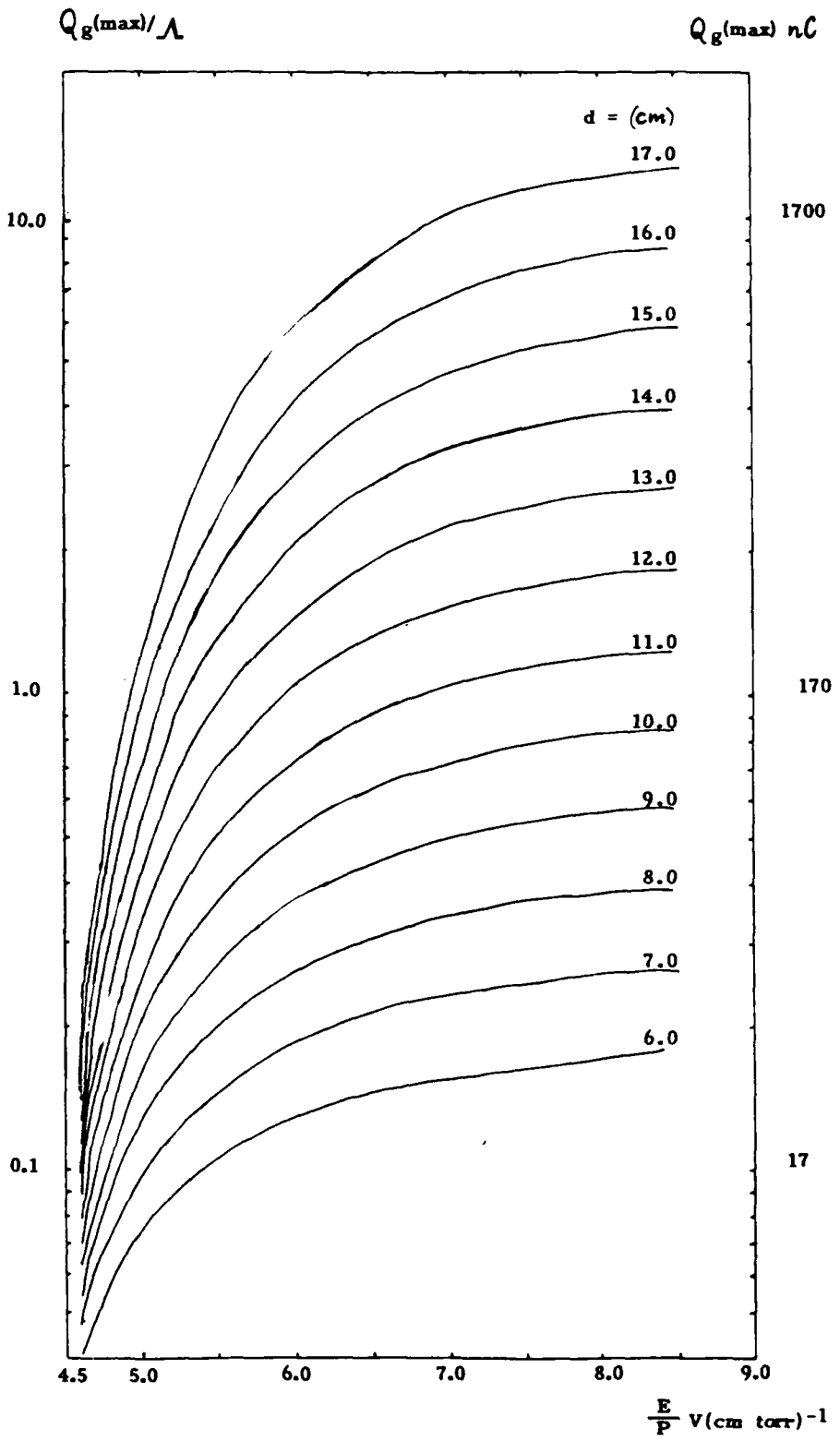
$Q_{g(max)}/\Lambda$
$Q_{g(max)}$ nC
d = (cm)
17.0
16.0
15.0
14.0
13.0
12.0
11.0
10.0
9.0
8.0
7.0
6.0
10.0
1.0
0.1
1700
170
17
4.5
5.0
6.0
7.0
8.0
9.0
$\frac{E}{P}$ V(cm torr)$^{-1}$

Fig. 5.5

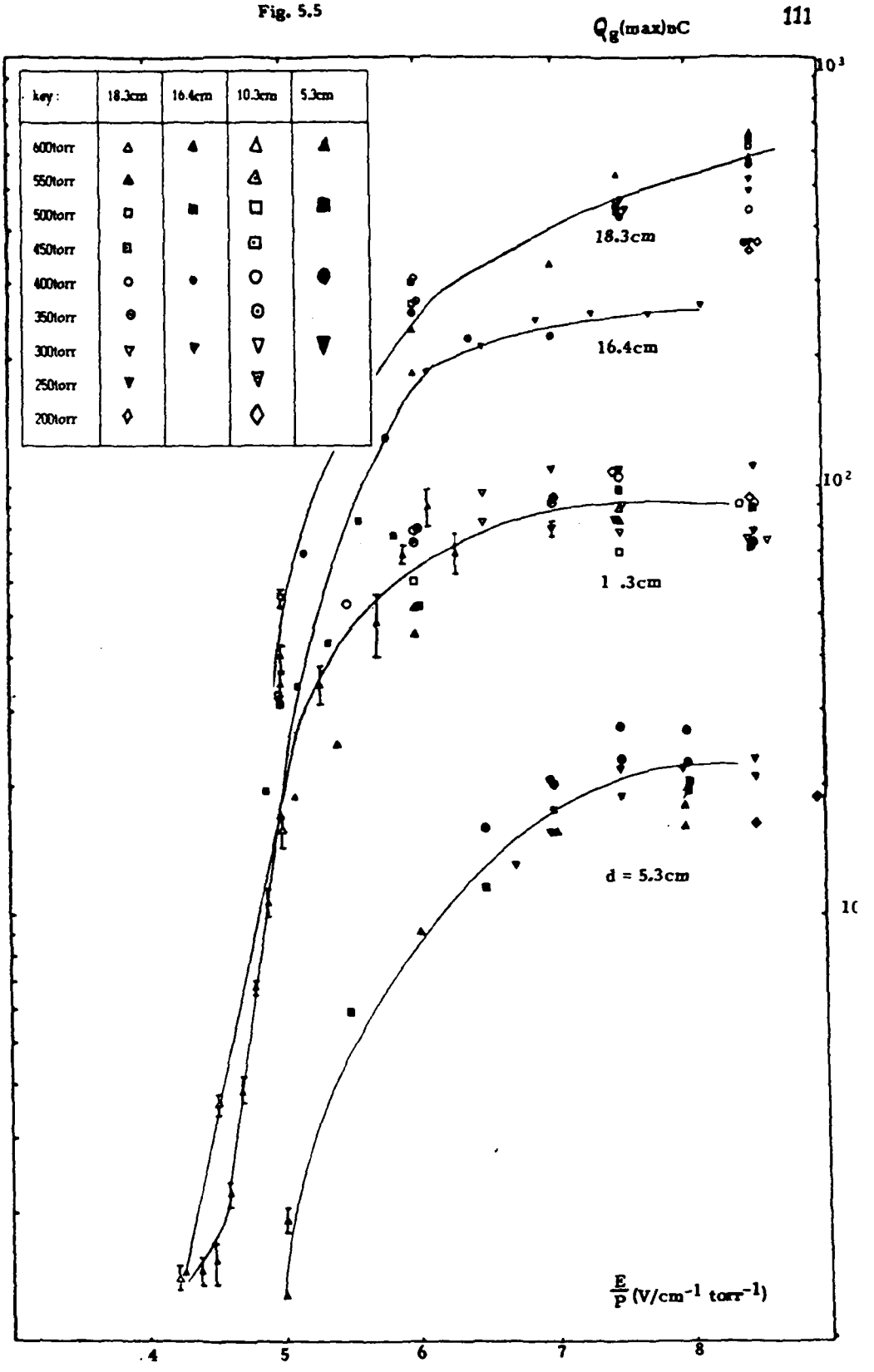
Q_g(max)nC
key :
18.3cm
16.4cm
10.3cm
5.3cm
600torr
550torr
500torr
450torr
400torr
350torr
300torr
250torr
200torr
18.3cm
16.4cm
1 .3cm
d = 5.3cm
10^3
10^2
10
.4
5
6
7
8
$\frac{E}{P}$ (V/cm^{-1} torr^{-1})

To obtain Q_g requires an estimate of the value of λ, the charge/unit length at the origin. This can be estimated from the minimum avalanche charge required for streamer formation, say q_{min}, together with the assumption that this charge is distributed over a channel length ~ channel diameter D so $\lambda \sim q_{min}/D$. With q_{min} 10^{-11}C (10^8) ions) and D~10^{-4}m then $\lambda \sim 10^{-7}$C m^{-1}. Using this value Q_g can be estimated as a function of reduced field and propagation distance. Typical values are shown in Fig. 6.4.

The problem of extrapolating a model which works perfectly well in the present electrode geometry to rather larger propagation distances is immediately apparent from this data. A reduced field of only 5 yields a free charge of ~10^{10}C in only 2m for example which is unrealistically large. These figures do however at least emphasise the rapid growth to be expected once the stability field is exceeded. It must be remembered also that this is not a net charge figure - there is an equal and opposite positive charge since the streamer channels contain a quasi-neutral plasma.

When assessing the growth of aircraft streamers from Fig.6.4 it is important to include two further factors:

(1) The streamers are unlikely to propagate in fields much greater than the stability field for the relevant pressure since any greater fields would most probably already have produced a breakdown:

(2) This stability field is pressure and, therefore, altitude dependent (Fig.4.1).

Given that just above the stability field growth would be expected to be significantly less than that indicated by Fig.6.4 then the growth in free charge would also be much lower than the 10^{10}C calculated above in the example given. More detailed measurements closer to the stability field than has been possible in the present investigation are required before making valid growth predictions.

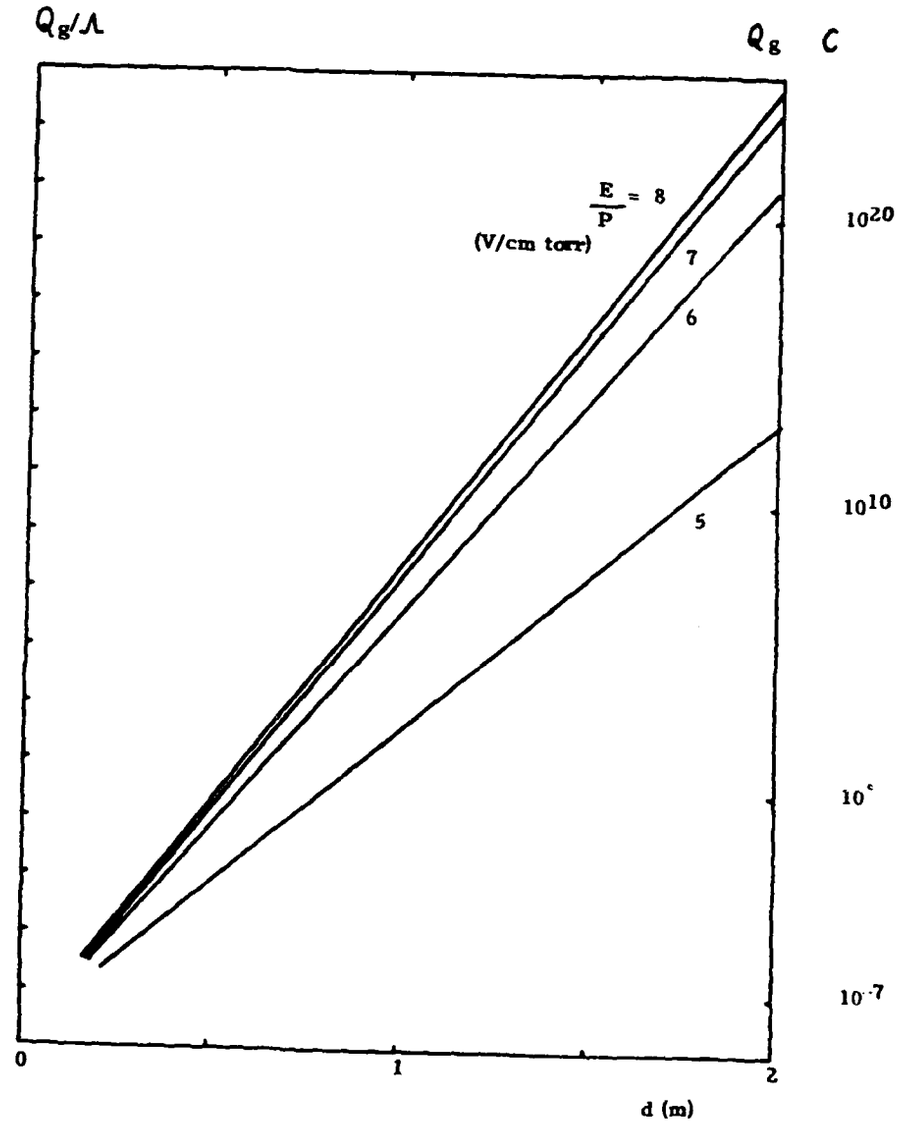

Fig. 6.4

Section 7: Summary and Conclusion

The concept of a positive corona streamer stability field such that streamer growth at large fields occurs leads naturally to the question of exactly how much growth might be expected for fields of large extent and what effect this growth might have on electrical breakdown. The fact that large scale quasi-uniform fields (i.e. >10's of metres) only occur in nature and that the behaviour is pressure dependent implies that this curiously neglected corner Of discharge physics may be enormously relevant to thundercloud conditions and the aircraft that fly in their vicinity.

This study has been aimed at characterising the streamer growth in quasi-uniform fields since the large scale fields in nature will necessarily be of this type (div $E = \sigma/\varepsilon_o$ and σ, the space charge density, is low). These streamers are typical of those that would be generated at aircraft surfaces. The 3-electrode arrangement employed together with the analytical procedure used, based on the Schockley-Ramo theorem, has allowed the free charge in the streamer system to be determined as a function of time and for a range of fields and pressures. In addition, the rate of addition of free charge - and generation current - has been found for the first time. The approach adopted also permits a simultaneous measurement of important parameters such as attachment frequency (coefficient) and streamer velocity together with the growth frequency which characterizes the streamer growth pattern in terms of a single parameter, Γ. Furthermore, the stability field for a given pressure may be determined unambiguously.

There is a natural range of fields and pressures - or more appropriately a range of reduced fields - the lower limit set by the streamer onset and the upper limit by breakdown. From onset to the immediate prebreakdown condition, the behaviour is one of variation on a single theme. Although, from a practical point of view the breakdown is arguably the most crucial event it is, of course, necessary to establish norm behaviour so that departures from this norm may be recognised. The data referred to above (Section 5) indeed quantify this norm.

Prebreakdown conditions are rather more difficult to quantify because of their statistical nature. In all cases, however, the usual primary streamer event with the asso-

ciated decay, due to electrical attachment, of both conduction and displacement currents - equivalent to the decay of the free charge - is interrupted by the appearance of new ionisation. The attempt to categorise this phenomena is contained in Section 6. There is nothing particularly novel about this observation: a similar pattern is observed in long rod-plane breakdown with the appearance of the second corona in the vicinity of the highly stressed electrode. What is unusual though is the low reduced field at which this phenomena is observed. A breakdown has been observed for a reduced field of only 6V/cm.torr whilst examples of multiple corona are shown in the text (e.g. Fig.5.14) for similar values; this kind of event has a low probability but which is, nonetheless, finite. At a pressure of 500 torr the breakdown field might than be 3kv/cm which is within the range measured for a thundercloud. An equally important observation concerns the effect of propagation distance.

Throughout, the effect of streamer propagation distance has been particularly closely observed because of the interest in extending any conclusion drawn to distances of several metres so that a valid comparison with aircraft streamers might be made. Generally, the effect of extending streamer length for otherwise similar conditions of field and pressure makes little difference to the measured parameters. Total free charge obviously increases because of increasing propagation but, surprisingly, peak conduction currents (due to the primary streamer) actually decrease (Section 5). However, for those prebreakdown events which include the appearance of additional ionisation there is a clear effect of distance. For the smallest gap studied (5.3cm) then the second corona event exhibits a peak current of the same order as the primary streamer current whilst, for longer gaps (up to 18.3cm) the second corona current may be 7-8 times larger than the primary current <u>for the same E/p</u>. Table 5.1/2 contain data illustrating this point. Unfortunately an insufficient number of events were recorded to provide an exhaustive study - because of the relative rarity of the events and the need to make comparisons for similar values of E/p at different propagation lengths - but the trend is unmistakable. If confirmed then this could well lower further the field required for breakdown in the presence of long streamers or, alternatively, increase the probability of a breakdown at the

higher reduced fields.

Phenomenology apart, the mechanism of such a breakdown is not clear. The model, developed in Section 3 and extended in Section 6, is useful because is calculates reasonably well the growth of free charge with distance as a function of reduced field and so provides useful predictive information since any breakdown must depend on the generation of such free charge. It is difficult to assess the role of the cathode definitively although two effects are observable, namely:

(i) electon injection at streamer arrival, and

(ii) the appearance of fast ionising waves, the generation of which appear to coincide with streamer arrival at the cathode. There is some evidence that the waves - if indeed they are waves - can enhance the ionisation near the origin of the streamer system (e.g. Fig.4.7).

The magnitude of the electron injection is relatively small and takes place at such large distances from the origin (i.e. d/v_e timescale of the breakdown) so that it is difficult to see how a contribution to the breakdown could be made in the present geometry and, if a valid mechanism must be equally relevant to aircraft streamers, then such a contribution must be ruled out since the only cathode-like structure, namely the precipitation, would provide considerably less local electron injection. That streamer impact with such precipitation might yield ionising waves must, however, remain a plausible possibility. An assessment of this has already been presented elsewhere by Bicknell and Shelton (1986).

The growth of free charge represented by equation 6.2

$$A(x) = \Lambda e^{\gamma x}. \qquad \gamma = T'/v_s$$

suggests an alternative approach to the problems of providing an explanation for long

streamer breakdown. Thermalisation of the streamer channel requires an electron density of $\tilde{>}10^{23}m^{-3}$ compared with a measured value for small gap streamers of $\sim10^{21}$ m^{-3}, If n(x) is the electron density at x then assuming a similar constant cross-section for each channel

$$n(x) = n(0)N(0)e^{\gamma x}/N(x)$$

where N(x) is the number of channels at x. Clearly the requirement that the electron density remains at the value n(0) ($\sim10^{21}m^{-3}$) implies that the channel number growth rate is similar to the charge growth rate or

$$N(x) = N(=.)e^{\gamma x}$$

There is little experimental data available regarding the behaviour of N(x) particularly at sub-atmospheric pressure but replotting the data of Bicknell, Sadik & Tang (1980) for the growth of N(x) at E/p=7.92 (atmospheric pressure) suggests a value for γ of 20.5. At the same E/p, results from this present study (Fig.6.2) provide γ ($=\Gamma/v_s$) of 35.6. On this evidence then the electron density is growing with propagation distance as

$$n(x) = n(\bullet)e^{\ 15.1x}$$

or if the required enhancement is 10^2 ($10^{23}/10^{21}$) then the required x is ln100/15.1 $\sim$ 30cm. For lower reduced fields this distance would be larger because of the smaller difference between the two growth rates. An investigation conducted in gaps larger than the present 20cm arrangement with facilities to monitor γ both for A(x) and N(x) may well be fruitful and conclusive.

REFERENCES

Bicknell, J A and Shelton R	1985	ICOLSE, Paris
	1986	IAGCLSE, Dayton, Ohio
Clifford, D W	1980	FAA/NASA/FIT Symp. Lightning Tech., Hampton, Virginia
Elliason and Kogelshatz	1986	Brown Boveri Report
Gallemberti, I	1972	J.Phys.D, 5, 2179
	1971	University of Padua Report
Hartmann, G	1974	C.R.Acad.Sci., Paris, B, 270, 309
Hudson, G C and Loeb, L B	1961	Phys.Rev., 123, 29-46
Jeans, J	1927	Electricity & Magnetism, p160, C.U.P.
Marode, E	1975	J.Appl.Phys, 46, 2005-20
Phelps, C T and Griffiths R F	1976	Phys.Rev., 123, 29-46
Ramo, S	1939	Proc. I.R.E., 27,584
Sadik, A and Bicknell, J A	1980	VI Int. Conf. Atmos. Elect., Manchester, 1980
Sigmund, R S	1978	Electrical Breakdown in Gases (ed. Meek & Craggs) Wiley

Appendix A

```
{*****************************************************************************
   program "h"
     by Rod Shelton, updated:06.04. 87
     this program reads data files created by "corona" and "sample".
     the data can be analysed in real time, using cursor-driven routines
     the input file must be called "B:D        .    "
*****************************************************************************}
PROGRAM DATAUSE1;
CONST
 SKEW = 105;
  TYPE
  MATRIX=ARRAY[0..3,0..3] OF REAL;
   VECTOR=ARRAY[0..3] OF REAL;
       RA=ARRAY[0..255] OF REAL;
  VAR
 INTC,INTD1,INTD2,INTD3:REAL;
 A:MATRIX;
 C,ERR:VECTOR;
 NA:INTEGER;
 HEADING:ARRAY[1..80]OF CHAR;
 ICMAX,TFK,IDPOSMAX, IDNEGMAX,TX,QGMAX,QRATE,QERROR,DOSTART,DOEND:REAL;
 DQRATE,DQERROR,DQINJECTED,REDUCEDFIELD:REAL;
 CALL23,CALL26,POLYFITFOUND:BOOLEAN;
 STATUS,PSTATUS:INTEGER;
  YH,VS,FITA,FITB,ERARATE:REAL;
 YG:INTEGER;
  GAPLEN,STRLEN,KVOLTS,VE,VS,VV,FIELD,PRE:REAL;
  FILENO:INTEGER;
 FILENUMBER,DATAFILE,DBASE:TEXT;
 BUTTONPRESSED,FIRSTTIME,UNDEFINED,DMP,GRSW,FITFOUND,CORRECTED:BOOLEAN;
 ENDPAGE,PFITFOUND:BOOLEAN;
 X1,X2,Y1,Y2,ZEROLEVEL,ARATE,INTEGRAL:REAL;
 XCUR,YCUR,XCHAN,YCHAN,BUTCHAN,IX1,IX2,IY1,IY2,IRESP,RBUT:INTEGER;
       IFREE:RA;
       PRESS,CLOCKVALUE,HUMID,XTIMB,YAMPL,RESISTOR:REAL;
 MINUS1,MINUS2:INTEGER;
 PZEROLEVEL,PARATE,PINTEGRAL:REAL;
 PIX1,PIX2,PIY1,PIY2:INTEGER;
 ICOND:RA;
 PPRESS,PCLOCKVALUE,PHUMID,PXTIMB,PYAMPL,PRESISTOR:REAL;
 PNRUN,PNXPTS,PNPOINTS,PFIRSTSAMPLE:INTEGER;
 PCHANNEL:CHAR;
       NRUN,NXPTS,NPOINTS,FIRSTSAMPLE,OLDXCUR,OLDYCUR:INTEGER;
 OLDIX1,OLDIX2:INTEGER;
       ACHAR,SELECTION,CHANNEL:CHAR;
{*****************************************************************************
   procedure wait
     no global usage
     waits for a time determined by the passed parameter
*****************************************************************************}
PROCEDURE WAIT(PERIOD:INTEGER);
  VAR COUNTER:INTEGER;
  BEGIN
  FOR COUNTER:=0 TO PERIOD DO COUNTER:=COUNTER
  END; (* of wait *)
{*****************************************************************************
   procedure svccode
     no global usage
     inserts machine code patch to enable svc data transfers
*****************************************************************************}
PROCEDURE SVCCODE;
  BEGIN  (*SVCCODE*)
  (* code for output to svc begins here *)
  (* the first n characters in memory starting at #F901 are read out *)
  (* n is the value in #F900 *)
  (* see assembler listing for more details *)
  (* ROD SHELTON... DEC '85 *)
  POKE16(#F910,#003A);  POKE16(#F912,#4FF9);
  POKE16(#F914,#0011);  POKE16(#F916,#13F9);
  POKE16(#F918,#471A);  POKE16(#F91A,#B2DB);
  POKE16(#F91C,#DA0F);  POKE16(#F91E,#F91A);
```

```
   POKE16(#F920,#D378);  POKE16(#F922,#0DB1);
   POKE16(#F924,#17C2);  POKE16(#F926,#C9F9);
   (* code for input from svc begins here *)
   (* n characters are read in from the svc, starting at #F901 *)
   (* n is the value in #F900 *)
   (* ROD SHELTON... DEC'85 *)
   POKE16(#F930,#003A); POKE16(#F932,#4FF9);
   POKE16(#F934,#0111); POKE16(#F936,#DBF9);
   POKE16(#F938,#0782); POKE16(#F93A,#37DA);
   POKE16(#F93C,#DBF9); POKE16(#F93E,#12B1);
   POKE16(#F940,#0D13); POKE16(#F942,#37C2);
   POKE16(#F944,#C9F9);
   (* CODE TO DUMP SVCSCREEN FOLLOWS *)
POKE(63824 ,CHR(62 ));
POKE(63825 ,CHR(32 ));
POKE(63826 ,CHR(50 ));
POKE(63827 ,CHR(255 ));
POKE(63828 ,CHR(255 ));
POKE(63829 ,CHR(50 ));
POKE(63830 ,CHR(255 ));
POKE(63831 ,CHR(255 ));
POKE(63832 ,CHR(14 ));
POKE(63833 ,CHR(5 ));
POKE(63834 ,CHR(30 ));
POKE(63835 ,CHR(13 ));
POKE(63836 ,CHR(205 ));
POKE(63837 ,CHR(5 ));
POKE(63838 ,CHR(0 ));
POKE(63839 ,CHR(14 ));
POKE(63840 ,CHR(5 ));
POKE(63841 ,CHR(30 ));
POKE(63842 ,CHR(10 ));
POKE(63843 ,CHR(205 ));
POKE(63844 ,CHR(5 ));
POKE(63845 ,CHR(0 ));
POKE(63846 ,CHR(14 ));
POKE(63847 ,CHR(5 ));
POKE(63848 ,CHR(30 ));
POKE(63849 ,CHR(27 ));
POKE(63850 ,CHR(205 ));
POKE(63851 ,CHR(5 ));
POKE(63852 ,CHR(0 ));
POKE(63853 ,CHR(14 ));
POKE(63854 ,CHR(5 ));
POKE(63855 ,CHR(30 ));
POKE(63856 ,CHR(76 ));
POKE(63857 ,CHR(205 ));
POKE(63858 ,CHR(5 ));
POKE(63859 ,CHR(0 ));
POKE(63860 ,CHR(14 ));
POKE(63861 ,CHR(5 ));
POKE(63862 ,CHR(30 ));
POKE(63863 ,CHR(0 ));
POKE(63864 ,CHR(205 ));
POKE(63865 ,CHR(5 ));
POKE(63866 ,CHR(0 ));
POKE(63867 ,CHR(14 ));
POKE(63868 ,CHR(5 ));
POKE(63869 ,CHR(30 ));
POKE(63870 ,CHR(2 ));
POKE(63871 ,CHR(205 ));
POKE(63872 ,CHR(5 ));
POKE(63873 ,CHR(0 ));
POKE(63874 ,CHR(6 ));
POKE(63875 ,CHR(255 ));
POKE(63876 ,CHR(197 ));
POKE(63877 ,CHR(219 ));
POKE(63878 ,CHR(178 ));
POKE(63879 ,CHR(7 ));
POKE(63880 ,CHR(218 ));
POKE(63881 ,CHR(132 ));
POKE(63882 ,CHR(249 ));
```

```
POKE(63883 ,CHR(219 ));
POKE(63884 ,CHR 177 ));
POKE(63885 ,CHR(95 ));
POKE(63886 ,CHR(14 ));
POKE(63887 ,CHR(5 ));
POKE(63888 ,CHR(213 ));
POKE(63889 ,CHR(245 ));
POKE(63890 ,CHR(197 ));
POKE(63891 ,CHR(205 ));
POKE(63892 ,CHR(5 ));
POKE(63893 ,CHR(0 ));
POKE(63894 ,CHR(193 ));
POKE(63895 ,CHR(241 ));
POKE(63896 ,CHR(209 ));
POKE(63897 ,CHR(205 ));
POKE(63898 ,CHR(5 ));
POKE(63899 ,CHR(0 ));
POKE(63900 ,CHR(193 ));
POKE(63901 ,CHR(5 ));
POKE(63902 ,CHR(194 ));
POKE(63903 ,CHR(132 ));
POKE(63904 ,CHR(249 ));
POKE(63905 ,CHR(219 ));
POKE(63906 ,CHR(178 ));
POKE(63907 ,CHR(7 ));
POKE(63908 ,CHR(218 ));
POKE(63909 ,CHR(161 ));
POKE(63910 ,CHR(249 ));
POKE(63911 ,CHR(219 ));
POKE(63912 ,CHR(177 ));
POKE(63913 ,CHR(95 ));
POKE(63914 ,CHR(14 ));
POKE(63915 ,CHR(5 ));
POKE(63916 ,CHR(213 ));
POKE(63917 ,CHR(245 ));
POKE(63918 ,CHR(197 ));
POKE(63919 ,CHR(205 ));
POKE(63920 ,CHR(5 ));
POKE(63921 ,CHR(0 ));
POKE(63922 ,CHR(193 ));
POKE(63923 ,CHR(241 ));
POKE(63924 ,CHR(209 ));
POKE(63925 ,CHR(205 ));
POKE(63926 ,CHR(5 ));
POKE(63927 ,CHR(0 ));
POKE(63928 ,CHR(58 ));
POKE(63929 ,CHR(255 ));
POKE(63930 ,CHR(255 ));
POKE(63931 ,CHR(61 ));
POKE(63932 ,CHR(194 ));
POKE(63933 ,CHR(85 ));
POKE(63934 ,CHR(249 ));
POKE(63935 ,CHR(201 ));
 (* ROUTINE FOR DOUBLE DENSITY *)
  END; (* OF SVCCODE *)
  (* N.B.
     the space from #F900 to #F945 is thus used by these routines
     the buffer is from #F902 to #F90F and can hold 15 characters only
     for the first character is clearly a control constant. *)
(*************************************************************************
   function entier
     returns the greatest integer <= x
*************************************************************************)
FUNCTION ENTIER(X:REAL):INTEGER;
BEGIN
 IF X<0 THEN ENTIER:=TRUNC(X)-1 ELSE ENTIER:=TRUNC(X);
END;
(*************************************************************************
   function frac
     returns the value x-entier(x)
*************************************************************************)
FUNCTION FRAC(X:REAL):REAL;
```

```
BEGIN
 FRAC:=X-ENTIER(X);
END;
(*****************************************************************************
Function Y(X)
*****************************************************************************)
FUNCTION Y(X:INTEGER):INTEGER;
BEGIN
Y:=YG+ENTIER(IFREE[X]/YH);
END;
PROCEDURE SHOWMATRIX(VAR A:MATRIX;VAR NA:INTEGER);
VAR
 ROW,COL:INTEGER;
BEGIN
 FOR ROW:=0 TO NA DO
  BEGIN
   WRITE('[ ');
   FOR COL:=0 TO NA DO WRITE(A[ROW,COL],    );
   WRITELN(']');
  END;
END;
PROCEDURE REDUCE(VAR A,B:MATRIX;VAR NA,NB,I,J:INTEGER);
VAR
 ROW,COL:INTEGER;
BEGIN
 FOR ROW:=0 TO NA DO
  FOR COL:=0 TO NA DO
   BEGIN
    IF (ROW<I) AND (COL<J) THEN B[ROW  ,COL  ]:=A[ROW,COL];
    IF (ROW<I) AND (COL>J) THEN B[ROW  ,COL-1]:=A[ROW,COL];
    IF (ROW>I) AND (COL<J) THEN B[ROW-1,COL  ]:=A[ROW,COL];
    IF (ROW>I) AND (COL>J) THEN B[ROW-1,COL-1]:=A[ROW,COL];
   END;
 NB:=NA-1;
 SHOWMATRIX(B,NB);
END;
FUNCTION DETERMINANT(VAR A:MATRIX;VAR NA:INTEGER):REAL;
VAR
 DET:REAL;
 B:MATRIX;
 NB,I,F:INTEGER;
 COL:INTEGER;
BEGIN
 IF NA=0 THEN DET:=A[0,0]
 ELSE
  BEGIN
   DET:=0;
   FOR I:=0 TO NA DO
    BEGIN
   COL:=0;
     REDUCE(A,B,NA,NB,COL,I); (* ELIMIATES COL(I) & ROW(0) ..RESULT:=B *)
     IF ODD(I) THEN F:=-1 ELSE F:=1;
     DET:=DET+F*A[0,I]*DETERMINANT(B,NB);
    END;
  END;
 DETERMINANT:=DET;
END;
FUNCTION COFACTOR(VAR A:MATRIX;VAR NA,I,J:INTEGER):REAL;
VAR
 B:MATRIX;
 ROW,COL,NB,F:INTEGER;
BEGIN
 REDUCE(A,B,NA,NB,I,J);
 IF ODD(I+J) THEN F:=-1 ELSE F:=1;
 COFACTOR:=F*DETERMINANT(B,NB);
END;
FUNCTION POLY(VAR X:INTEGER):REAL;
VAR
 A:REAL;
 N:INTEGER;
BEGIN
 A:=0;
```

```
 FOR N:=0 TO 3 DO A:=A+C[N]*POWER(X,N);
 POLY:=A;
END;
PROCEDURE POLYFIT;
VAR
 J,K,NB,ROW,COL,I:INTEGER;
 RESIDUAL,DETA,HHH:REAL;
 B:MATRIX;
 Y:VECTOR;
BEGIN
 FOR J:=0 TO 3 DO
  BEGIN
   Y[J]:=0;
   C[J]:=0;
   FOR K:=0 TO 3 DO A[J,K]:=0;
  END;
 FOR J:=IX1 TO IX2 DO
  BEGIN
   FOR K:=0 TO 3 DO
    BEGIN
     Y[K]:=Y[K]+IFREE[J]*POWER(J,K);
     A[0,K]:=A[0,K]+POWER(J,K);
    END;
   FOR K:=1 TO 3 DO A[K,3]:=A[K,3]+POWER(J,(K+3));
  END;
 FOR ROW:=1 TO 3 DO
  FOR COL:=0 TO 2 DO
   A[ROW,COL]:=A[ROW-1,COL+1];
 NA:=3;
 WRITELN('MATRIX COMPUTED');
 SHOWMATRIX(A,NA);
 DETA:=DETERMINANT(A,NA);
 WRITELN('DETERMINANT FOUND');
 FOR I:=0 TO 3 DO
  FOR J:=0 TO 3 DO
   C[I]:=C[I]+COFACTOR(A,NA,J,I)*Y[J];
 WRITELN('COFACTOR MATRIX & INVERSION COMPLETE');
 WRITELN('DETA:= ',DETA);
 FOR I:=0 TO 3 DO C[I]:=C[I]/DETA;
 RESIDUAL:=0;
 FOR I:=IX1 TO IX2 DO
  RESIDUAL:=RESIDUAL+SQR(IFREE[I]-POLY(I));
 HHH:=RESIDUAL/(DETA*(IX2-IX1+1-4));
 WRITELN('RESIDUALS COMPUTED');
 FOR I:=0 TO 3 DO
  BEGIN
   REDUCE(A,B,NA,NB,I,I);
   ERR[I]:=SQRT(HHH*DETERMINANT(B,NB));
  END;
 WRITELN('ABSOLUTE ERRORS IN COEFFICIENTS CALCULATED');
 POLYFITFOUND:=TRUE;
 WRITE('>'); READLN;
END;
(*****************************************************************************
   fuction yfit;
     finds the (real) value of the exponential fit done by expfit
*****************************************************************************)
FUNCTION YFIT(X:INTEGER):INTEGER;
VAR J:REAL;
BEGIN
 IF FITFOUND THEN
  BEGIN
   J:=EXP(FITB);
   IF (IFREE[IX1]<0) THEN J:=J*(-1);
   J:=J*EXP(FITA*X)/YH;
(* YFIT:=YG+ENTIER(J);*)
  END
  ELSE IF POLYFITFOUND THEN J:=POLY(X)/YH;
 YFIT:=YG+ENTIER(J);
END;
(*****************************************************************************
   procedure normalscreen
```

```
      no global usage
      restores 80 column format to svc display
*****************************************************************************)
PROCEDURE NORMALSCREEN;
  VAR C:INTEGER;
BEGIN
  C:=CPM(6,27);
  C:=CPM(6,49);
END; (* of normalscreen *)
(*****************************************************************************
   procedure clearscreen
     no global usage
     clears the screen exiting with svc in graphics format
*****************************************************************************)
PROCEDURE CLEARSCREEN;
  VAR C:INTEGER;
  BEGIN
  NORMALSCREEN;
  C:=CPM(6,26);  (*  CURSOR HOME & CLEAR SCREEN  *)
  C:=CPM(6,27);
  C:=CPM(6,52);  (*  BACK TO GRAPHICS MODE  *)
  END;
(*****************************************************************************
   procedure point
     global usage: none
     requires graphics format
     draws a point at XX,YY
*****************************************************************************)
PROCEDURE POINT(XX,YY:CHAR);
VAR
 SKEWX:CHAR;
  BEGIN (* point *)
 IF (YY<=CHR(255)) AND (YY>=CHR(0)) THEN
BEGIN
 SKEWX:=CHR(ORD(XX)+SKEW);
  POKE(#F900,CHR(6));
  POKE(#F901,CHR(27));
  POKE(#F902,CHR(83));
  POKE(#F903,SKEWX);
  POKE(#F904,CHR(00));
  POKE(#F905,YY);
  POKE(#F906,CHR(00));
  USER(#F910);
 END;
  END;  (* of point *)
(*****************************************************************************
   procedure unpoint
      global usage: none
      requires graphics format
      rubs out anything at XX,YY
*****************************************************************************)
PROCEDURE UNPOINT(XX,YY:CHAR);
VAR
 SKEWX:CHAR;
BEGIN
 IF (YY>=CHR(0)) AND (YY<=CHR(255)) THEN
 BEGIN
 SKEWX:=CHR(ORD(XX)+SKEW);
  POKE(#F900,CHR(6));
  POKE(#F901,CHR(27));
  POKE(#F902,CHR(82));
  POKE(#F903,SKEWX);
  POKE(#F904,CHR(00));
  POKE(#F905,YY);
  POKE(#F906,CHR(00));
  USER(#F910);
 END;
END;
(*****************************************************************************
procedure cursorrow(x)
*****************************************************************************)
PROCEDURE CURSORROW(X:INTEGER);
```

```
 BEGIN
  POKE(#F900,CHR(4));
  POKE(#F901,CHR(27));
  POKE(#F902,CHR(#3D));
  POKE(#F903,CHR(X));
  POKE(#F904,CHR(5));
  USER(#F910);
END;
(*****************************************************************************
procedure move
*****************************************************************************)
PROCEDURE MOVE(XX,YY:CHAR);
VAR
 SKEWX:CHAR;
BEGIN
 SKEWX:=CHR(ORD(XX)+SKEW);
 POKE(#F900,CHR(6));
 POKE(#F901,CHR(27));
 POKE(#F902,CHR(109));
 POKE(#F903,SKEWX);
 POKE(#F904,CHR(0));
 POKE(#F905,YY);
 POKE(#F906,CHR(0));
 USER(#F910);
END;
(*****************************************************************************
procedure complement
*****************************************************************************)
PROCEDURE COMPLEMENT(XX,YY:CHAR);
VAR
 RESULT,SKEWX:CHAR;
BEGIN
 SKEWX:=CHR(ORD(XX)+SKEW);
 POKE(#F900,CHR(6));
 POKE(#F901,CHR(27));
 POKE(#F902,CHR(#54));
 POKE(#F903,SKEWX);
 POKE(#F904,CHR(0));
 POKE(#F905,YY);
 POKE(#F906,CHR(0));
 USER(#F910);
 POKE(#F900,CHR(1));
 USER(#F930);
 RESULT:=PEEK(#F901,CHAR);
 CASE RESULT OF CHR(0): POINT(XX,YY);
                CHR(1): UNPOINT(XX,YY)
                END;
END;
(*****************************************************************************
   procedure line
*****************************************************************************)
PROCEDURE LINE(XX,YY:CHAR);
VAR
 SKEWX:CHAR;
BEGIN
 SKEWX:=CHR(ORD(XX)+SKEW);
 POKE(#F900,CHR(7));
 POKE(#F901,CHR(27));
 POKE(#F902,CHR(108));
 POKE(#F903,SKEWX);
 POKE(#F904,CHR(0));
 POKE(#F905,YY);
 POKE(#F906,CHR(0));
 POKE(#F907,CHR(1));
 USER(#F910);
END;
(*****************************************************************************
   procedure dmprq
     global usage: none
     requests svc to dump screen
*****************************************************************************)
PROCEDURE DMPRQ;
```

```
VAR
 C:INTEGER;
BEGIN
C:=CPM(6,#1B);
 C:=CPM(6,#64);
 C:=CPM(6,#50);
END;
(*****************************************************************************
   procedure graphics
     global usage: none
     enters graphics mode
*****************************************************************************)
PROCEDURE GRAPHICS;
  VAR C:INTEGER;
  BEGIN (* graphics *)
  C:=CPM(6,27);
  C:=CPM(6,52);
  END; (* of graphics *)
(*****************************************************************************
   procedure initialise
     global usage:UNDEFINED,FIRSTTIME,X1,X2,Y1,Y2
           OLDX1,OLDX2,RBUT,XCHAN,YCHAN,BUTCHAN,XCUR,YCUR,IX1,IX2,IY1,IY2
           OLDXCUR,OLDYCUR,PRESS,FIRSTSAMPLE,CLOCKVALUE,HUMID,XTIME,YAMPL
           RESISTOR,RUN,NXPTS,NPOINTS
     sets initial values
*****************************************************************************)
PROCEDURE INITIALISE;
  VAR A:INTEGER;
BEGIN
 ICMAX:=0;
 IDNEGMAX:=0;
 TPK:=0;
 TX:=0;
 IDPOSMAX:=0;
 QGMAX:=0;
 QERROR:=0;
 DQSTART:=0;
 DQEND:=0;
 DQRATE:=0;
 DQERROR:=0;
 PFITFOUND:=FALSE; FITFOUND:=FALSE;
 WRITELN('THIS VERSION READS DATAFILES FROM DRIVE "A".....');
 WRITELN;
 WRITELN('V20.05.87, corrected for cable impedance ');
 WRITELN;
 WAIT(1000);
 VS:=0;
 IX1:=30;
 IX2:=90;
 ENDPAGE:=FALSE;
 GRSW:=FALSE;
 DMP:=FALSE;
 MINUS1:=1;
 MINUS2:=-1;
 UNDEFINED:=TRUE;
 FIRSTTIME:=TRUE;
 X1:=0; Y1:=0; X2:=0; Y2:=0;
 OLDIX1:=IX1; OLDIX2:=IX2;
 RBUT:=100;
 XCHAN:=11;
 YCHAN:=12;
 BUTCHAN:=8;
 XCUR:=IX1;
 YCUR:=200;
 IY1:=100;
 IY2:=150;
 OLDXCUR:=XCUR;
 OLDYCUR:=YCUR;
  PRESS:=0;
  FIRSTSAMPLE:=0;
  CLOCKVALUE:=0;
  HUMID:=0;
```

```
  XTIMB:=0;
  YAMPL:=0;
  RESISTOR:=0;
  NRUN:=0;
  NXPTS:=0;
  NPOINTS:=0;
  END; (* of initialise *)
(*****************************************************************************
   procedure beginning
      global usage:DATAFILE
      reads the heading in the input file
*****************************************************************************)
PROCEDURE BEGINNING;
VAR A:INTEGER;
  BEGIN
  RESET(DATAFILE,'A:D$      .   ');
 RESET(FILENUMBER,'A:LOOKING .AT ');
 REWRITE(DBASE,'A:DATABASE.NEW');
 A:=1;
  REPEAT READ(DATAFILE,ACHAR);
  HEADING[A]:=ACHAR;
  WRITE(ACHAR);
  A:=A+1;
 UNTIL ACHAR='$';
  WRITELN;
  WRITELN;
  WRITE('ENTER file numer >>>>>'); READ(FILENUMBER,FILENO);WRITELN(FILENO);
  WRITELN;
  WRITELN;
  WRITELN('ENTER D (cm)  needle height (mm)  V (KV) and p (mmHg)');
  WRITE('>>>');
  READ(GAPLEN,STRLEN,KVOLTS,PRE);
 WRITE('E/p= ',(KVOLTS/GAPLEN/PRE*1000),' V/cm.torr ; enter approx. value>');
  READ(REDUCEDFIELD); WRITELN;
  STRLEN:=GAPLEN-(STRLEN/10);
  FIELD:=KVOLTS/GAPLEN*1.0E+5; (* VOLTS PER METRE *)
  VE:=1.0E+6*POWER((FIELD*1.0E-5/PRE*1.0E+3),0.715)*1.0E-2;
   (* from gallimberti ref. data: Ve (cm/s)=10^6*(e/p)^0.715
      where e/p is in v/cm.torr ... I have converted to Ve (m/s)  *)
  END; (* of beginning *)
(*****************************************************************************
   procedure zero
     global usage:RAW,FIRSTSAMPLE,
     finds the mean of the ten RAW datapoints, the zerolevel.....
     if any one differs by more than +/- 6 from the first, then the
     GARBAGE flag is set
*****************************************************************************)
PROCEDURE ZERO(VAR A:REAL);
 VAR
B:INTEGER;
BEGIN
 A:=0;
 FOR B:=FIRSTSAMPLE TO FIRSTSAMPLE+4 DO   A:=A+IFREE[B];
 A:=A/5
END; (* of zero *)
(*****************************************************************************
   procedure newevent
     global usage:CHANNEL,NXPTS,NPOINTS,PRESS,CLOCKVALUE,FIRSTSAMPLE
                  HUMID,XTIMB,YAMPL,RESISTOR,RAW
     reads the parametric datafield for the next record
     reads the integer data into the array RAW
*****************************************************************************)
PROCEDURE NEWEVENT;
  VAR A,B:INTEGER;
      ACHAR:CHAR;
BEGIN
  REPEAT READ(DATAFILE,ACHAR) UNTIL ACHAR='\';
  READ(DATAFILE,CHANNEL,NXPTS,NPOINTS,PRESS,CLOCKVALUE,FIRSTSAMPLE);
  READ(DATAFILE,HUMID,XTIMB,YAMPL,RESISTOR);
  IF CHANNEL='A' THEN YAMPL:=YAMPL*RESISTOR/35.3; (* correction ' *)
  (* Z0=78 OHMS, R=64.3 OHMS : FINAL CORRECTION!!!*)
  IF CHANNEL='B' THEN YAMPL:=YAMPL*RESISTOR/33.3;
```

```
x

   (* I0=74 OHMS, R=60.6 OHMS *)
  FOR A:=FIRSTSAMPLE TO NPOINTS DO
    BEGIN
      READ(DATAFILE,B);
      IFREE[A]:=B*YAMPL/128;
    END;
   ZERO(ZEROLEVEL);
   FOR A:=FIRSTSAMPLE TO NPOINTS DO IFREE[A]:=IFREE[A]-ZEROLEVEL;
  END;
{*************************************************************************
   procedure display
     global usage:NRUN,NPOINTS,NXPTS,FIRSTSAMPLE,CLOCKVALUE,RESISTOR
                  PRESS,HUMID,XTIME,YAMPL
     tabulates the parametric data field for this record
*************************************************************************}
PROCEDURE DISPLAY;
VAR A:INTEGER;
 BEGIN
 A:=1;
REPEAT WRITE(HEADING[A]) ; A:=A+1 UNTIL HEADING[A]='$';
 WRITELN;
  WRITE('#',FILENO:4,'.');
 WRITE(NXPTS:2,'  ');
  CASE STATUS OF
       1: WRITE('Ic ');(*,YH*2.5E+4:8:3,'mA/cm ',XTIME*1.0E+6:8:3,'us/cm');*)
       2: WRITE('Id ');(*,YH*2.5E+4:8:3,'mA/cm ',XTIME*1.0E+6:8:3,'us/cm');*)
       3: WRITE('Ie ');(*,YH*2.5E+4:8:3,'mA/cm ',XTIME*1.0E+6:8:3,'us/cm');*)
       4: WRITE('Qg ');(*,YH*2.5E+12:8:3,'nC/cm ',XTIME*1.0E+6:8:3,'us/cm');*)
       5: WRITE('dQ ');(*,YH*2.5E+12:8:3,'nC/cm ',XTIME*1.0E+6:8:3,'us/cm');*)
      6: BEGIN
     WRITE('Ax ');(*,YH*2.5E+10:8:3,'nC/cm ',XTIME*VE*VS/(VE+VS)*100:8:3);*)
       WRITE('cms')
     END
      END; (* OF CASE *)
 WRITELN;
  WRITE(GAPLEN:4:1,' cm  ',PRE:3:0,' mmHg ');
  WRITE(FIELD*1.0E-5:5:2,' KV/cm ',(FIELD*1.0E-5/PRE*1.0E+3):5:2);
  WRITELN(' V/cm.torr');
 WRITE('Ve= ',(VS/1000):5:1,' Km/s');
 WRITELN;
 WRITE(ICMAX,' ; ',TPK,' ; ',IDPOSMAX,' ;');
 WRITELN(IDNEGMAX);
 WRITELN(TX,' ; ',VS,' ; ',QGMAX,' ; ',QERROR);
 WRITE(DQSTART,' ; ',DQEND,' ; ',DQRATE);
 WRITELN(' ; ',DQERROR);
 WRITE(DQINJECTED,' ; ',CALL23,' ; ');
 WRITELN(CALL26);
  END; (* of display *)
{*************************************************************************
   procedure analmenu
     global usage:X1,X2,Y1,Y2,INTEGRAL,MU,UNDEFINED,NXPTS,CHANNEL
     displays the cursor data and the calculated quantities
     then displays a user prompt for response choice
*************************************************************************}
PROCEDURE ANALMENU;
VAR
 SF:REAL;
BEGIN
 IF NOT DMP THEN NORMALSCREEN;
 DISPLAY;
  CASE STATUS OF
       1,2,3: SF:=1.0E+3;
         4,5: SF:=1.0E+9
     END; (* of case *)
(*  WRITE('uS');
  CASE STATUS OF
     1,2,3: WRITE(',mA');
       4,5: WRITE(',nC')
     END; *)(* of case *)(*
  WRITE(',',X1*1.0E+6:8:3,',',Y1*SF:8:3,',',X2*1.0E+6:8:3);
  WRITELN(',',Y2*SF:8:3);*)
 WRITE('dT= ',(X2-X1)*1.0E+6:5:2,' uS  Ve= ',(VE/1000):4:2,' Km/s');
```

```
WRITELN;
IF STATUS  4 THEN
IF NOT UNDEFINED THEN
WRITE(  ;int.   ,INTEGRAL*1.0E+9:12:4,  nC );
 IF FITFOUND THEN
WRITE(  ;att. fr. (x1)  ,ARATE*1.0E-6:12:4,  MHz );
WRITELN;
IF NOT DMP THEN
 BEGIN
 WRITELN;
  WRITELN('enter selection to....');
  WRITELN;
  WRITE('1: add (X1,Y1)                    11: find Ie ');
  IF CORRECTED THEN WRITELN('=Id+Ic.(d-n)/d') ELSE WRITELN('=Id+Ic');
  WRITELN('2: add (X2,Y2)                    12 : find Qg');
  WRITELN('3: find attachment rate at X1     13: screendump');
  WRITELN('4: find integral                  14: graticule');
  WRITELN('5 : go to next record             15 : find dQ');
  WRITELN('6: quit program                17 : find streamerfunction A(z)');
  WRITELN('7: show data                      18 : find streamer velocity');
  WRITELN('8 : swap cursor 1&2               19: cubic polynomial fit');
  WRITELN('9: swap old & new datafield       20: Ie=Id+Ic');
 WRITELN('21  Ic pk  22  +Id pk  23  Ts & -Id pk  24  Qg pk % decay');
 WRITELN(' 25  dQ growth, start & end  26  -dQ pk  27  output to disc. ');
  END;
END; (* of analmenu *)
(*****************************************************************************
   procedure adc
      global usage:none
      returns the voltage for a particular channel of the adc card
*****************************************************************************)
PROCEDURE ADC(VAR ANS,CHANNEL:INTEGER);
VAR
 A,B:INTEGER;
 INPUT:CHAR;
 RESULT:REAL;
BEGIN
   OUT(32+CHANNEL,CHR(0));
   FOR A:=0 TO 5 DO A:=A;
   INPUT:=INP(32);
 ANS:=ORD(INPUT);
END; (* of adc *)
(*****************************************************************************
   procedure cursor
     global usage:OLDXCUR,OLDYCUR,XCUR,YCUR,RBUT
     finds new cursor position,stores old one so it can be erased,
     and assigns an appropriate value to BUTTONPRESSED
*****************************************************************************)
PROCEDURE CURSOR;
BEGIN
 OLDXCUR:=XCUR;
 OLDYCUR:=YCUR;
 ADC(XCUR,XCHAN);
 ADC(YCUR,YCHAN);
 ADC(RBUT,BUTCHAN);
 IF RBUT<125 THEN BUTTONPRESSED:=TRUE ELSE BUTTONPRESSED:=FALSE;
 IF XCUR<FIRSTSAMPLE THEN XCUR:=FIRSTSAMPLE;
 IF XCUR>NPOINTS THEN XCUR:=NPOINTS;
END; (* of cursor *)
(*****************************************************************************
   procedure drawgraticule
     global usage:none
     draws scope graticule on svc screen
     requires graphics mode
*****************************************************************************)
PROCEDURE DRAWGRATICULE;
VAR
 A,B,C:INTEGER;
BEGIN
 (* SQUARE GRID *)
 (*  FOR B:=0 TO 250 DO
   FOR A:=0 TO 10 DO
```

```
    BEGIN
     POINT(CHR(A*25),CHR(B));
     POINT(CHR(B),CHR(A*25));
    END; *)
(* AXES ONLY *)
FOR A:=0 TO 250 DO
BEGIN
POINT(CHR(0),CHR(A));
POINT(CHR(150),CHR(A));
END;
FOR A:=0 TO 150 DO
 BEGIN
 POINT(CHR(A),CHR(0));
 POINT(CHR(A),CHR(250));
 END;
FOR B:=1 TO 9 DO FOR C:=1 TO 3 DO
BEGIN
  POINT(CHR(C),CHR(25*B));
 POINT(CHR(150-C),CHR(25*B));
 END;
FOR B:=1 TO 5 DO FOR C:=1 TO 3 DO
BEGIN
 POINT(CHR(25*B),CHR(C));
 POINT(CHR(25*B),CHR(250-C));
END;
C:=CPM(6,#1B); C:=CPM(6,#0C);
END;
(*************************************************************************
   procedure autorange(scale:real,range:integer)
     global usage:IFREE
     finds the parameters needed by drawtrace to plot the data in IFREE[a]
*************************************************************************)
PROCEDURE AUTORANGE(VAR C:REAL;VAR A:INTEGER);
VAR
 B:INTEGER;
 G,INT,MAX,MIN:REAL;
BEGIN
 MAX:=0; MIN:=0;
 FOR B:=FIRSTSAMPLE TO NPOINTS DO
  BEGIN
   IF IFREE[B]>MAX THEN MAX:=IFREE[B];
   IF IFREE[B]<MIN THEN MIN:=IFREE[B];
  END;
 INT:=MAX-MIN;
 A:=TRUNC(-1*MIN/INT*10);
 IF A>0 THEN
 G:=LN(-1*MIN/A)/LN(10.0)
 ELSE
  BEGIN
   A:=1;
   G:=LN(MAX/9)/LN(10.0);
  END;
 C:=((POWER(10,FRAC(G))*10)+1)/10*POWER(10,ENTIER(G));
 C:=C/25; A:=A*25;
END;
(*************************************************************************
procedure curdraw(x);
*************************************************************************)
PROCEDURE CURDRAW(X:INTEGER);
VAR
A:INTEGER;
BEGIN
(*FOR A:=-2 TO 2 DO
 BEGIN
  COMPLEMENT(CHR(X+A),CHR(Y(X)+A));
  COMPLEMEN(CHR(X+A),CHR(Y(X)-A));
 END;
COMPLEMENT(CHR(X),CHR(Y(X)));*)
 FOR A:=-2 TO 1 DO
 BEGIN
   COMPLEMENT(CHR(X+A),CHR(Y(X)-2));
   COMPLEMENT(CHR(X+2),CHR(Y(X)+A));
```

```
    COMPLEMENT(CHR(X-A),CHR(Y(X)+2));
    COMPLEMENT(CHR(X-2),CHR(Y(X)-A));
  END;
END;
{*****************************************************************************
   procedure drawtrace
     global usage:FIRSTSAMPLE,NPOINTS,RAW
     requires graphics mode
     draws crude data straight from RAW
*****************************************************************************}
PROCEDURE DRAWTRACE;
VAR
 A,B,C,D:INTEGER;
BEGIN
 CLEARSCREEN;
 AUTORANGE(YH,YG);
 IF GRSW THEN
  BEGIN
   DRAWGRATICULE;
   FOR A:=FIRSTSAMPLE TO NPOINTS DO
    IF (A<5) OR (Y(A)<5) OR (Y(A)>245) THEN
    BEGIN
     D:=YG+ENTIER(IFREE[A]/YH);
     FOR B:=-3 TO 3 DO
       FOR C:=-3 TO 3 DO
        UNPOINT(CHR(A+B),CHR(D+C));
   END;
  END;
  MOVE(CHR(FIRSTSAMPLE),CHR(Y(FIRSTSAMPLE)));
  FOR A:=FIRSTSAMPLE TO NPOINTS DO
    LINE(CHR(A),CHR(Y(A)));
 IF FITFOUND OR POLYFITFOUD THEN
  BEGIN
   A:=FIRSTSAMPLE;
     REPEAT
      A:=A+1;
     UNTIL (YFIT(A)>0) AND (YFIT(A)<250);
     A:=A+1;
     WHILE (YFIT(A)>0) AND (YFIT(A)<250) AND (A<=NPOINTS) DO
      BEGIN
       MOVE(CHR(A-1),CHR(YFIT(A-1)));
       LINE(CHR(A),CHR(YFIT(A)));
       IF (A>=IX1) AND (A<=IX2) THEN LINE(CHR(A),CHR(Y(A)));
       A:=A+1;
      END;
  END;
  C:=CPM(6,#1B); C:=CPM(6,#0C);
  FOR C:=1 TO 4 DO WRITELN;
  WRITE('fig d',FILENO:3,'.',NXPTS:1);
  CASE STATUS OF
       1: BEGIN
    WRITELN('a');
    WRITELN;
       WRITELN('conduction');
      WRITELN('current, Ic');
      END;
       2: BEGIN
         WRITELN('b');
      WRITELN;
          WRITELN('displacement');
          WRITELN('current, Id');
       END;
       3: BEGIN
  WRITELN('c');
     WRITELN;
   WRITELN('simple ');
     WRITELN('current, Is');
     END;
       4;
        BEGIN
        WRITELN('d');
       WRITELN;
```

```
          WRITELN( total free );
          WRITELN( charge, Qg );
        END;
       5: BEGIN
        WRITELN( e );
        WRITELN;
         WRITELN( generation of );
           WRITELN( charge dQ/sec );
         END;
      6: BEGIN
   WRITELN( f );
   WRITELN;
WRITELN( Ax  );
  WRITELN;
  END
     END;
   WRITELN;
WRITELN( d    ,GAPLEN:4:1,'  cms' );
 WRITELN( p   ,PRE:7:0,'   mmHg' );
 WRITELN( E   ,FIELD*1.0E-5/:4:1);
WRITELN(          kV/cm' );
WRITELN( E/p  ',(FIELD*1.0E-5/PRE*1.0E+3):4:2);
WRITELN(     V/cm.torr' );
WRITELN( Vs  ,(VS*1.0E-3):5:1,' km/s' );
 WRITELN( Ve   ,(VE*1.0E-3):5:2,'  " );
 IF FITFOUND THEN
 BEGIN
  IF (ARATE<0) THEN WRITELN('decay freq. = ') ELSE WRITELN('growth freq. = ');
 WRITELN((ARATE*1.0E-6):9:2);
WRITELN( +/- ,(ERARATE*1.0E-6):6:2,' MHz' );
  END;
IF NOT UNDEFINED THEN
 BEGIN
  WRITELN;
  WRITELN('integral =');
  WRITELN((INTEGRAL*1.0E+9):9:2,' nC');
 END;
IF UNDEFINED AND (FITFOUND=FALSE) THEN BEGIN WRITELN; WRITELN; WRITELN END;
WRITELN;
 WRITELN('ver/hor scale');
 WRITE( y: );
 CASE STATUS OF
    4: WRITELN((YH*2.5E+10):6:2,' nC');
    1,2,3: WRITELN((YH*2.5E+4):6:2,' mA');
    5,6: WRITELN((YH*2.5E+1):6:3,' C/s')
   END;
  WRITELN('x:',(XTIMB*1.0E+6):7:2,' uS');
IF UNDEFINED THEN
BEGIN
CURDRAW(IX1);
CURDRAW(IX2);
END
 ELSE
 BEGIN
 FOR A:=IX1 TO IX2 DO
 BEGIN
  MOVE(CHR(A),CHR(YG));
  LINE(CHR(A),CHR(Y(A)));
  END;
END;
IF (NOT UNDEFINED) OR (STATUS=5) THEN
BEGIN
 MOVE(CHR(FIRSTSAMPLE),CHR(YG));
  LINE (CHR(NPOINTS),CHR(YG));
END;
  END;
PROCEDURE DRAWCUR;
BEGIN
 CURDRAW(OLDIX1); CURDRAW(OLDIX2);
 CURDRAW(IX1);    CURDRAW(IX2);
END;
(*****************************************************************************
```

```
   procedure rout1
    global usage:X1,IX1,XCUR,XTIMB,Y1,IY1,RAW,ZEROLEVEL,RBUT,YAMPL
                 OLDIX1,OLDXCUR
     requires graphics mode
     finds cursor position,makes this new cursor1,stores old value
     repeats until button is pressed
*****************************************************************************)
PROCEDURE ROUT1;
BEGIN
 UNDEFINED:=TRUE;
 DRAWTRACE;
  OLDIX1:=OLDXCUR;
 REPEAT
 DRAWCUR;
  CURSOR;
  X1:=XCUR*XTIMB/25;
  Y1:=IFREE[XCUR];
  IX1:=XCUR; OLDIX1:=OLDXCUR;
 UNTIL RBUT 125;
END;
(*****************************************************************************
   procedure rout2
     global usage:XCUR,X2,IX2,OLDIX2,OLDXCUR,XTIMB
                  Y2,RAW,ZEROLEVEL,YAMPL,RBUT
     same as rout1 but gets cursor position and maps it onto cursor2
     calculating the real values X2,Y2 of the cursor positon.
     again the old ones are saved for erasure
*****************************************************************************)
PROCEDURE ROUT2;
BEGIN
 UNDEFINED:=TRUE;
 DRAWTRACE;
  OLDIX2:=OLDXCUR;
 REPEAT
  DRAWCUR;
   CURSOR;
   X2:=XCUR*XTIMB/25;
   Y2:=IFREE[XCUR];
   IX2:=XCUR; OLDIX2:=OLDXCUR;
  UNTIL RBUT>125;
END;
(*****************************************************************************
procedure expfit;
  performs a least squares fit to the data between the cursors
  to the function y=a exp(bx)
*****************************************************************************)
PROCEDURE EXPFIT;
VAR
 YS,SX,SY,SXX,SYY,SXY,SD,DD,ED:REAL;
 S,N:INTEGER;
FUNCTION Q(X:INTEGER):REAL;
VAR
 J,K:REAL;
 C:INTEGER;
BEGIN
 J:=IFREE[X];
 IF J<0 THEN J:=J*(-1);
 IF J>0 THEN
  K:=LN(J)
  ELSE
  K:=-40;
 IF K=-40 THEN C:=CPM(6,7); (* BEEP *)
 Q:=K;
END;
FUNCTION D(VAR X:INTEGER):REAL;
BEGIN
 D:=FITA*X+FITB-Q(X);
END;
BEGIN
 FITFOUND:=FALSE;
 SX:=0; SY:=0; SXX:=0; SYY:=0; SXY:=0; SD:=0;
 FOR S:=IX1 TO IX2 DO
```

```
  BEGIN
   SX:=SX+S;
   SXX:=SXX+SQR(S);
  YS:=Q(S);
   SY:=SY+YS;
   SYY:=SYY+SQR(YS);
   SXY:=SXY+S*YS;
  END;
 N:=IX2-IX1+1;
 DD:=N*SXX-SQR(SX);
 FITA:=(N*SXY-SX*SY)/DD;
 FITB:=(SY*SXX-SX*SXY)/DD;
 ARATE:=FITA*25/XTIMB;
 FOR S:=IX1 TO IX2 DO SD:=SD+SQR(D(S));
 EQ:=SD/(N-2);
 ERARATE:=SQRT(N*EQ/DD)*25/XTIMB;
 WRITELN(' [X]n := ',SX,   [XX]n := ',SXX,  [Y]n := ',SY,   [Y]n := ',SYY);
 WRITELN(' [XY]n := ',SXY,   [DD]n := ',SD,   N:= ',N);
 WRITELN('n[XX].N- [X]n.[X]n := ',DD, [DD]n/(N-2) := ',EQ);
 WRITE(' a := ',FITA,'  b:= ',FITB,'  +- att.freq  := ',ARATE,  +/-  );
 WRITELN(ERARATE);
 READLN;
END;
{*****************************************************************************
   procedure rout4
      global useage:INTEGRAL,IX2,IX1,RAW,ZEROLEVEL,YAMPL,XTIMB,UNDEFINED
      requires graphics mode
      displays data, calculates integral between X1&X2, displays result.
      on return to program, negates undefined flag
*****************************************************************************}
PROCEDURE ROUT4;
VAR
A:INTEGER;
BEGIN
 FITFOUND:=FALSE;
 IF (STATUS <> 4)  THEN
  BEGIN
 DRAWTRACE;
 INTEGRAL:=0;
 DRAWCUR;
 IF IX2>IX1 THEN
  FOR A:=IX1 TO IX2 DO INTEGRAL:=INTEGRAL+IFREE[A]
  ELSE
  FOR A:=IX2 TO IX1 DO INTEGRAL:=INTEGRAL+IFREE[A];
 INTEGRAL:=INTEGRAL*XTIMB/25;
 WRITE(INTEGRAL*1.0E+9:12:4,' nC');
 UNDEFINED:=FALSE;
 READLN;
  END
  ELSE
   BEGIN
    WRITELN(' meaningless ');
    UNDEFINED:=TRUE;
    READLN;
   END; (* of if status < 4 *)
END;
{*****************************************************************************
   procedure rout5
     gloal usage:FIRSTTIME,PZEROLEVEL,ZEROLEVEL,PARATE,ARATE
                 PINTEGRAL,INTEGRAL,PRAW,RAW,PPRESS,PRESS
                 PCLOCKVALUE,CLOCKVALUE,PHUMID,HUMID,PXTIMB,XTIMB
                 PYAMPL,YAMPL,PRESISTOR,RESISTOR,PNRUN,NRUN,PNXPTS,NXPTS
                 PNPOINTS,NPOINTS,PFIRSTSAMPLE,FIRSTSAMPLE,PCHANNEL,CHANNEL
                 X1,IX1,Y1,X2,IX2,Y2
     stores the parameters and gets more data from file
     i.e. (field2):=(field1); then new (field1). (field2) is lost.
*****************************************************************************}
PROCEDURE ROUT5;
VAR
 A:INTEGER;
 RTEMP:REAL;
BEGIN
```

```
 POLYFITFOUND:=FALSE;
 CALL23:=FALSE;
 CALL26:=FALSE;
 FIRSTTIME:=FALSE;
 (* SAVE OLD PARAMETERS AND DATA *)
 PZEROLEVEL:=ZEROLEVEL;
 PARATE:=ARATE;
 PINTEGRAL:=INTEGRAL;
 FOR A:=0 TO 255 DO ICOND[A]:=IFREE[A];
 PPRESS:=PRESS;
 PCLOCKVALUE:=CLOCKVALUE;
 PHUMID:=HUMID;
 PXTIMB:=XTIMB;
 PYAMPL:=YAMPL;
 PRESISTOR:=RESISTOR;
 PNRUN:=NRUN;
 PNXPTS:=NXPTS;
 PNPOINTS:=NPOINTS;
 PFIRSTSAMPLE:=FIRSTSAMPLE;
 PCHANNEL:=CHANNEL;
 PFITFOUND:=FITFOUND;
 (* END OF SAVING PARAMETERS *)
 FITFOUND:=FALSE;
 NEWEVENT;
  X1:=IX1*XTIMB/25;
  Y1:=IFREE[IX1];
   X2:=IX2*XTIMB/25;
   Y2:=IFREE[IX2];
 UNDEFINED:=TRUE;
END;
(*****************************************************************************
   procedure rout7
     global usage:none
     calls other routines to draw (field)
*****************************************************************************)
PROCEDURE ROUT7;
VAR
 A,B:INTEGER;
BEGIN
 DRAWTRACE;
 IF NOT DMP THEN READLN;
END;
(*****************************************************************************
   procedure rout3
     global usage:IX1,XCUR,IY1,RAW,OLDIX1,OLDXCUR,X1,XTIMB
                  Y1,ZEROLEVEL,YAMPL,ARATE,BUTTONPRESSED
     requires graphics mode
     gets a new cursor1 value, calculates the attachment freq.
     here, and displays the value.
     stops when button is pressed.
*****************************************************************************)
PROCEDURE ROUT3;
BEGIN
 EXPFIT;
 FITFOUND:=TRUE;
 ROUT7;
END;
(*****************************************************************************
   procedure rout8
     global usage:IX1,IX2,IY1,IY2,XCUR,YCUR,X1,X2,Y1,Y2
     interchanges the cursor fields; cursor1:=cursor2, cursor2:=cursor1
*****************************************************************************)
PROCEDURE ROUT8;
VAR
 ITEMP:INTEGER;
 RTEMP:REAL;
BEGIN
 ITEMP:=IX1; IX1:=IX2; IX2:=ITEMP;
 ITEMP:=IY1; IY1:=IY2; IY2:=ITEMP;
 XCUR:=IX1;
 YCUR:=IY1;
 RTEMP:=X1; X1:=X2; X2:=RTEMP;
```

```
 RTEMP:=Y1; Y1:=Y2; Y2:=RTEMP;
END;
{*****************************************************************************
   procedure rout9
     global usage:FIRSTTIME,ZEROLEVEL,PZEROLEVEL,ARATE,PARATE
                  INTEGRAL,PINTEGRAL,RAW,PRAW,PRESS,PPRESS,HUMID,PHUMID
                  CLOCKVALUE,PCLOCKVALUE,XTIMB,PXTIMB,YAMPL,PYAMPL
                  RESISTOR,PRESISTOR,NRUN,PNRUN,NXPTS,PNXPTS
                  NPOINTS,PNPOINTS,FIRSTSAMPLE,PFIRSTSAMPLE,CHANNEL,PCHANNEL
                  X1,IX1,Y1,X2,IX2,Y2
   interchanges the datafields; (field1):=(field2), (field2):=(field1).
*****************************************************************************}
PROCEDURE ROUT9;
VAR
 A,ITEMP:INTEGER;
 RTEMP:REAL;
 BTEMP:BOOLEAN;
 CTEMP:CHAR;
BEGIN
 UNDEFINED:=TRUE;
 IF FIRSTTIME THEN ROUT5;
 RTEMP:=ZEROLEVEL; ZEROLEVEL:=PZEROLEVEL; PZEROLEVEL:=RTEMP;
 RTEMP:=ARATE; ARATE:=PARATE; PARATE:=RTEMP;
 RTEMP:=INTEGRAL; INTEGRAL:=PINTEGRAL; PINTEGRAL:=RTEMP;
 BTEMP:=FITFOUND; FITFOUND:=PFITFOUND; PFITFOUND:=BTEMP;
 FOR A:=0 TO 255 DO
  BEGIN
   RTEMP:=IFREE[A];
   IFREE[A]:=ICOND[A];
   ICOND[A]:=RTEMP;
  END;
 ITEMP:=STATUS; STATUS:=PSTATUS; PSTATUS:=ITEMP;
 RTEMP:=PRESS; PRESS:=PPRESS; PPRESS:=RTEMP;
 RTEMP:=CLOCKVALUE; CLOCKVALUE:=PCLOCKVALUE; PCLOCKVALUE:=RTEMP;
 RTEMP:=HUMID; HUMID:=PHUMID; PHUMID:=RTEMP;
 RTEMP:=XTIMB; XTIMB:=PXTIMB; PXTIMB:=RTEMP;
 RTEMP:=YAMPL; YAMPL:=PYAMPL; PYAMPL:=RTEMP;
 RTEMP:=RESISTOR; RESISTOR:=PRESISTOR; PRESISTOR:=RTEMP;
 ITEMP:=NRUN; NRUN:=PNRUN; PNRUN:=ITEMP;
 ITEMP:=NXPTS; NXPTS:=PNXPTS; PNXPTS:=ITEMP;
 ITEMP:=NPOINTS; NPOINTS:=PNPOINTS; PNPOINTS:=ITEMP;
 ITEMP:=FIRSTSAMPLE; FIRSTSAMPLE:=PFIRSTSAMPLE; PFIRSTSAMPLE:=ITEMP;
 CTEMP:=CHANNEL; CHANNEL:=PCHANNEL; PCHANNEL:=CTEMP;
  X1:=IX1*XTIMB/25;
  Y1:=IFREE[IX1];
   X2:=IX2*XTIMB/25;
   Y2:=IFREE[IX2];
END;
PROCEDURE ROUT10;
VAR
 A:INTEGER;
BEGIN
 FOR A:=FIRSTSAMPLE TO NPOINTS DO IFREE[A]:=LN(SQRT(SQR(IFREE[A])));
END;
{*****************************************************************************
   procedure rout11;
     global usage:RAW,ZEROLEVEL,PRAW,PZEROLEVEL,YAMPL,PYAMPL
     performs the mapping described in rout10.
     note: data in RAW is lost !
*****************************************************************************}
PROCEDURE ROUT11;
VAR
 A:INTEGER;
 FACTORX:REAL;
BEGIN
 FITFOUND:=FALSE;
 IF CORRECTED THEN FACTORX:=STRLEN/GAPLEN ELSE FACTORX:=1;
 UNDEFINED:=TRUE;
 IF (STATUS=2) AND(PSTATUS=1) THEN
  BEGIN
   FOR A:=FIRSTSAMPLE TO NPOINTS DO IFREE[A]:=IFREE[A]+FACTORX*ICOND[A];
   STATUS:=3;
```

```
  END
  ELSE
  IF (STATUS=1) AND (FSTATUS=2) THEN
   BEGIN
    WRITELN('<9, ?');
    READLN
   END
   ELSE
    BEGIN
     WRITELN('<5 ???');
     READLN
    END;
END;
(*****************************************************************************
   procedure rout12
     global usage: none
     calls rout5,rout5,rout11,rout4 : a convenience
*****************************************************************************)
PROCEDURE ROUT12;
VAR
 A:INTEGER;
 B:REAL;
BEGIN
 UNDEFINED:=TRUE;
 FITFOUND:=FALSE;
 IF (STATUS=3) AND (PSTATUS=1) THEN
  BEGIN
   B:=VE/GAPLEN*100; (* 1/D in metres *)
   FOR A:=FIRSTSAMPLE TO NPOINTS DO IFREE[A]:=IFREE[A]/B;
   STATUS:=4;
  END
  ELSE
  IF (STATUS=1) AND (PSTATUS=3) THEN
   BEGIN
    WRITELN('<9,???');
    READLN
   END
   ELSE
    BEGIN
     WRITELN('<11> ???');
     READLN
    END; (* OF IF *)
END;
(*****************************************************************************
   procedure rout13
     global usage:none
     draws the current field, outputs it to the printer
     then lists the parameters associated with it
*****************************************************************************)
PROCEDURE ROUT13;
VAR
 A,B,C:INTEGER;
BEGIN
 GRSW:=TRUE;
 DMP:=TRUE;
 C:=CPM(5,27);
 C:=CPM(5,51);
 C:=CPM(5,24); (* SET EPSON LINESPACING FOR GRAPHICS *)
 GRAPHICS;
 DRAWTRACE;
  DMPRQ;
 USER(#F950); (* GRAPHICS DUMP *)
 C:=CPM(5,27);
 C:=CPM(5,50); (* RESTORE DEFAULT LINESPACING TO EPSON *)
 DMP:=FALSE;
(* IF ENDPAGE THEN
  BEGIN
   C:=CPM(5,12);*) (* FORM FEED *)
(*   ENDPAGE:=FALSE;
  END
  ELSE ENDPAGE:=TRUE;*)
 WRITELN;
```

```
 POKE1o(#E159,#EB96); (* RESTORE O/P JUMP IN BIOS TO CRT: *)
 GRSW:=FALSE;
END;
(*****************************************************************************
   procedure rout14
      global usage:GRSW
      turns on/off the graticule drawing routine
*****************************************************************************)
PROCEDURE ROUT14;
BEGIN
 IF GRSW THEN GRSW:=FALSE ELSE GRSW:=TRUE
END;
(*****************************************************************************
   procedure rout15
     global usage:none
     reads in a new record (ic and id) and displays id
*****************************************************************************)
PROCEDURE ROUT15;
BEGIN
 (* SET RETURNED VALUES TO 0 *)
 ICMAX:=0;
 IDPOSMAX:=0;
 IDNEGMAX:=0;
 TX:=0;
 VS:=0;
 QGMAX:=0;
 DQINJECTED:=0;
 QRATE:=0;
 DQRATE:=0;
 QERROR:=0;
 DQERROR:=0;
 TPk:=0;
 DQSTART:=0;
 DQEND:=0;
 INTC:=0;
 INTD2:=0;
 INTD3:=0;
 ROUT5; ROUT5;
 STATUS:=2;
 PSTATUS:=1;
 ROUT7;
END;
(*****************************************************************************
   procedure rout16
      global usage:none
      finds gap charge generation, dQ
*****************************************************************************)
PROCEDURE ROUT16;
VAR
 ICTERM,OMYGODWHATAMESS,RTEMP,RRTEMP:REAL;
 A:INTEGER;
BEGIN
 UNDEFINED:=TRUE;
 IF (STATUS=4) AND (PSTATUS=1) AND FITFOUND THEN
  BEGIN
   OMYGODWHATAMESS:=ICOND[FIRSTSAMPLE];
   FOR A:=FIRSTSAMPLE+1 TO NPOINTS DO
    BEGIN
     ICTERM:=(ICOND[A]+OMYGODWHATAMESS)*XTIMB/50;
     OMYGODWHATAMESS:=ICOND[A];
     ICOND[A]:=IFREE[A]-(IFREE[A-1]-ICTERM)*EXP(ARATE*XTIMB/25);
     ICOND[A]:=ICOND[A]/XTIMB*25; (* dQ/sec *)
    END;
    PSTATUS:=5;
      END
    ELSE IF (STATUS=1) AND (PSTATUS=4)
 THEN BEGIN  WRITELN('<9>??'); READLN END
  ELSE BEGIN WRITELN('<15>??'); READLN END;
 IF NOT FITFOUND THEN WRITELN('<3>??');
 FFITFOUND:=FALSE;
   ICOND[FIRSTSAMPLE]:=0;
    FIRSTSAMPLE:=FIRSTSAMPLE+1;
```

```
 ROUT7;
 END;
{*****************************************************************************
   procedure rout17
      forms the streamerfunction A(x) in IFREE
*****************************************************************************}
{*PROCEDURE ROUT17;
VAR
A,B:INTEGER;
CC,VELO,D:REAL;
BEGIN
 FFITFOUND:=FALSE;
 IF (PSTATUS=1) AND FITFOUND AND (VS<>0) THEN
  BEGIN
   STATUS:=0;
   VELO:=VE*VS/(VE+VS);
   CC:=(SQRT(SQR(ARATE))/VE)*VELO*XTIMB/25;
  WRITELN('CC:=',CC);
  WRITELN('ARATE:=',ARATE);
   WRITELN('VELO:=',VELO);
   FOR A:= IX1 TO IX2 DO  IFREE[A-IX1]:=(ICOND[A]/VELO)*EXP((A-IX1)*CC);
   FOR A:=(IX2+1-IX1) TO NPOINTS DO IFREE[A]:=0;
 END
  ELSE WRITELN('18.2 <3.2 <12.22');
  READLN;
 FITFOUND:=FALSE;
 FFITFOUND:=TRUE;
END;   *)
{*****************************************************************************
   procedure rout18;
     finds the streamer velocity
*****************************************************************************}
PROCEDURE ROUT18;
BEGIN
 VS:=STRLEN/(ABS(X2-X1)*100);
END;
PROCEDURE ROUT19;
BEGIN
 POLYFIT;
 ROUT7;
END;
{*****************************************************************************
   procedure rout20
     global usage: CORRECTED;
     changes ROUT11 such that it finds Ie=Id+Ic; and not the default
     which is Ie=Id+(d-n)/d.Ic
*****************************************************************************}
PROCEDURE ROUT20;
BEGIN
 IF CORRECTED THEN CORRECTED:=FALSE ELSE CORRECTED:=TRUE;
 IF CORRECTED THEN WRITELN('finds Ie=Id+Ic.(d-n)/d')
              ELSE WRITELN('finds Ie=Id+Ic');
 READLN;
END;
PROCEDURE ROUT21;
VAR
 A:INTEGER;
BEGIN
 ICMAX:=Y2;
 TPk:=(X2-X1);
 INTC:=0;
 FOR A:=FIRSTSAMPLE TO NPOINTS DO INTC:=INTC+IFREE[A];
 INTC:=INTC*XTIMB/25;
END;
PROCEDURE ROUT22;
BEGIN
 IDPOSMAX:=Y2;
END;
PROCEDURE ROUT23;
VAR
 A:INTEGER;
BEGIN
```

```
  CALL23:=TRUE;
  IDNEGMAX:=Y2;
  TX:=(X2-X1);
  ROUT18;
  INTD2:=0;
  INTD3:=0;
  FOR A:=(IX1) TO IX2 DO INTD2:=INTD2+IFREE[A];
  FOR A:=(IX1) TO NPOINTS DO INTD3:=INTD3+IFREE[A];
  INTD2:=INTD2*XTIMB/25;
  INTD3:=INTD3*XTIMB/25;
END;
PROCEDURE ROUT24;
BEGIN
  QGMAX:=Y1;
  QRATE:=ARATE;
  QERROR:=ERARATE;
END;
PROCEDURE ROUT25;
BEGIN
  DQSTART:=Y1;
  DQEND:=Y2;
  DQRATE:=ARATE;
  DQERROR:=ERARATE;
END;
PROCEDURE ROUT26;
BEGIN
  CALL26:=TRUE;
  DQINJECTED:=Y2;
END;
PROCEDURE ROUT27;
VAR A:INTEGER;
BEGIN
  WRITELN(DBASE,' ');
  WRITE(DBASE,'\ ',FILENO,' ',NXPTS,' ');
  WRITE(DBASE,FIELD,' ',(FIELD/PRE),' ',GAPLEN,' ',PRE,' ');
  WRITE(DBASE,ICMAX,' 0 ',IDPOSMAX,' 0 ',IDNEGMAX,' 0 ');
  WRITE(DBASE,QGMAX,' 0 ',DQINJECTED,' 0 ',QRATE,' ',QERROR,' ');
  WRITE(DBASE,DQRATE,' ',DQERROR,' ',VS,' 0 ',VE,' 0 ');
  WRITE(DBASE,INTC,' 0 ',INTD2,' 0 ',INTD3,' 0 ');
  WRITE(DBASE,VE,' 0 ',TX,' 0 ',STRLEN,' 0 ',TPK,' 0 ',DQSTART,' 0 ');
  WRITE(DBASE,DQEND,' 0 ');
  IF CALL23 THEN WRITE(DBASE,'  1    ') ELSE WRITE(DBASE,'   0    ');
  IF CALL26 THEN WRITE(DBASE,'  1    ') ELSE WRITE(DBASE,'   0    ');
END;
(*************************************************************************
   procedure analysis
     global usage:IRESP
     drives the sub-menu for the cursor-oriented analysis package
*************************************************************************)
PROCEDURE ANALYSIS;
BEGIN
 REPEAT
  NORMALSCREEN;
(*(*  WRITELN('YOURE SO SMART !');*)
  WAIT(2);
  NORMALSCREEN;
  ANALMENU;
  READ(IRESP);
  CASE IRESP OF
   1:ROUT1;
   2:ROUT2;
   3:ROUT3;
   4:ROUT4;
   5:ROUT15;
(*   6:ROUT6;*)
   7:ROUT7;
   8:ROUT8;
   9:ROUT9;
  10:ROUT10;
   11:ROUT11;
   12:ROUT12;
   13:ROUT13;
```

```
    14:ROUT14;
    16:ROUT16;
(*    17:ROUT17;   *)
    18:ROUT18;
    19:ROUT19;
    20:ROUT20;
    21:ROUT21;
    22:ROUT22;
    23:ROUT23;
    24:ROUT24;
    25:ROUT25;
    26:ROUT26;
    27:ROUT27
     END;
  UNTIL IRESP=6;
END; (* of analysis *)
(*****************************************************************************
   program begins here
*****************************************************************************)
BEGIN  (* program *)
  SVCCODE;
  INITIALISE;
  BEGINNING;
  ANALYSIS;
END. (* of program *)
```

Appendix B

A complete data list is available from the author.

The data has not been included in order to reduce the bulk of the report.

END

DATE
FILMED

588